Effect of discontinuity adaptive MRF models with Noise classifier

ARAVIND HARIKUMAR
March, 2014

ITC SUPERVISOR
Prof. Dr. Ir. A. Stein

IIRS SUPERVISOR
Dr. Anil Kumar

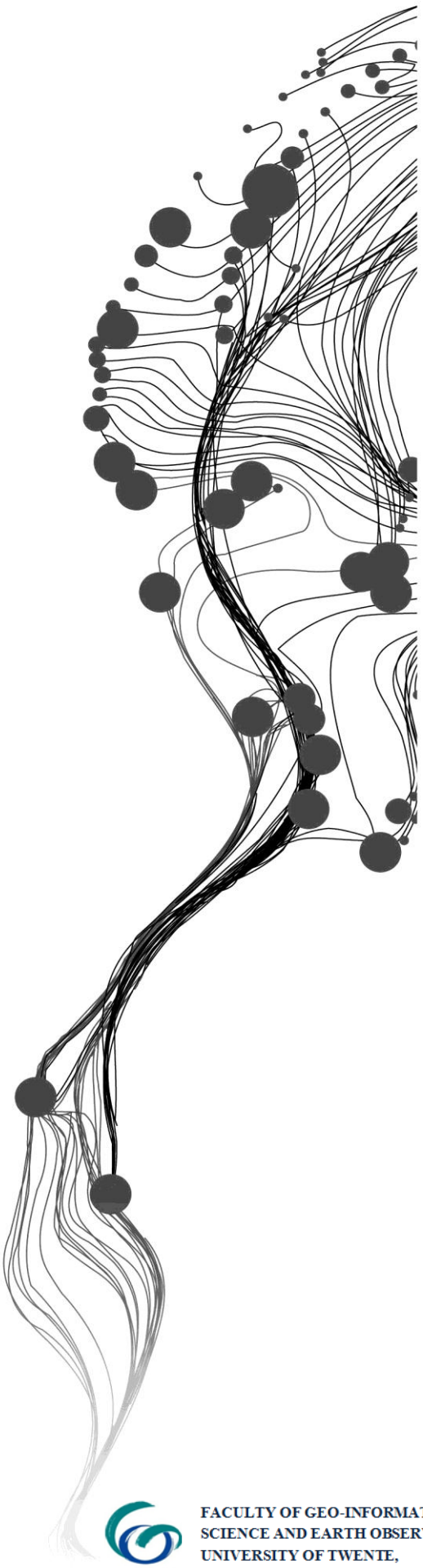

Effect of discontinuity adaptive MRF models with Noise classifier

ARAVIND HARIKUMAR
Enschede, The Netherlands [March, 2014]

Thesis submitted to the Faculty of Geo-information Science and Earth Observation of the University of Twente in partial fulfilment of the requirements for the degree of Master of Science in Geo-information Science and Earth Observation.

Specialization: Geoinformatics

THESIS ASSESSMENT BOARD:

Chair	: Prof. Dr. V. G. Jetten
ITC Professor	: Prof. Dr. Ir. A. Stein
External Examiner	: Prof. Dr. P. K. Garg (IIT, Roorkee)
IIRS Supervisor	: Dr. Anil Kumar
ITC Supervisor	: Prof. Dr. Ir. A. Stein

OBSERVERS:

IIRS Observer	: Dr. S. K. Srivastav
ITC Observer	: Dr. N. A. S. Hamm

FACULTY OF GEO-INFORMATION SCIENCE AND EARTH OBSERVATION, UNIVERSITY OF TWENTE, ENSCHEDE, THE NETHERLANDS

INDIAN INSTITUTE OF REMOTE SENSING
Indian Space Research Organisation
Department of Space, Government of India

DISCLAIMER

This document describes work undertaken as part of a programme of study at the Faculty of Geo-information Science and Earth Observation (ITC), University of Twente, The Netherlands. All views and opinions expressed therein remain the sole responsibility of the author, and do not necessarily represent those of the institute.

Dedicated to my mother and father!

ABSTRACT

Fuzzy based classifiers were found to be relatively efficient in generating accurate and realistic results in image classification. The presence of noise in the input dataset is found to causes a decrease in classification accuracy. Noise clustering was identified as a technique that is potentially robust against the presence of noise in remote sensing images. In this research, a supervised version of fuzzy noise clustering was used and it had been referred to in this thesis as Noise classifier. The use of spatial contextual information along with the spectral information from an image has a positive impact on the classification accuracy. Markov Random Fields (MRF) were used for modelling spatial contextual information and integrated into the objective function of the noise classifier. The novelty of this research lies in the use of contextual information with noise classifier. By means of this research, the effect of smoothness prior and discontinuity adaptive prior MRF models on the classification was studied using AWIFS and LISS-III datasets from Resourcesat-1 and 2. The fuzzy error matrix (FERM) accuracy for AWIFS data was found to be equal to 87.26% for Resourcesat-1 and 89.40% for Resourcesat-2. FERM accuracy for LISS-III data was found to be 85.27% for Resourcesat-1 and 89.37% for Resourcesat-2. Classification was also conducted, by leaving one class untrained, to study the effect of untrained classes on the classifier accuracy. A relative decrease in user's accuracy was observed when compared with the fully trained case. A decrease in user's accuracy of 9.93% and 7.25% was observed for AWIFS data from Resourcesat-1 and Resourcesat-2 respectively. A decrease in user's accuracy of 6.04% and 9.63% was observed for LISS-III data from Resourcesat-1 and Resourcesat-2 respectively. The study concludes that, the use of discontinuity adaptive priors improves the accuracy of the classification at the cost of slight increase in entropy.

Keywords: *Noise clustering, Noise robustness, Classification, Markov Random Fields, Fuzzy Error Matrix*

ACKNOWLEDGEMENTS

First of all I take this opportunity to thank the almighty for bringing me into this MSc program, helping me to successfully complete it and thus improve myself. Alongside I thank my mother and father for loving me so much.

I thank all my teacher form Indian Institute of Remote Sensing (IIRS) and ITC - Faculty of Geoinformation Science and Earth Observation for giving me knowledge, morally and technically supporting me and guiding me.

Dr. Anil Kumar, my supervisor and favourite teacher at Indian Institute of Remote Sensing is indeed very unique, as teacher and also as a supervisor. He is bestowed with qualities which draws respect from his students. I am indebted to him for the help, guidance and time he gave me in regard to my research.

I thank Prof. Dr. Alfred Stein for his guidance and help throughout my research phase. I have been really lucky and feel privileged to have a supervisor like him. The deep knowledge he has in geo-information science, his promptness and clarity in e-mail replies (even on holidays) and willingness to help his students are qualities worth mentioning.

I respect Dr. Valentyn Tolpekin for his kind, polite and helpful nature. I thank him for helping me at times when I was stuck with programming and technical challenges.

I also thank Dr. S K Srivastav, Head of Department, Department of Geoinformatics for being a very approachable person. I also thank him for his valuable advices which have really helped me during my research. I also thank Mr. P L N Raju, Group Head, Remote Sensing and Geoinformatics group for his valuable advices and providing me necessary resources to complete my project.

At last but not least I would like to thank all my friends at IIRS and ITC for being with me, encouraging me and also for their timely help and support.

Aravind Harikumar

TABLE OF CONTENTS

LIST OF FIGURES

LIST OF TABLES

1. INTRODUCTION

1.1. Research Background

The information about the earth and its atmosphere, conceived by analyzing the data acquired using remote sensing techniques has been helping society ever since the idea of remote sensing was realized. But information extraction from raw data is a challenging step in spatial sciences, and so is the case with remote sensing. Raw images collected most by remote sensor can easily be interpreted by a human, but not by computers. Still automation is critical for processing the large amount of data accumulating from these sensors. The concepts in image processing implemented in the form of algorithms, have helped in utilizing the potential of computers for automating and simplifying the information extraction process from remote sensing imageries.

Thematic maps have a wide application among the end products of remote sensing. In the digital domain, thematic maps are created by assigning labels to each pixel in an image and, this process is called as Digital Image Classification. This labelling allows computers to do further processing on the image and hence extract the required information. Achieving a high accuracy for thematic maps such as land use land cover maps has been a challenging problem to researchers. In the past, several methodologies were implemented as algorithms with the objective to create better classifiers and thus accurate thematic maps.

Conventional classification technique presumes that, each pixel in an image contains a single homogeneous class. It follows the classical set theory where, it is assumed that a pixel either has to completely belong to a class or completely not belong to the class i.e. if a pixel belongs to the forest class, the corresponding ground area is presumed be consisting of only forest and no other class, irrespective of its cell size. This type of classification is called hard classification. Due to the crisp nature of hard classifier, its classification result is a coarse approximation of reality.

In reality, each pixel might contain multiple classes and even for the case in which a class completely fills one pixel, the probability of getting hundred percent homogeneity equals zero i.e. pixels are never pure. This problem of having multiple classes within a pixel is referred to as mixed pixel problem. Mixed pixels mainly arise due the following reasons as discussed (Zhang and Foody, 1998).

1. Land use land cover classes are never found to be homogeneous in real world. A change from one class to another has always been found to be gradual, except in the case of manmade classes i.e. the boundaries of natural classes are fuzzy in nature.
2. Due to the unavoidable interaction of electromagnetic radiation with the atmosphere and ground objects, the reflected radiation reaching the sensor may not always provide

the actual spectral information. Hence the pixel values (DN) can also be a little different.

3. If the spatial resolution of a sensor is not very fine, it might result in the inclusion of multiple classes in one Ground Resolution Cell (GRC). Hence the resulting reflectance will be a spectral mixture of different classes within the GRC.

The concept of fuzzy sets (Zadeh, 1965) was found suitable for addressing the mixed pixel problem. Fuzzy logic basically assigns membership values to a pixel i.e. any real value between 0 and 1 for every class, rather than forcing a hard label from among any presumed pure class label set. This kind of membership value assignment helped in creating more realistic classification results. Fuzzy c-Means (FCM) is one successful classification technique which is built on top of fuzzy logic. In FCM membership values are provided to each class in a pixel and they always add up to one. The membership values in FCM basically show the degree of sharing of different classes in a pixel. But classification results of the popular FCM classifier was found inaccurate in the presence of noise and outliers (Krishnapuram and Keller, 1993). To solve this issue associated with FCM, a Possibilistic *c*-Means algorithm (PCM) was developed by slightly modifying the objective function of FCM and relaxing the membership restriction which exists for FCM i.e. for PCM all membership values for one pixel need not add up to one and each membership value for each pixel class can have any value between 0 and 1. The membership values in the case of PCM represent the degree of belongingness, rather than degree of sharing (Krishnapuram and Keller, 1993).

Noise in remote sensing imagery degrades the interpretability of the data. It is undesirable for any classifier including FCM and PCM, for the classification accuracy degrades in the presence of noise in the input dataset. The different sources of noise in an image includes,

1) Sensors or detector noise (Shot noise, Salt and pepper noise, thermal noise, mixed pixels etc) and noise due to processing errors.
2) Atmospheric noise or Speckle noise in case of radar images.
3) It is always possible to have classes other than the classes of interest in the study area. These classes are also considered as noise as far as a classifier is concerned.

Noise classifier (NC) is a classification technique which was found to be robust against these types of noises. It is basically the supervised version of Noise Clustering technique. It achieves noise robustness by allocating all the pixels which are at a constant distance 'δ' (delta) in the feature space to a separate class called the noise class, rather than forcing them to any on the existing classes. An interesting fact is that, NC membership can be represented as the product of two terms where, one term is the FCM component responsible for data partitioning, and the other is the possibilistic component that achieves a mode seeking effect and imparts robustness. The noise membership can be written as (Davé and Sen, 1997), $NC_{u_{ij}} = FCM_{u_{ij}} * PCM_{u_{ij}}$, where $FCM_{u_{ij}}$ represents the membership value estimated using FCM for the ith pixel in the jth class and $PCM_{u_{ij}}$ represents the membership value estimated using PCM for the ith pixel in the jth class for the same input image. In most classification techniques the classification was performed on the basis of spectral information only. Here the base assumption is that all pixels in an image

are independent to one another. But in reality a pixel will always end up having some correlation with its neighbouring pixels. This occurs due to the fact that, on ground, most classes are found to be spread across more than one pixel and also the energy collected by sensor i.e. for a pixel, is never entirely from its own GRC but from the surrounding GRC's as well. Thus it was thought of by researches as a wise idea to include the information about the surrounding i.e. to include spatial contextual information also as input to the classifier. There are many ways to use this contextual information for better classification.

1. **Image pre-processing**: In this case, each pixel value is modified by considering the information about the surrounding i.e. contextual information is used to enhance information contained in each pixel. The different preprocessing operations include Mean Filter, Average filter, etc. This pre-processed image is used as the input for classification.
2. **Post classification**: Here the classification is conducted first and then the classification output is further subjected to image processing operators such as Median Filter.
3. **Label relaxation**: Here the classifier uses information from both spatial and spectral domain simultaneously while classifying. Markov Random Field (MRF) is a widely accepted technique used to model the contextual information. MAP-MRF theory provided a convenient and consistent way of modeling the contextual information. This was possible after the establishment of equivalence between MRF and Gibbs distribution (Besag, 1974). In this method the contextual information modeled using MRF (i.e. prior) is incorporated into the objective function of the base classifier and the resulting optimization problem is solved using optimization techniques like Simulated Annealing (SA).

The possible kinds of MRF priors that can be used include the Smoothness prior and discontinuity Adaptive Priors. Usage of Smoothness Prior creates the problem of over-smoothening at the edges and in order to overcome this problem discontinuity Adaptive Priors were introduced. This research primarily aims at studying the effect of using different discontinuity Adaptive Priors when integrated with the Noise classifier operated in fuzzy mode (base classifier) on classification accuracy.

1.2. Motivation and Problem Statement

It was proved that, fuzzy classification provides better or realistic classification results when compared to hard classification. It is also true that noise in an input imagery affects the classification accuracy. Noise classifier (fuzzy mode) was identified as one such classifier which was found to be more robust against noise as when compared to other fuzzy classification techniques such as FCM and PCM. Adding contextual information to the base classifier for improving the classifier accuracy proved to be a good idea. Considering this, it was proposed to study the effect of different Smoothness Prior & discontinuity Adaptive Priors with Noise classifier (fuzzy mode).

1.3. Research Identification

Almost all classification algorithms are affected by noise and outliers present in the input data. The sources of noise have already been discussed. Among the various robust classifiers, Noise classifier was identified as to be one of the best which can mitigate the effect of noise and outliers on the accuracy of image classification (Dave and Fu, 1994, Dave, 1991, Dave, 1993). The Noise classifier assigns a separate class/cluster for noise and its cluster center would be equidistant from all other data points. The algorithm starts with the base assumption that all the points have equal probability of belonging to the noise cluster and then, as the algorithm progresses the probability shifts (Dave, 1991). Noise classifier and its variations have been successfully used in many applications (Sen and Dave, 1999, Ma et al., 2003). The ability of Noise classifier to incorporate the fuzzy nature of objects in an image helps in generating more realistic results (Richards, 2013). The objective function of Noise clustering is shown in Equation 1.1,

$$J(B,U;X) = \sum_{i=1}^{C}\sum_{j=1}^{N}(u_{ij})^m\, d^2(x_j,\beta_i) + \sum_{j=1}^{N}\delta^2\left(1-\sum_{i=1}^{C}u_{ij}\right)^m \quad (Equation\ 1.1)$$

In equation 1.1, $d^2(x_j,\beta_i)$ represents the distance from feature point x_j to cluster center(β_i), δ represents the noise distance, (u_{ij}) represents the membership values, *C* is the number of clusters, N is total number of feature points and m represents the degree of fuzziness.

It was found that the usage of spatial contextual information in the classification process could improve the classifiers robustness against noise and untrained classes as when compared to purely spectral based classification algorithm. (Krishnapuram and Keller, 1993, Foody, 2000). As it was mentioned earlier in this thesis, the MRF modelling technique was found to be widely accepted technique for modelling contextual information and hence was used for modelling the contextual information in this thesis.

The spatial contextual information thus modelled goes as the prior information into the Bayesian model where the basic assumption is that, the process under consideration always changes gradually. This property was considered to help in modelling any natural process better and so smoothness priors was preferred (Mather and Tso, 2010). But the use of smoothness priors' results in the problem of over smoothness at the boundaries and this was solved to some extend by adopting the discontinuity Adaptive Prior models. Four discontinuity Adaptive models have been mentioned in literature and the same was used in this research (Li, 2009).

Through this research an effort was made to study the effect of various discontinuity Adaptive MRF models while using the Noise classifier (fuzzy mode). In this research work a coarse resolution (AWiFS) and medium resolution (LISS-III) datasets would be used for evaluating the efficiency of the proposed algorithm. Finally the accuracy would be accessed using reference data created from finer resolution LISS-IV sensor and also with the help of field observations.

1.4. Research objectives

The main objective of this research is to incorporate spatial contextual information with Noise classifier using discontinuity Adaptive MRF models. The specific objectives are,

- ✓ To incorporate spatial contextual information with Noise classifier (NC) using the smoothness prior model.
- ✓ To study the effect of the four discontinuity adaptive MRF (DA-MRF) models when incorporated with the Noise classifier.
- ✓ To evaluate the performance of the Noise clustering algorithm while applying discontinuity adaptive MRF models for both trained and untrained classes.

1.5. Research questions

The following are the research questions identified from the research objectives, which will ultimately help in addressing the objectives of this research.

1. How can the Noise classifier (NC) parameters be estimated.
2. How can the Noise classifier objective function be modified to incorporate spatial contextual information modeled using S-MRF and DA-MRF models?
3. Which DA-MRF prior model would be best suited for the Noise Classifier?
4. To what degree does the classification accuracy improve upon using the NC DA-MRF classifiers when compared to NC Classifier with and without training?

1.6. Innovation aimed at

Incorporating contextual information into Noise classifier was proposed to overcome sensitivity of noise and outliers on the classification result to an extent. In this research work, it was aimed to quantify the performance of Noise classifier which incorporates spatial contextual information using S-MRF or DA-MRF models.

1.7. Methodology

The core objective of this research is to frame an objective function for noise classifier which incorporates the contextual information in an image using Markov Random Fields technique, which includes smoothness prior MRF models and discontinuity Adaptive MRF models. Before estimating the MRF model parameters, the optimal NC parameters, m (fuzzification factor) and δ (noise distance) need to be estimated, so as to maximize the efficiency of the Noise classifier.

Before classification, the LISS-III, LISS-IV, and AWIFS images from Resourcesat-1 and Resourcesat-2 sensors have been geometrically corrected and geo-registered. Survey of India toposheet was used initially to geometrically correct the LISS-IV dataset which was then used for the geo-registration of AWIFS and LISS-III datasets. This would be followed by a classification of the data by the NC, NC S-MRF and four different NC DA-MRF classifiers. Finally the accuracy will be accessed using soft classified finer resolution data from LISS-IV sensor and also with the help of field observation data. The performance of the classifier would

be evaluated in case of untrained classes as noise and or outliers also. The methodology adopted for this research is shown in Figure 1.1.

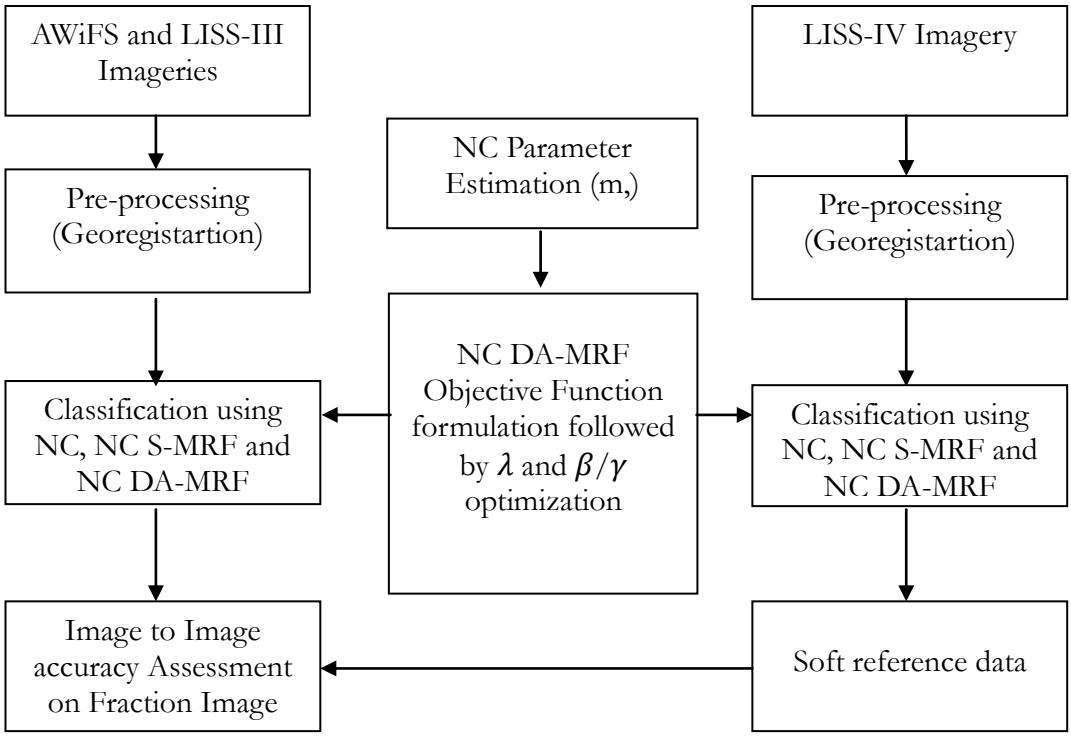

Figure 1-1: Methodology adopted for this study

1.8. Thesis Structure

The thesis portraits the whole research in eight chapters. The *First chapter* gives an introduction to the research, the objectives that need to be achieved and the high level view of the methodology adopted. The *Second chapter* briefs about the various research works that were conducted in the field of image classification and various accuracy assessment techniques. The T*hird chapter* describes in detail about the idea of noise clustering and also its mathematics behind it. The *Fourth chapter* describes on why and how the use of MRF modelling can be used to model spatial contextual information. The *Fifth chapter* describes in details about the hybrid classifier what is realized. The mathematical expression formulated for this novel classifier is also explained in detail. The *Sixth chapter* says about the study area considered for this research, the reasons for selecting it and various datasets used. The *Seventh chapter* show and describes the various results that were obtained in this study. The *Eighth chapter* concludes the research, answers all the research questions and also gives some possibilities for improving the current research outcomes.

2. LITERATURE REVIEW

2.1. Fuzzy c-Means and Possibilistic c-Means Clustering

The widespread use of fuzzy logic for classification began with the introduction of Fuzzy *c*-Means (FCM) Clustering. In FCM, the objective is to represent the similarity of a data point to its cluster center rather than bluntly representing the data point by the cluster center properties (Bezdek et al., 1984). It would be rather intuitive to say that FCM gives information about the degree of sharing of each data point with the different cluster centers or class prototypes (Krishnapuram and Keller, 1993). FCM had been successfully used for estimation and mapping of sub-pixel level land cover composition (Foody, 2000, Fisher and Pathirana, 1990).

Initial fuzzy classification approaches considered fuzziness in the class allocation stage but ignored to address the fuzziness involved in the testing and training stages (Zhang and Foody, 1998). Fuzzy ground data derived with the help of indicator kriging enabled in addressing the fuzziness at the training and testing stages (Zhang and Kirby, 1997). This fully fuzzy FCM approach gave an improvement in accuracy of 1.6% and 20% over partially fuzzy approach and hard approach respectively while using Landsat TM dataset (Zhang and Foody, 1998, Zhang and Foody, 2001).

FCM was found to generate membership values which represented the degree of sharing rather than degree of typicality (i.e. belongingness to a class and for the same reason), and it failed to mitigate the effect of noise points and outliers. Possibilistic c-means (PCM) was developed to address the drawback of FCM. It was developed by adding an additional term (η – distance at which membership value reach 0.5 for a class) to the objective function of FCM and relaxing constrain on the membership. PCM generated membership values that represented degree of belongingness (Krishnapuram and Keller, 1996).

Soon after the development of FCM many variations of the classifiers such as supervised fuzzy c-means classification (Foody, 2000) and unsupervised possibilistic clustering (Yang and Wu, 2006) were realized. Kumar et al. (2006) compared the accuracy of FCM against PCM and found that, PCM with Euclidean norm has the highest overall accuracy among them (Kumar et al., 2006). The performance of PCM was found to be better than FCM because PCM was able to surpass the effect of hyperline constant found in FCM (Chawla, 2010). Successful effort to reduce the uncertainty associated with the data while doing the segmentation of magnetic resonance (MR) image happed when, Noise clustering concept was incorporated into entropy based FCM.

2.2. Noise clustering

The performance of a clustering algorithm is affected by two main factors which are, apriori knowledge of clusters and presence of noise in the data. To certain level of accuracy the number of clusters can be found using cluster validity measures (Bezdek, 1981) and even better results have been obtained using compatible cluster merging algorithm (Krishnapuram and Freg, 1992).

The challenging problem of noise removal was looked upon at different perspectives (Jolion and Rosenfeld, 1989, Krishnapuram and Freg, 1992) and among them Noise clustering was found to give the best performance (Dave, 1991).

Noise clustering algorithm was proposed to overcome sensitivity of FCM algorithms to noisy data. In Noise clustering algorithm, those feature space points which are at a constant minimum distance (Noise distance) from all the cluster centers are considered as noise. But later the assumption of constant noise distance was found restrictive and thus the algorithm was designed to allow different Noise distances for different feature vectors (Davé and Sen, 1997). A Kernel Noise clustering algorithm was also proposed (Chotiwattana, 2009) based on distances of kernel method and was found to be relatively more resistant against noise. Here the idea was to replace the Euclidian distance in the objective function of NC algorithm with distance of kernel.

Surprisingly, it is also proved that the Noise clustering algorithm is a generalization, where PCM and FCM are its special cases (Davé and Sen, 1997).The mathematical proof can be found in (Davé and Sen, 1997). The main disadvantage of PCM, which is a mode seeking algorithm, is its performance dependence on good cluster initialization. FCM (a partitioning algorithm) is capable of providing good cluster initialization and is hence used estimate prospective cluster centers for PCM. Noise clustering combines the mode seeking ability of PCM combined with the FCM's power of partitioning and was found to give a relatively better performance (Davé and Sen, 1997).

2.3. Markov Random Field

Among the different techniques for modelling the contextual information, MRF modelling was found to improve the classification accuracy (Solberg et al., 1996) and for the same reason MRF was widely used for modelling contextual information. Initial applications of MRF included tomographic reconstruction (Geman and Graffigne, 1986), computer vision (Geman and Graffigne, 1986), surface reconstruction (Geiger and Girosi, 1991). In the field of remote sensing image analysis, it was used for image restoration (Geman and Geman, 1984), texture classification (Derin and Elliott, 1987), image and texture segmentation (Rangarajan et al., 1991) etc.

The equivalence existing between Gibbs distribution and MRF opened up the possibility of using an energy function for embodying image attributes conveniently followed by maximum-a-posteriori (MAP) parameter estimation using an optimization method (Geman and Geman, 1984). From among the different optimization methodologies developed, Simulated Annealing (stochastic relaxation) guaranties to provide global MAP estimates i.e. the algorithm do not get carried away by local optima's (Geman and Geman, 1984).

MRF based contextual methods were used for classification and fusion of multi-source data and it was proven that the classification accuracy have improved over other contextual methods (Solberg et al., 1996). Contextual information modelled using MRF was integrated into multi source classification scheme using fuzzy based classifier helped in generating maps which are

more reliable (Binaghi et al., 1997). A Robust Fuzzy *c*-Means (RFCM) algorithm was developed by adding contextual information to the objective function of FCM using MRF, while performing image segmentation of Magnetic Resonance Images of brain (Pham, 2001). An Adaptive Bayesian Contextual classifier, which combines the advantages of Adaptive classifier and Bayesian Contextual classifier demonstrated, on how MRF modelling of joint probabilities of classes of each pixel and its neighbourhood could improve the classification accuracy by mitigating the effect of Speckle error (Jackson and Landgrebe, 2002).

MRF was also used successfully to integrate contextual and spatio-temporal information, while classifying Landsat TM and ERS-1 SAR images (Melgani and Serpico, 2003). Kasetkasem et al. used MRF model for super-resolution land cover mapping of IKONOS MSS and Landsat ETM+ images and found it to be better than Linear Optimization approaches (Kasetkasem et al., 2005). Moser and Serpico integrated contextual information onto support vector machines classifier using MRF model. It was achieved by reformulating the prior energy function in terms of suitable SVM-like kernel expansion (Moser and Serpico, 2010).

2.4. Dealing with Over-smoothening

The smoothness prior MRF model creates the problem of over smoothening at the boundaries and in order to overcome this discontinuity adaptive (DA) MRF models which could control the smoothening strength at the boundaries were introduced (Li, 1995, Li, 2009) i.e. at discontinuities, the model minimizes the smoothing strength accordingly.

Smits and Dellepiane used MRF based contextual information modelling with adaptive neighbourhood segmentation on synthetic aperture radar (SAR) images (Smits and Dellepiane, 1997) and it was found to have the advantage of preserving the edges in the image. A method for automatically controlling the smoothing strength by adjusting smoothening parameter in discontinuity adaptive MRF function was also proposed (Kang and Roh, 2001).

The effect of adding Contextual Information using DA-MRF models in Possibilistic *c*-Means classification was studied by (Dutta, 2009). Classification based on fuzzy *c*-Means incorporating spatial contextual information by using Markov Random Field was also studied using multispectral data (Singha, 2013). Singha also studied the effect of different DA-MRF models on the accuracy of Fuzzy *c*-Means classification.

2.5. Accuracy Assessment

Accuracy assessment is an essential step for projecting the usability of any remote sensing end product. Producer's accuracy, user's accuracy, overall accuracy and kappa derived from confusion matrix have been used for validating hard classification results. But validation of soft classification result is not straightforward as sub-pixel class boundaries are unknown. As of now there is no standard accuracy assessment technique available for soft classification results. Efforts to access the accuracy of a soft classification result after hardening it resulted in loss of information (Foody, 1997, Silván-Cárdenas and Wang, 2008).

Various methods have been suggested over the past two decades for conducting soft classification accuracy assessment (Binaghi et al., 1999, Congalton, 1991, Green and Congalton, 2004, Pontius Jr and Cheuk, 2006). It is not possible to find the exact spread of a class within a pixel in both fuzzy classified and fuzzy reference sets (i.e. ground data) and hence various operators such as MIN, PROD and even hybrid operators such as MIN-MIN, MIN-PROD was introduced to do fuzzy accuracy assessment (Pontius Jr and Cheuk, 2006). Among the various methods proposed, the fuzzy error matrix (FERM) is a popular but not standard one and was used for generating accuracy indices such as overall accuracy (Binaghi et al., 1999). A Sub-pixel Confusion Uncertainty Matrix (SCM), where the uncertainty in the confusion matrix elements is also represented in the form of a center value plus–minus maximum error was also developed (Silván-Cárdenas and Wang, 2008).

Entropy measure proved to be useful to a great extent in the absence of reference data. It gives an absolute measure of uncertainty for a classified output. (Dehghan and Ghassemian, 2006, Foody, 1996, Kumar and Dadhwal, 2010, Zhang and Foody, 1998). Cross-entropy measure for accuracy assessment also was implemented for fuzzy datasets (Foody, 1995).

3. NOISE CLUSTERING

3.1. Cluster Analyis

There are situations in scientific data analysis where it is necessary but difficult to effectively group similar data due to lack on information about the data. Clustering is an unsupervised classification technique which helps in grouping similar data points such that data points within the clusters are more similar to each other rather than their counterparts in other clusters (Soman et al., 2006). Clustering has wide application in many scientific fields such as artificial intelligence, data mining, image processing, pattern recognition and statistics.

It is a fact that, there is no single clustering methodology which performs best for all the datasets or solves all the clustering problems and hence there exists different clustering techniques. Clustering algorithms are broadly classified as hierarchical and partitional. Hierarchical clustering builds a dendorum structure of the data but partitional clustering divide data into a specified or estimated number for clusters (Soman et al., 2006). Clustering algorithms are also classified into 'Hard' and 'Soft' algorithms (Dave, 1991). In Hard clustering each data point is allotted to exactly one class as where as in the case of Soft or Fuzzy clustering each data point will have a partial allotment to each of the clusters with a measure of belongingness (Babu and Murty, 1994).

For reducing the time required for clustering algorithm to reach an optimal solution, initial seed values i.e. vague cluster centers, are selected (Babu and Murty, 1994). Most clustering algorithm can be represented as an optimization problem. For Hard clustering the parameters to be optimized includes only the cluster centers but in case of soft classifier, the parameters to be optimized include the membership values and the cluster centers.

Fuzzy c-Means clustering (FCM) and Possibilistic c-Means (PCM) are two popular clustering techniques. In case of FCM, the membership values represent degree to which a class is shared to a cluster but in case of PCM it refers to the degree of belongingness (Krishnapuram and Keller, 1993). PCM is found to be more stable against noise when compared to FCM.

3.2. Noise clustering

Noisy data and outliers has always been a problem for effective clustering. The presence of noise biases the clustering algorithm and hence results in unrealistic clusters. In case of k-Means or FCM, the algorithm finds a relation between each data point and a cluster i.e. each data point is forcefully assigned/related to a particular cluster irrespective of whether the point under consideration is a noise data point or not (Dave, 1991). PCM solves the problem of noise and outliers by working on the degree of belongingness of each data point to a cluster numerically represented using membership values (Krishnapuram and Keller, 1993).

Noise clustering algorithm was introduced by Dave, R.N as an alternative approach to overcome the sensitivity of FCM algorithm to noisy data. It stressed on the concept of having a separate cluster (noise cluster) into which, all the noisy data points/outlier in the data may be

dumped. The noise cluster center is selected such that, it is equidistant from all the points in the dataset and physically it means that each data point have an equal prior probability of belonging to the noise cluster (Dave, 1991). This estimated distance of noise cluster center from all the data points is called as 'Noise distance' (δ) and is a critical parameter which affects the performance of the Noise clustering (Dave, 1991). Its value is ideally dependent on the data but a close approximation can be obtained using equation 3.1 (Dave, 1991, Dave, 1993).

$$\delta^2 = \lambda \left[\frac{\sum_{i=1}^{N} \sum_{j=1}^{c} D(\vec{x}_i, \vec{v}_j)}{Nc} \right] \tag{3.1}$$

The Figure 3.1 (a) shows the a sample data set taken from (Dave, 1993) and Figure 3.1 (b) shows the result of Noise clustering on the dataset. The ' ○', ' ☆' and '◇' represents three valid clusters and '+' represents the outliers and noisy data points which belongs to the noise cluster. From Figure 3.1 (b) we can see that the clusters formed are realistic. All the points beyond a threshold (noise distance) from all the cluster centers are allocated to noise cluster. For FCM the constant on the membership value (for each pixel) is that, membership values for all the classes should add up to 1 i.e. $\sum_{j=1}^{c+1} u_{ij} = 1,\ 1 \le i \le N$ where c is the number of clusters and N is the total number of pixels in the image. Hence all data points including noisy data and outliers are forcefully assigned to one cluster or the other and as a result, the cluster centers might get shifted more from the optima. (Dave, 1993). In case of PCM the membership constraint is $\sum_{j=1}^{c+1} u_{ij} > 1,\ 1 \le i \le N$, and thus each class within a pixel could be assigned with a membership value between 0 and 1 (both 0 and 1 include). This constraint relaxation enabled PCM to give high membership values for valid data points (up to 1) and low values for on the membership values (close to 0) for noisy data points. In case of Noise clustering, the constraint on membership is $\sum_{j=1}^{c+1} u_{ij} \le 1,\ 1 \le i \le N$ and so the sum of class membership values for a pixel can even be less than 1. This creates way for the noise points to have small membership values (Dave, 1993, Davé and Krishnapuram, 1997). Thus noisy points will have little impact on deciding the cluster centers and hence better clustering.

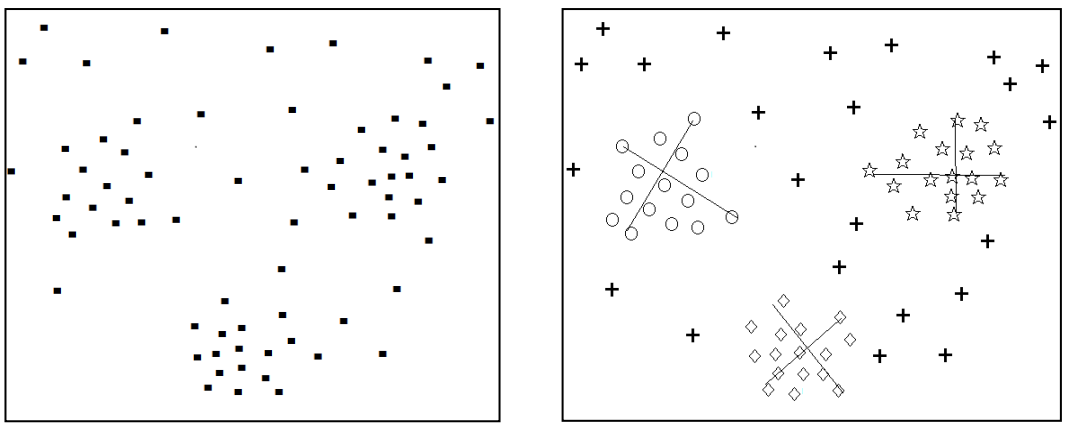

(a) Noisy data (b) Result of Noise clustering

Figure 3-1: Noise clustering (Dave, 1993)

3.3. Why Noise Clustering?

The strength of PCM lies in its mode seeking capability, which helps in locating meaningful clusters i.e. those defined by dense regions. But PCM has a few disadvantages. For optimal performance, PCM expects good cluster center initialization which is obtained with the help of FCM (Barni et al., 1996). The relaxation of the membership constraint for PCM makes the cluster forming process independent of one another and hence sometimes exaggerate the dependence on initial partitions and also the probability of ending up in a local minima goes up for PCM (Barni et al., 1996).

The main advantage of Noise clustering over its counterparts is its robustness to noise and outliers. It achieves the same by allocating all the noisy data and outliers to the noise cluster as discussed in the section 3.2. The Noise classifier and its variations have been successfully used in many applications and had shown better performance in noisy environment. The ability of Noise classifier (fuzzy approach) to deal with the fuzzy nature of objects in an image, at the same time allocating a separate class for noise would help in producing more realistic classification results (Richards, 2012). Even in case of untrained classes, i.e. classes which were actually present in the data but no training data was given to the classifier, Noise clustering will not forcefully allocate the data points to any available class but will be looked upon as noise only.

3.4. Mathematics behind Noise clustering

The objective function of Noise clustering (fuzzy mode) is shown in equation 3.2. The first term in equation 3.2 is exactly the objective function of FCM and the second term is placed in the objective function to ensure that the optimization problem (here a minimization problem) also has a grab on the noise cluster membership values while optimizing.

$$J_{nc}(U;V) = \sum_{i=1}^{N}\sum_{j=1}^{C}(u_{ij})^m D(\vec{x}_i, \vec{v}_j) + \sum_{i=1}^{N}(u_{i,c+1})^m \delta. \qquad (3.2)$$

In equation 3.2, *C* is the number of classes, N is the total number of pixels in the image, m is the fuzzification factor, u_{ij} represent the membership value of i^{th} pixel in the j^{th} class, $u_{i,c+1}$ represents the membership values of the noise class, v_j is the mean value (cluster center) of the j^{th} class, x_i is the vector value of the i^{th} pixel, D is the Euclidian distance between $\bar{x}_i$ and $\bar{v}_j$ and δ is a positive constant called the Noise distance. The value of the membership values(u_{ij}), membership values for noise class $(u_{i,c+1})$ and mean class $(\bar{v}_j)$ vectors can be obtained from the equations 3.3, 3.4 and 3.5 respectively.

$$u_{ij} = \left[\sum_{k=1}^{C}\left(\frac{D(\vec{x}_i, \vec{v}_j)}{D(\vec{x}_i, \vec{v}_k)}\right)^{\frac{1}{m-1}} + \left(\frac{D(\vec{x}_i, \vec{v}_j)}{\delta}\right)^{\frac{1}{m-1}}\right]^{-1}, \quad 1 \le j \le C \qquad (3.3)$$

$$u_{i,c+1} = \left[\sum_{k=1}^{C} \left(\frac{\delta}{D(\vec{x}_i, \vec{v}_j)} \right)^{\frac{2}{m-1}} + 1 \right]^{-1} \tag{3.4}$$

$$\overline{v}_j = \frac{\sum_{i=1}^{N} (u_{ij})^m \vec{x}_i}{\sum_{i=1}^{N} (\bar{u}_{ij})^m}, \quad 1 \leq j \leq C \tag{3.5}$$

The second term in equation 3.3 ensures that outliers get low membership values. Also unlike FCM, the constraint on membership is effectively relaxed i.e. sum of class membership values for a pixel can even be less than 1. This creates way for the noise points to have small membership values (Dave, 1993, Davé and Krishnapuram, 1997). For NC, the constrain on membership is mathematically expressed as shown in equation 3.6.

$$0 \leq \sum_{j=1}^{c+1} u_{ij} \leq 1, \quad 1 \leq i \leq N \tag{3.6}$$

It has also been proved mathematically, that the objective function of NC and PCM are the just the same when number of clusters C equals 1, and when $C > 1$, the PCM is equivalent to C separate noise functional each looking for a cluster (Davé and Sen, 1997). Also the equation to find the optimal membership values was decomposed into two components, which exactly are the equations for finding the membership values of PCM and FCM correspondingly i.e. $NC_{u_{ij}} = FCM_{u_{ij}} * PCM_{u_{ij}}$, where $FCM_{u_{ij}}$ represents the membership value estimated using FCM for the i^{th} pixel in the j^{th} class and $PCM_{u_{ij}}$ represents the membership value estimated using PCM for the i^{th} pixel in the j^{th} class for the same input image. In the light of this equation NC is said to be a hybrid of FCM and PCM with individual qualities inherited (Davé and Sen, 1997). The Noise clustering algorithm can be found in Appendix A.

4. MARKOV RANDOM FIELDS – A CONTEXTUAL MODELLING TECHNIQUE

The chapter aims at shedding light on the concept on Markov Random Field theory and how it can be used in the context of images. Markov Random Field is a technique which helps in effectively modelling context-dependent entities such as image pixels and other correlated features (Li, 2009). Contextual information basically refers to the relationship of an entity with its neighbourhood and in context of an image pixel it refers to the information obtained from the neighbourhood pixels.

In case of an image, the contextual information can be obtained from spectral, spatial or temporal domains and this additional information obtained could be used to improve the accuracy of image classification. MRF had been applied widely in the image processing domain including image restoration and segmentation, surface reconstruction, edge detection, texture analysis, data fusion, etc (Li, 2009). In case of remote sensing image, each pixel represents a square region on the ground and it is a fact that digital number of each pixel is influenced by the neighbouring pixels. This is caused due to the reflection coming from the adjacent ground resolution cell. Hence it is also true to say that there is a statistical dependence between the DN values of neighbouring pixels (Pizurica, 2002). In case of a remote sensing image, inclusion of contextual information while classifying helps in removing isolated pixel problem i.e. a pixel which is surrounded by water pixels is assigned with more possibility of being a water class rather than any other class. Fuzzy classifiers achieve the same by assigning high membership value to the class mostly surrounding the isolated pixels.

4.1. Defining Markov Random Field

"Let a set of random variable $d = \{d_1, d_2, \ldots . d_m\}$ be defined on the set S containing m number of sites in which each random variable $y_i(1 \leq \mathrm{i} \leq \mathrm{m})$ takes a label from label set L. This family d is called random field" (Mather and Tso, 2010). An image can be considered as one such random field where m would represent number of pixels, d is the possible set of DN values, and L would represent possible class labels, e.g. dry agriculture, forest, water etc. "A random field with respect to a neighbourhood system is called a Markov Random Field if its probability density function satisfies the following three properties:" (Mather and Tso, 2010).

1) **Positivity**: It means that there are no label configurations which isn't possible i.e. $P(w) > 0$
2) **Markovianity**: This states that the labeling of a particular site is entirely dependent on the labels of its neighbors, i.e. $P(w_r|w_{S-r}) = P\left(w_r\middle|w_{N_r}\right)$.
3) **Homogeneity**: The conditional probability of label of site r, given the labels of its neighborhood is independent of the relative position of the site r in S. i.e. $P\left(w_r\middle|w_{N_r}\right)$ is a constant.

Apart from these, the dependency with the neighbourhood can also vary as a function of direction, this directional variation in dependency is sometime undesirable and the property of direction independence is referred to as Isotropy.

4.2. Neighbourhood Systems

In this thesis, we are interested in modelling the spatial contextual information from an image. The neighbourhood is relevant in the context of MRF as it deals with local interaction as when compared to Gibbs Random Field (GRF) which deals with global interaction. The order of neighbourhood system represents the range of pixels over which a center pixel has some interaction. Figure 4.1 shows the some spatial neighbourhood systems possible for a pixel, where r denotes the target site.

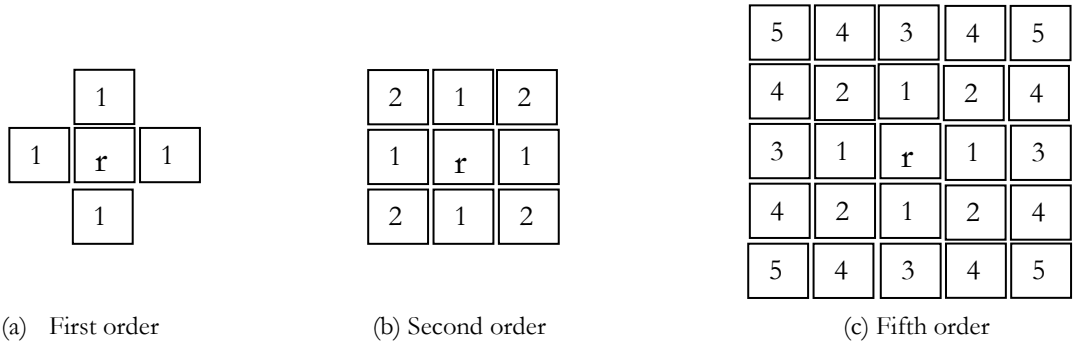

(a) First order (b) Second order (c) Fifth order

Figure 4-1: Neighbourhood systems (Mather and Tso, 2010)

Mathematically a neighbourhood system can be represented as a set. E.g. a first order neighbourhood system is represented as $N(i,j) = [(i-1,\ j), (i+1,\ j), (i,\ j-1), (i,\ j+1)]$, where i and j represents the row index and column index of site r in the image.

4.3. Gibbs Random Field (GRF) and Equivalence to MRF

Both GRF and MRF can be used for modelling the spatial contextual information in an image. The main difference is that GRF describes the global properties of an image whereas, MRF is defined in terms of local properties. An image can be represented by specifying a p.d.f as shown in equation 4.1

$$\mathrm{P(w)} = \frac{1}{Z} exp\left[-\frac{U(w)}{T}\right] \qquad (Equation\ 4.1)$$

In equation 4.1, T is a constant called Temperature, $U(w)$ is called Energy function and Z is called Partition function and it represents the sum of energy of all possible combination of w and is mathematically represented as (Mather and Tso, 2010),

$$\mathrm{Z} = \sum_{\substack{all\ possible \\ configuration\ of\ w}} exp\left[-\frac{U(w)}{T}\right] \qquad (Equation\ 4.2)$$

But calculating the value of Z is not a possible thing to do for most of the real life situations. Even an image of size 256 x 256 will have $8^{256*256}$ number of possible configurations. Looking at equation 4.1, it is true to say that maximizing $P(w)$ is equivalent to minimizing the Energy function $U(w)$ which is mathematically expresses as,

$$\mathrm{U(w)} = \sum_{c \epsilon C} V_c(w) \qquad (Equation\ 4.3)$$

In equation 4.3, C refers to the collection of all possible Cliques, and $V_c(w)$ is called the potential function against each Clique type C. A clique is a site subset from the neighbourhood system where members of the site are mutual neighbours. They can either be first order clique or second order clique. Second order clique includes pair-site, triple-sites and quadruple-site cliques. Consider that we have a neighbourhood as shown in Figure 4.2 (a), then Figure 4.2 (b) shows the cliques that can be formed from the first order and second order neighbourhood systems respectively.

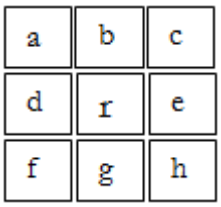

(a) Neighborhood System

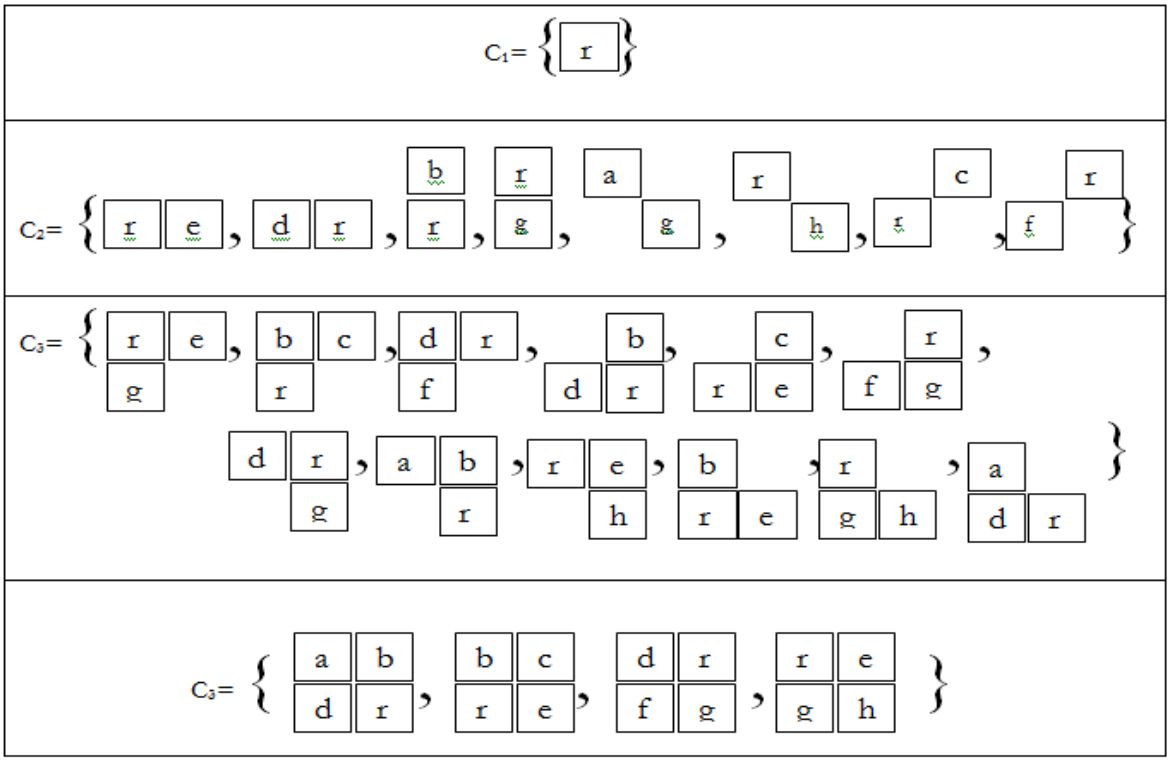

(b) First and second order cliques

Figure 4-2: Cliques

The Hammersley-Clifford theorem states that, a unique GRF exist for every MRF if the GRF is defined in terms of cliques of neighbourhood system, the proof of which is available in (Besag, 1974). This equivalence between MRF and GRF reduces the computation involved in calculating the joint probability by shifting the problem from global context to local context. Hence the Energy function in equation 4.3 can be re-written as shown in equation 4.4.

$$\mathrm{U(w)} = \sum_{\{r\}\epsilon C_1} V_1(w_r) + \sum_{\{r,r'\}\epsilon C_2} V_1(w_r, w_{r'}) + \sum_{\{r,r',r''\}\epsilon C_3} V_1(w_r, w_{r'}, w_{r''}) + ..$$

$(Equation\ 4.4)$

In equation 4.4, $V_1(w_r)$, $V_1(w_r, w_{r'})$and $V_1(w_r, w_{r'}, w_{r''})$ represents the potential function against single-site (C_1), pair-site (C_2) and triple site (C_3) cliques respectively.

4.4. Bayes Theorem

Using Bayesian theorem, the information from the data can be combined with the prior information to produce the required posterior distribution (Bernardo, 2003). According to Bayesian theorem the posterior probability can be expressed mathematically as shown in equation 4.5.

$$\mathrm{P}\left(\frac{\mathrm{w}}{\mathrm{y}}\right) \propto \mathrm{P(w)} * \mathrm{P}\left(\frac{\mathrm{y}}{\mathrm{w}}\right) \qquad (Equation\ 4.5)$$

Here $\mathrm{P(w/y)}$ refers to the posterior probability, $\mathrm{P(y/w)}$ referes to the conditional probability of getting the image y given the label configuration w and $\mathrm{P(w)}$ refers to the prior probability. From equation 4.5, the global posterior energy can be represented as shown in equation 4.6 (Tolpekin and Stein, 2009).

$$\mathrm{U}\left(\frac{\mathrm{w}}{\mathrm{y}}\right) = \mathrm{U(w)} + \mathrm{U}\left(\frac{\mathrm{y}}{\mathrm{w}}\right) \qquad (Equation\ 4.6)$$

4.5. The Prior

A prior in an image context, refers to the information about the image data available before hand. Prior energy is represented by $P(w)$ and is calculated equation shown in equation 4.5. In the case of image classification, the sum of pair-site interactions form the prior energy (Tolpekin and Stein, 2009). Various techniques generally called as Smoothness priors are available to model the prior information, it includes Ising model, Auto and Auto-Logistic model (Mather and Tso, 2010).

4.6. Smoothness Priors

Smoothness is a generic assumption while using priors. It is assumed that the changes in the physical properties of a system are never abrupt. In the case of images, the assumption is that, the DN values do not change abruptly. The smoothness assumption can be represented

mathematically by a prior probability which again can be represented as an energy (Li, 2009). Analytical regularizers are used for representing the prior energy. The general form of the regularizer is given in equation 4.7.

$$\mathrm{U(f)} = \sum_{\mathrm{n=1}}^{\mathrm{N}} \mathrm{U_n(f)} = \sum_{\mathrm{n=1}}^{\mathrm{N}} \lambda_{\mathrm{n}} \int_{n}^{b} g\left(f^{(n)}(x)\right) dx \qquad (Equation\ 4.7)$$

Here $U(f)$ is the prior energy represented using the n^{th} order regularizers, $g\left(f^{(n)}(x)\right)$ is the Potential function which in turn is dependent on the irregularity in $f^{(n-1)}(x)$, N is the highest order considered and λ_n is the weighting factor and is always greater than or equal to 0. In case of smoothness prior standard regularizers are used and as it is just a quadratic function as we can see in equation 4.8.

$$g\left(f^{(n)}(x)\right) = g(\eta) = \eta^2 \qquad (Equation\ 4.8)$$

From equation 4.8 it is implied that the value of $g(x)$ will increase as the irregularities in $f^{(n-1)}(x)$ increases and this in turn triggers more smoothening. In other words one can say that, at the discontinuities, the smoothening strength increases drastically thus resulting in the problem of over smoothening. Also the unbiased interaction with the neighbourhood sites is a matter of concern (Li, 1995).

4.7. Discontinuity Adaptive Priors

The problem of over smoothening blurs the boundaries in an image and hence is an issue to be looked into. The smoothening strength is controlled by the Adaptive Potential Function (APF) placed within the regularizers and hence four different APF was used in this study. The derivative of APF is expressed as shown in equation 4.9.

$$g'(\eta) = 2\,\eta\,h(\eta) \qquad (Equation\ 4.9)$$

Where $h(\eta)$ is called as Adaptive Interaction Function (AIF). This is the function which actually controls the nature of interaction of a site with its neighbours in the case of discontinuity adaptive priors. The smoothening strength for the regularizers is given by equation 4.10.

$$|g'(f'(x))| = |2\,f'\,h(f'(x))| \qquad (Equation\ 4.10)$$

4.8. Mathematical design of DA priors

"The necessary condition for a regularizer to be discontinuity adaptive is given by equation" 4.11 (Li, 1995)

$$\lim_{\eta\to\infty} |g'(\eta)| = \lim_{\eta\to\infty} |2\,\eta\,h(\eta)| = C \qquad (Equation\ 4.11)$$

Here, $C \in [0, \infty]$ is a constant which determines the smoothening strength at discontinuities. So if the value of C is taken as 0, the smoothening strength would be the lowest and for any value $C > 0$, the smoothening strength increases correspondingly. Again at larger values of η, the interaction decreases and approaches 0, at $\eta = \infty$.

4.9. DA model used

There are four different Adaptive Potential Function (APF) used in this study and hence four different DA models. Each function has a different shape and hence results in a unique kind of interaction between the study site and its neighbours. The APF functions $g(\eta)$, that have been used in the study are shown from equation 4.11 – 4.14 (Li, 2009).

$$g_{1\gamma}(\eta) = -\gamma e^{-\frac{\eta^2}{\gamma}} \qquad (Equation\ 4.11)$$

$$g_{2\gamma}(\eta) = -\frac{\gamma}{1 + \frac{\eta^2}{\gamma}} \qquad (Equation\ 4.12)$$

$$g_{3\gamma}(\eta) = \gamma \ln\left(1 + \frac{\eta^2}{\gamma}\right) \qquad (Equation\ 4.13)$$

$$g_{4\gamma}(\eta) = \gamma|\eta| - \gamma^2 \ln\left(1 + \frac{|\eta|}{\gamma}\right) \qquad (Equation\ 4.14)$$

A plot of the four APF, the corresponding derivative of APF and corresponding AIF can be seen in Figure 4.3. The figure clearly shows the decrease in smoothening strength at the discontinuities (i.e. near $\eta = 0$)

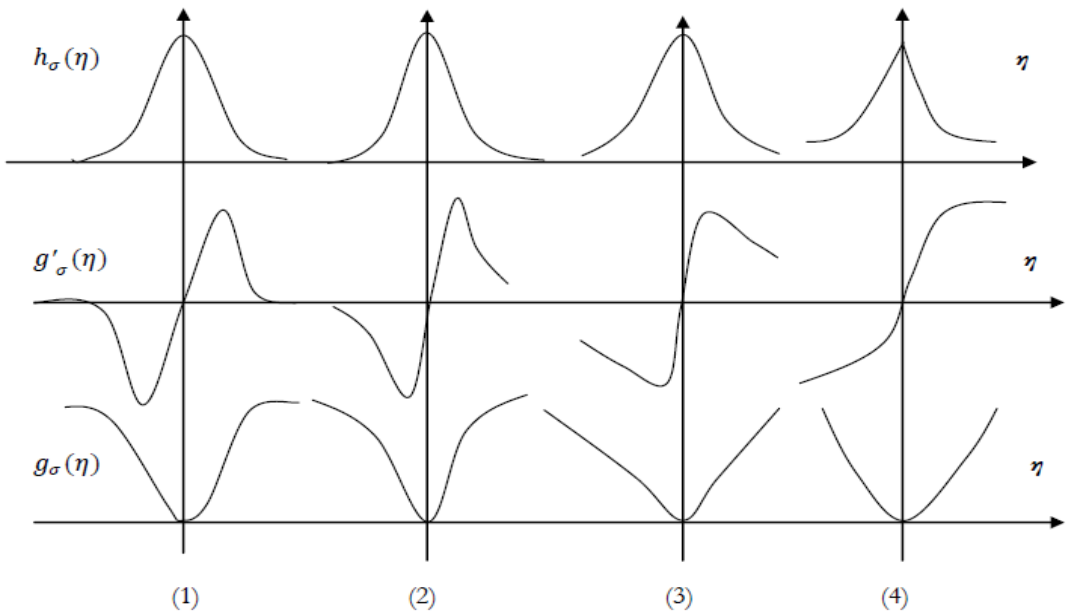

Figure 4-3: Qualitative shape of the four DA function (Li, 1995)

4.10. MAP-MRF Framework

The label configuration which gives the minimum global posterior energy (equation 4.6) will be the most probable configuration for the sites in the image. The Bayesian theorem was used to combine the prior probability with the maximum likelihood to obtain the posterior probability as shown in equation 4.5. The maximization of the posterior probability or the minimization of the posterior energy can be achieved by finding the MAP-MRF estimates, which are nothing but the parameter y (μ in case of fractional images). This is mathematically expressed as shown in equation 4.15.

$$\mathrm{y} = \arg\max\left\{\mathrm{p}\left(\frac{\mathrm{w}}{\mathrm{d}}\right)\right\} = \arg\min\left\{\mathrm{U}\left(\frac{\mathrm{d}}{\mathrm{w}}\right) + \mathrm{U}(\mathrm{w})\right\} \qquad (Equation\ 4.15)$$

5. PROVIDING CONTEXTUAL SUPPORT TO NOISE CLASSIFIER

5.1. Formulating NC-MRF objective function

The main objective of this research is to use spatial contextual information in an image along with its spectral information to obtain better classification accuracy. The objective function of Noise clustering is given by equation 5.1. In this research, the estimation of u_{ij} is conducted by minimizing the product of membership values and distance, for each data point to the cluster centers. In other words, only information from the spectral domain was the deciding factor while estimating the membership values. The objective function of Noise classifier (fuzzy mode) is given in equation 5.1.

$$J_{nc}(U;V) = \sum_{i=1}^{N}\sum_{j=1}^{C}(u_{ij})^m D(\vec{x}_i, \vec{v}_j) + \sum_{i=1}^{N}(u_{i,c+1})^m \delta. \qquad (Equation\ 5.1)$$

For including spatial context of the pixel as yet another factor for estimating the membership values, the objective function of Noise clustering has to be modified as shown in equation 5.2. Here the spatial contextual information was modelled using the smoothness prior and incorporated into the objective function of Noise clustering.

Bayesian theorem was utilized for combining information from the two domains. To solve the problem using MAP-MRF framework, it is required to frame an objective function which incorporates the spectral information and spatial information. The MAP-MRF framework works by maximizing the posterior probability (mentioned in section 4.4). Also, in order to balance the contribution of information from the spectral and spatial domain a new term 'λ' was introduced.

$$U\left(\frac{u_{ij}}{\mathrm{d}}\right) = (1-\lambda)\left[\sum_{i=1}^{N}\sum_{j=1}^{C}(u_{ij})^m D(\vec{x}_i, \vec{v}_j) + \sum_{i=1}^{N}(u_{i,c+1})^m \delta\right] + (\lambda)\left[\sum_{i=1}^{N}\sum_{j=1}^{C}\sum_{j\in N_j}\beta(u_{ij}-u_{ij})^2\right]$$

(Equation 5.2)

In equation 5.2, $\mathrm{U}\left(\frac{\mathrm{u_{ij}}}{\mathrm{d}}\right)$ represents the posterior probability, β is the weight factor associated with a pixel's neighbours and $\mathrm{N_j}$ represents the neighbourhood window around pixel i. For reasons mentioned in section 4.7 the spatial contextual information modelling has also be conducted using discontinuity adaptive (DA) prior. The objective function of NC combined with discontinuity adaptive (DA) prior is shown in equation 5.3 to 5.6. There are four discontinuity adaptive priors introduced by Li, 2009 and which taken up for study here. Each equation now represents the objective function of a new hybrid classifier. The four hybrid

classifier formed will be referred from now on in this thesis as NC DA1-MRF, NC DA2-MRF, NC DA3-MRF and NC DA4-MRF classifiers respectively.

$$U\left(\frac{u_{ij}}{\mathrm{d}}\right) = (1-\lambda)\left[\sum_{i=1}^{N}\sum_{j=1}^{C}(u_{ij})^{m}\, D(\vec{x}_i, \vec{v}_j) + \sum_{i=1}^{N}\left(u_{i,c+1}\right)^{m}\delta\right] + (\lambda)\left[\sum_{i=1}^{N}\sum_{j=1}^{C}\sum_{j\in N_j}\left(-\gamma e^{-\frac{\eta^2}{\gamma}}\right)\right]$$

(Equation 5.3)

$$U\left(\frac{u_{ij}}{\mathrm{d}}\right) = (1-\lambda)\left[\sum_{i=1}^{N}\sum_{j=1}^{C}(u_{ij})^{m}\, D(\vec{x}_i, \vec{v}_j) + \sum_{i=1}^{N}\left(u_{i,c+1}\right)^{m}\delta\right] + (\lambda)\left[\sum_{i=1}^{N}\sum_{j=1}^{C}\sum_{j\in N_j}\left(\frac{-\gamma}{1+\frac{\eta^2}{\gamma}}\right)\right]$$

(Equation 5.4)

$$U\left(\frac{u_{ij}}{\mathrm{d}}\right) = (1-\lambda)\left[\sum_{i=1}^{N}\sum_{j=1}^{C}(u_{ij})^{m}\, D(\vec{x}_i, \vec{v}_j) + \sum_{i=1}^{N}\left(u_{i,c+1}\right)^{m}\delta\right] + (\lambda)\left[\sum_{i=1}^{N}\sum_{j=1}^{C}\sum_{j\in N_j}\left(\gamma \ln\left(1+\frac{\eta^2}{\gamma}\right)\right)\right]$$

(Equation 5.5)

$$U\left(\frac{u_{ij}}{\mathrm{d}}\right) = (1-\lambda)\left[\sum_{i=1}^{N}\sum_{j=1}^{C}(u_{ij})^{m}\, D(\vec{x}_i, \vec{v}_j) + \sum_{i=1}^{N}\left(u_{i,c+1}\right)^{m}\delta\right] + (\lambda)\left[\sum_{i=1}^{N}\sum_{j=1}^{C}\sum_{j\in N_j}\left(\gamma|\eta| - \gamma^2 \ln\left(1+\frac{\eta^2}{\gamma}\right)\right)\right]$$

(Equation 5.6)

In equation 5.3 – 5.6, $\mathrm{U}\left(\frac{\mathrm{u_{ij}}}{\mathrm{d}}\right)$ represents the posterior probability, βis the weight for neighbors and $\mathrm{N_j}$ represents the neighbourhood window around pixel i, γ is a positive constant.

5.2. Simulated Anneling

This hybrid classification technique considered here aims at estimating the membership values (or parameters) for each pixel and for each class. The optimal membership values in our case would be those which minimize the posterior energy as represented by equations 5.2 - 5.6 which are the objective functions for the NC S-MRF and four NC DA-MRF classifiers respectively. Various optimization techniques are available to solve an optimization problem. Some of the commonly used ones are Iterated Conditional Modes (ICM), Simulated Annealing (SA) and Maximizer of Posterior Marginals (Mather and Tso, 2010). In this research, Simulated Annealing was chosen for the MAP-MRF estimation. This was chosen by considering its ability to reach the global minimum/maximum with minimum computation time.

Simulated Annealing algorithm emulates the steel annealing process where, steel is heated to a high temperature close to its melting point and cooled down gradually to room temperature. The steel so formed would be very hard due to its minimal energy configuration (Bertsimas and Tsitsiklis, 1993). When SA is applied in case of an image, the 'Temperature' controls the number of random pixel label changes throughout the image. This iterative algorithm will finally bring the fractional image to the minimal energy state. The SA algorithm has the following steps (Mather and Tso, 2010).

1) Choose a neighbourhood system, the initial temperature (T_0), the temperature decrement rate (k) and maximum number of iterations (N). The fuzzification factor (m) and Noise distance (δ) need to be estimated as a pre-requisite.
2) The membership values from the Noise classifier results should be set as the initial state of the image to enable the SA to reach the optimal value quickly.
3) Update the temperature value using the equation $T_1 = kT_0$ where T_1 is the updated temperature (Li, 2009).
4) Calculate the new membership values for all classes using Gibbs sampler.
5) Calculate the initial posterior energy $U(x/d)$ and the posterior energy obtained after label adjustments $U'(x/d)$
6) Find $\Delta = U(x/d) - U'(x/d)$ for each cite and if is either found to be greater than 0 or $exp(\Delta) \geq random[0,1]$, then replace the previous membership value at the site with the new membership value.
7) Repeat steps 4 and 5 for N times.
8) For the $(N+1)^{th}$ iteration update the temperature as mentioned in step 3.
9) Repeat steps 4 to 7 until the frozen state is reached.

5.3. Parameters to be estimated

The objective function of all NC S-MRF and NC DA-MRF classifiers involves certain parameters which need to be initialized before the optimization of the membership values is conducted. The different parameters to be estimated includes,

1) Fuzzification factor (m)
2) Noise distance (δ)
3) Lambda (λ)
4) Beeta/gamma (β/γ)
5) Initial temperature (T_0) and Temperature Update Rate (k)

All these parameters are dependent on the input images and have to be estimated. But there is no standard technique to estimate these parameters (Li, 2009). The fuzzification factor and noise distance are parameters of Noise clustering and is estimated first through a combination of DN value change method and entropy method. The values of Lambda and Beeta/Gamma for NC S-MRF and NC DA-MRF correspondingly are estimated by considering the edge preservation measured using the mean-variance method. Even though there is no standard method for finding the initial value of temperature (T_0), entropy method can be used to estimate the same (Chawla, 2010, Singha, 2013). The normally used initial temperature in case of image analysis was found to be 3 or 4 (Geman and Geman, 1984, Li, 2009, Dutta, 2009, Chawla, 2010). In Temperature Update technique used in Simulated Annealing algorithm is that which was introduced by Kirkpatrick et. al. in 1983. The optimal value of k is found to be between 0.85 and 0.99 (Li, 2009).

5.4. Accuracy Assessment

The assessment of the quality of information derived from a classification process is referred to as accuracy assessment (Okeke and Karnieli, 2006). Accuracy assessment of conventional hard allocation process was conducted primarily using the Kappa accuracy derived from the confusion matrix. And the confusion matrix can be created when knowledge of the actual class on the ground for a point in the classified image is known. For soft classification accuracy assessment it would be impossible to find a class within a pixel, as multiple classes might be assigned to the same pixel and hence the normal error matrix cannot be realized (Silván-Cárdenas and Wang, 2008). Many suggestions have been made to do soft image accuracy assessment (Binaghi et al., 1999, Congalton, 1991, Green and Congalton, 2004, Pontius Jr and Cheuk, 2006). The section further describes few of the soft classification techniques.

5.4.1. Fuzzy Error Matrix (FERM)

While accuracy of hard classification results can be calculated using error matrix, a slightly different technique is required for deriving the accuracy for soft classified results (Zhang and Foody, 1998). Among the various methods suggested, Fuzzy Error Matrix was found as one of the most appealing approaches developed to do the accuracy assessment of soft classified results. It has much similarity to tradition error matrix, but the difference is that, it takes fractional images as input. Hence the cell values also will be real values between 0 and 1. This is based on MIN operator (Intersection operator) which shows the maximum possible overlap between reference and classified dataset as shown in equation 5.7 (Silván-Cárdenas and Wang, 2008).

$$P_{n_{ij}} = MIN\left(S_{n_k}, r_{n_k}\right) \qquad (Equation\ 5.7)$$

Where S_{n_k} represents membership value of class k with pixel n in the assessed dataset and r_{n_l} represents membership value of class k with pixel n in the reference dataset.

5.4.2. Sub-pixel Confusion Uncertainty Matrix (SCM)

Comparing just the membership values to access the fractional image accuracy may not be the best method, as it does not take care of the actual spatial extend of a class within a pixel and hence is incapable of analytically determining the actual confusion. This problem is referred to as sub-pixel area allocation problem. To overcome this problem the idea of accuracy was defined in terms of sub-pixel overlap among the reference and assessed pixels rather than a mere comparison of membership values (Silván-Cárdenas and Wang, 2008).

A new error matrix called the sub-pixel confusion uncertainty matrix (SCM) that used confusion interval in the form of center value plus or minus its uncertainty was developed. The intervals were defined by MIN-LEAST and MIN-MIN composite operators which basically provide minimum and maximum possible sub-pixel class-overlap at pixel level. The MIN-MIN operator uses the MIN operator for calculating both the diagonal and off-diagonal elements of the matrix but in case of MIN-LEAST operator the MIN operator calculates the

diagonal elements and the LEAST operator gives the off-diagonal elements of the matrix (Silván-Cárdenas and Wang, 2008).

5.4.3. Root Mean Square Error

The Root Mean Square Error (RMSE) is the square root of sum of squared difference between the membership values from the reference and classified fractional images (Dehghan and Ghassemian, 2006). It is a measure of the closeness of the membership values of classified data to the reference data. A lower value of RMSE shows more similarity of the classified image to the reference image and vice versa. The global or total RMSE is calculated using equation 5.8 (Dehghan and Ghassemian, 2006).

$$\mathrm{RMSE} = \frac{\sqrt{\sum_{i=1}^{C}\sum_{j=1}^{N}\left(u_{ij} - u'_{ij}\right)^2}}{N} \qquad (Equation\ 5.8)$$

In equation 5.8, u_{ij} and u'_{ij} represents the membership values of classified and reference image respectively, N is the total number of pixels in the image and C is the total number of classes. The RMSE per class can be calculated by equation 5.9.

$$\mathrm{RMSE(class\ i)} = \frac{\sqrt{\sum_{j=1}^{N}\left(u_{ij} - u'_{ij}\right)^2}}{N} \qquad (Equation\ 5.9)$$

5.4.4. Entropy – An Uncertainty measure

Methods such a Mean Relative Error (MRE), Root Mean Square Error (RMSE) and Linear Correlation Coefficient (LCC) give the measure of differences between the expected and actual measurement and hence are relative measures. But the entropy value is an absolute measure of the uncertainty involved in the classified data. Entropy is defined based on only the actual classified data and does not require any reference data for its calculation. Entropy represents the classification uncertainty as a single number per pixel per class (Dehghan and Ghassemian, 2006). From the class membership values entropy can be calculated using equation 5.10.

$$H(x_j) = \sum_{i=1}^{c} u_{ij} \log_2(u_{ij}) \qquad (Equation\ 5.10)$$

Here u_{ij} represent the membership values of the i^{th} pixel in the j^{th} class (or fractional image). Higher entropy shows more uncertainty in membership values of the pixel and vice versa. In case of Noise classifier where the membership value of a pixel can have values less than one (i.e. $\sum u_{ij} \leq 1$) and hence the average entropy is given by equation 5.11 (Ricotta and Avena, 2002).

$$H(x_j) = \frac{\sum_{i=1}^{c} u_{ij} \log_2(u_{ij})}{\sum_{i=1}^{c} u_{ij}} \qquad (Equation\ 5.11)$$

In this research entropy measure was used in combination with other measures to estimate the optimal value of m and δ.

5.4.5. Mean Variance Method

Mean variance method is mainly used as a means for measuring the fuzziness in the edges. The research deals with studying the effect of different discontinuity adaptive MRF models on the classification accuracy. Discontinuity adaptive MRF models helps in preserving the edges and mean variance method is the best way to measure the same.

In an image, edges are formed due to gradual or sudden change in DN values, and can be represented using a step function or a slope plot respectively. The significance of an edge can be found by taking the mean of pixel values from either side of the edge and calculating the difference which turns out to be the slope. As per Wen and Xia an edge point is retained if it satisfies the following condition.

$$|X_i - Y_i| > c + \sqrt{2}SZ_a \qquad (Equation\ 5.12)$$

Where X_i and $Y_i$represent the DN values of pixels on either side of the edge point, S is the standard deviation of DN values of the region and Z_a is the standardized sample mean and c is a constant threshold.

In this research the hybrid fuzzy classifier produces fractional images for each class under consideration. And for each parameter mentioned in section 5.3 the set of fractional images generated will be slightly different. A fractional image will have high values for the regions where a particular class is present and for all other areas the membership value will be small. Prospective fractional images would be those with minimal variability on either side of the boundaries and maximum membership value change across the boundary.

6. STUDY AREA AND DATA PREPARATION

The chapter describes in detail about the considered study area and the dataset that had been used for this research. The various image pre-processing operations that were conducted as part data preparation is also explained. In this research accuracy assessment was conducted using soft reference datasets. The chapter also explains about the methods that have been used to derive the same.

6.1. Study Area

Selection of study area is an important requirement for most earth science related studies. For this research, the study area selected was Sitarganj's Tehsil, Udham Singh Nagar District, Uttarakhand State, India (Chawla, 2010). The bounds of the considered area is 28^0 52' 29"N to 28^0 54' 20" N and 79^0 34' 25" E 79^0 36' 34"E (Chawla, 2010). Based on ground data as well as satellite imageries, Sitarganj's Tehsil was identified to have six classes which includes, sal forest, eucalyptus plantations, both wet and dry, agricultural land without crop and two water reservoirs – Baigul and Dhora reservoirs. The reasons for selecting the study area include the following.

1. The current research aims at testing the capability of a novel classifier; and Sitarganj's Tehsil has a large diversity of distinguishable classes.
2. Data from the LISS-III, LISS-IV and AWiFS sensors aquired on the same date from Resourcesat-1 and 2 separately, are available for the area.
3. The area have both fuzzy and crisp boundaries and hence would help in studying the effect of DA-MRF models on boundaries for both cases.

The Figure 6.1 shows the geographic location of the study area and the various classes identified within. Field visits were also conducted during 2009 November to identify and validate the six classes identified from remotely sensed data (LISS-III and LISS-IV both Resourcesat-1 and Resourcesat-2).

6.2. Datasets used

The datasets used here are obtained from LISS-III (Linear Imaging Self Scanner-III), LISS-IV (Linear Imaging Self Scanner-IV) and AWIFS (Advanced Wide Field Sensor) which are sensors onboard both Resourcesat-1 also known as IRS-P6 (Indian Remote Sensing Satellite) and Resourcesat-2. LISS-III, LISS-IV and AWiFS datasets were acquired at the same time. Sensors onboard Resourcesat-2 has a slightly higher radiometric accuracy and is considered in this research to study the effect of this novel fuzzy hybrid classifier accuracy on radiometric accuracy of the input dataset. Soft classification results from finer resolution LISS-IV image have been used for validation of the soft classification results obtained for both AWIFS and LISS-III datasets. The dataset available from Resourcesat-1 is dated 15th October 2007 and the one from Resourcesat-2 is dated 23rd November 2011 (Chawla, 2010). The Table 6.1 shows the features of referred sensors onboard Resourcesat-1 and Resourcesat-2.

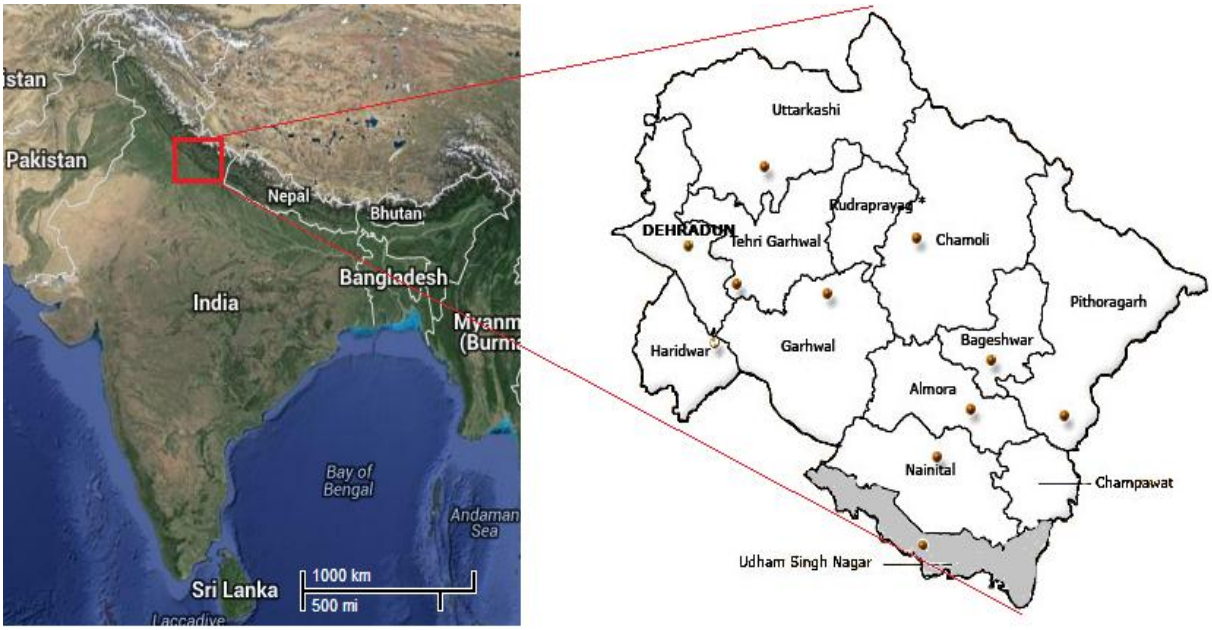

(A) Geographic location of study area

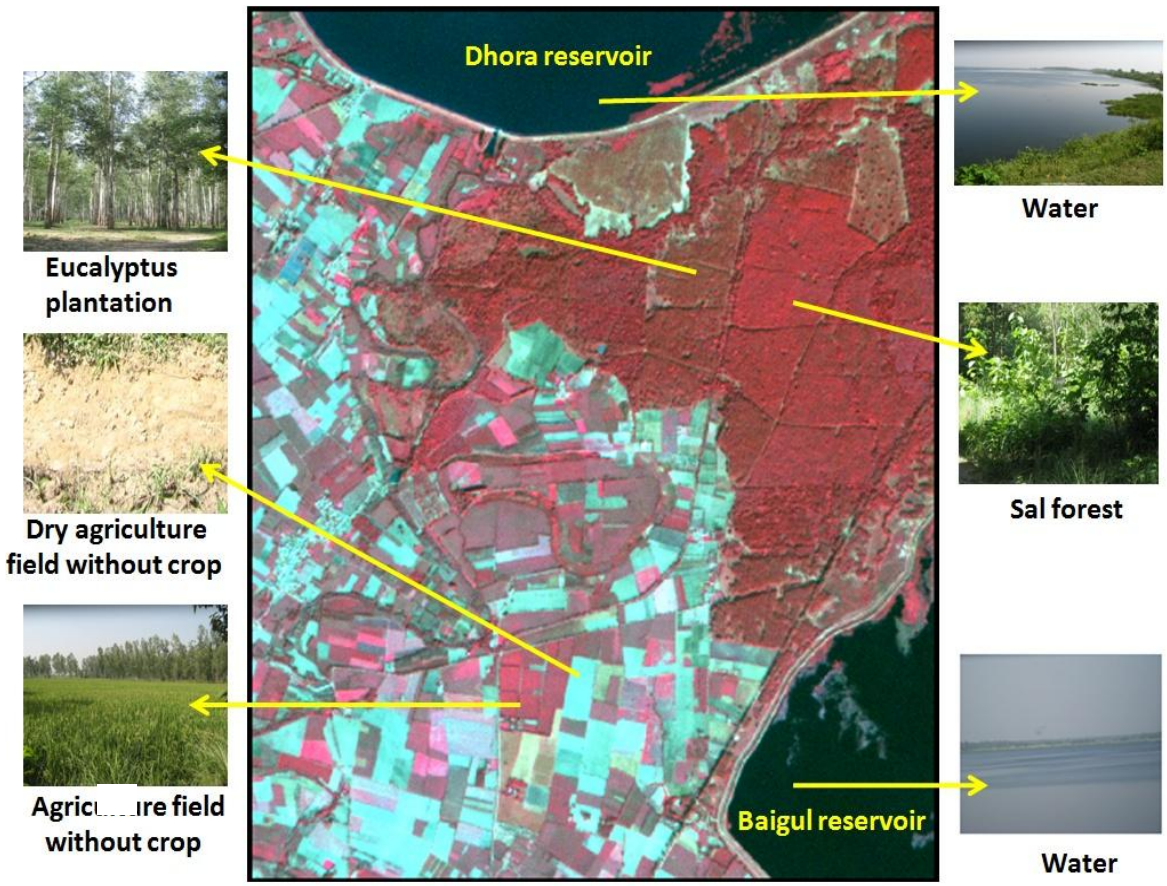

(B) LISS-IV (Resourcesat 2) image of Sitarganj's Tehsil with various identified classes

Figure 6-1: Study Area

Specification	AWIFS		LISS-III		LISS-IV	
	Resourcesat-1	Resourcesat-2	Resourcesat-1	Resourcesat-2	Resourcesat-1	Resourcesat-2
Spatial Resolution(m)	56	56	23.5	23.5	5.8	5.8
Spectral Resolution	0.52 - 0.59 0.62 - 0.68 0.77 - 0.86 1.55 – 1.70	0.52 - 0.59 0.62 - 0.68 0.77 - 0.86 1.55 – 1.70	0.52 - 0.59 0.62 - 0.68 0.77 - 0.86 1.55 - 1.70	0.52 - 0.59 0.62 - 0.68 0.77 - 0.86 1.55 - 1.70	0.52 - 0.59 0.62 - 0.68 0.77 - 0.86	0.52 - 0.59 0.62 - 0.68 0.77 - 0.86
Swath (km)	740	740	141	141	23.9 (Max Mode) 70.3 (Pan Mode)	70 (Max Mode) 70 (Mono Mode)
Radiometric Resolution	10	12	7	10	7	10

Table 6-1: Resourcesat-1 and Resourcesat-2 sensors specification

6.3. Data Preparation

Geo-registration is a highly important pre-processing step for remote sensing image analysis. But for geo-registration it is mandatory to have a geometrically corrected reference data set against which the corrections have to be made. In this research, high resolution LISS-IV dataset was rectified using Survey of India (SOI) toposheet numbered, 53 P/9. The Survey of India toposheet was scanned and georeferenced before it could be used for rectification of LISS-IV dataset. The LISS-IV image was geo-registered in UTM projection, Zone 44N. The vertical datum used was Everest. Further, the Georegistartion of LISS-III and LISS-IV was conducted using the geometrically corrected LISS-IV image with same specification of datum spheroid and projection as mentioned before. Also the AWIFS, LISS-III and LISS-IV have been resampled to resolutions 5m, 20 m and 60 m which achieves the ratio 1:4:12 to favour the accuracy assessment process. The resampling method used in this case is *Nearest Neighbour Resampling*, considering its ability to give fast results and also that it creates only geometric discontinuities in the order of half a pixel (Chawla, 2010).

6.4. Reference dataset generation

In this research, the reference images have been derived from high resolution LISS-IV image due to unsuitability of ground data. The possibility of acquiring aerial photographs was ruled out considering its expense and the government regulations. It has not been possible to acquire ground data for the following reasons.

1. It is not possible to pin point classes within a pixel on the ground neither is it possible to accurately quantify the spread of class within a pixel.
2. The ground data might contain errors; hence conventional accuracy assessment may be described as a degree of agreement and not true reflection of reality (Foody, 2002).

3. Some regions in the area were inaccessible and hence obtaining ground data was not realistic.

In outputs of NC S-MRF and NC DA-MRF classifiers are fractional images and there is a fractional image generated for each class under consideration. For accuracy assessment of these soft classification results, fractional images generated by the same classifiers for high resolution LISS-IV dataset have been used. But the resolutions of the so generated test and reference datasets are not the same and in this case and hence accuracy assessment was not directly possible. *Multiple resolution technique* was used in this research to address this issue. In this method, the pixels of high resolution LISS-IV image were aggregated to form a coarser resolution pixel (Chawla, 2010). The AWIFS, LISS-III and LISS-IV datasets were resampled suitably such that the cell resolutions were in the ratio 1:4:12 and hence 16 pixels (4 x 4) of LISS-III and 144 pixels (12 x 12) of AWIFS have to be combined to reach the pixel dimension of LISS-IV. The image so obtained from aggregating the LISS-IV pixels is then classified and was used for accuracy assessment of AWIFS and LISS-III classification results. FERM technique was used in this research for accuracy assessment. The accuracy degradation of datasets that happens on resampling and the usage of aggregated mean of pixels from the reference pixel while doing accuracy assessment were sources of error and hence was a disadvantage for this method (Chawla, 2010).

7. RESULTS AND DISCUSSION

7.1. Base Classifier Parameter Estimation

The base classifier used in this study was the Noise Classifier and it was necessary to estimate its optimal parameters to ensure best performance. The Noise classifier parameters that needed to be estimated were the fuzzification factor (m) and noise distance (δ). Since the classification approach used was fuzzy, the output of the classifier was fractional images. Fractional image is a pictorial representation of the membership values assigned for a class within each pixel. Also for each class under consideration a separate fractional image would be generated. In this research, a combination of uncertainty (entropy) and 'membership values change' methods were used to find the optimal values of 'm' and 'δ'. The two methods are explained in sections 7.1.1 and 7.12.

7.1.1. Uncertainty calculation

Each fractional image highlights regions of a particular class due to high membership values and other regions will be relatively dark due to low membership values. For each fractional image, random pixels were selected from the bright regions class of interest of the fraction is selected from inside its bright region for calculating the entropy of the class. In this research, instead of picking random pixels from the bright region, a small square region was selected from within the bright region of the fractional image, and then the entropy was calculated over the membership vector for each pixel inside the square region and then its mean was determined. The membership vector was generated by compiling membership values form all the fractional images over a same pixel. The equation for calculating the average entropy at a single pixel is given by equation 7.1.

$$H_{avg} = \frac{\sum_{i=1}^{C} -u_{ij}\, log_2(u_{ij})}{\sum_{i=1}^{C} u_{ij}} \qquad (Equation\ 7.1)$$

Here C is the number of classes, u_{ij} is the membership value for i^{th} row and j^{th} column in the fractional image. In the case of Noise classifier, the sum of membership values for all the classes for a particular pixel always sums up to 1 and hence denominator of equation 7.1 becomes 1. For example, if the interest is on calculating the entropy of water class (i.e. fractional image 0), a small square region in the water class would be selected as shown in the Figure 7.1. A pixel showing high membership values in the fractional image corresponding to water class is expected to show low membership values for same locations in the other fractional images. Let us now take a case where we have 3 classes. Let us assume that we are interested in calculating the entropy involved in the classification of class 0 and assume the following possible cases,

Case 1: If membership values of class 0 = 0.8, class 1= 0.1 and class 3 = 0.1. The entropy at the pixel is calculated as ((-0.8 * $\log_2(0.8)$) + (-0.1 * $\log_2(0.1)$) + (-0.1 * $\log_2(0.1)$)) = 0.9219.

Case 2: If membership values of class 0 = 0.6, class 1= 0.2 and class 3 = 0.2. The entropy at the pixel is calculated as $((-0.6 * \log_2(0.6)) + (-0.2 * \log_2(0.2)) + (-0.2 * \log_2(0.2))) = 1.3710$.

Clearly the numbers shows that, the uncertainty is more in case 2 when compared to case 1. In this research work, fractional outputs (from class 0 to class 5) was generated for all combination of 'δ' (0.1, 0.2…1) and 'm' (1.1, 1.2…10). Then for each fractional image, the mean entropy is calculated for pixels within the selected region. It can also be seen that, whenever there is a large difference in membership values within the membership vector, i.e. between the interested class and the other class for the same pixel, the entropy will be less and low entropy in the classification result is good thing to have. The combination of 'δ' and 'm' which gives the minimal entropy is considered the best. But the 'δ' and 'm' combination might be different for every class (i.e. fractional image) and so, their individual means are calculated and found as the optimal value for a particular set of inputs.

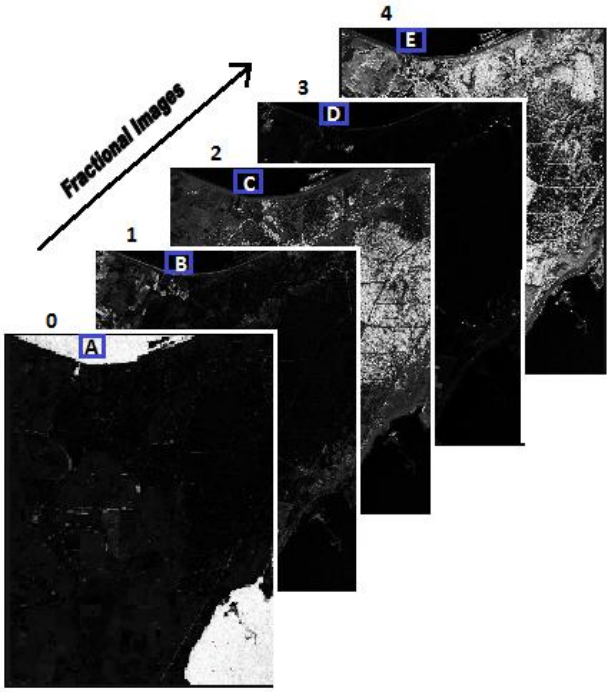

Figure 7-1: Fractional Images generated for LISS-III dataset from Resourcesat-1 (δ: 10000 and m: 3.0)

7.1.2. Membership Value Change calculation

Considering just the entropy as a criterion for optimal parameter estimation is not enough, as the minimum entropy may belong to a 'm – δ' combinations which gives bad/inaccurate classification. This is why the second method was considered. Here the stress is given to, finding the best combination of 'm' and 'δ' for which the difference between the membership value in the interested class locations and average of membership values in other class locations is a maximum. The method is explained in an algorithmic fashion with an example in this section. In this example it is assumed that the number of classes is 5 ('1', '2', '3', '4' and '5'), no. of soft classification outputs is also 5, where each output will have high membership values in the region (i.e. pixels) where the class is probably present and low membership values in other regions.

Algorithm:

1. Consider the soft classification output layers (i.e. fractional images) one at a time. To start with consider fractional image corresponding to class 1.
2. Consider a fixed number of random pixels in the area of the class of interest (Figure 7.2, pixels inside square box within class 1).
3. Similarly select random pixels from regions of all other classes (class 2, 3, 4 and 5) as shown in Figure 7.2.
4. Calculate the mean of the selected random pixel from within the class of interest (e.g. class 1). It is highly probable that, the mean value would be large.
5. Consider the random pixels of all the other classes and calculate the mean i.e. mean of random pixel from class 2, 3, 4 and 5 put together.
6. Calculate the difference between the mean of random pixels of class 1 and the mean calculated in step 5.
7. Do steps 1 – 6, for other classes also. I.e. For class 2, 3, 4 and 5.

This difference for each class have to calculated for each set of fractional images generated from all combinations of 'm' and 'δ'

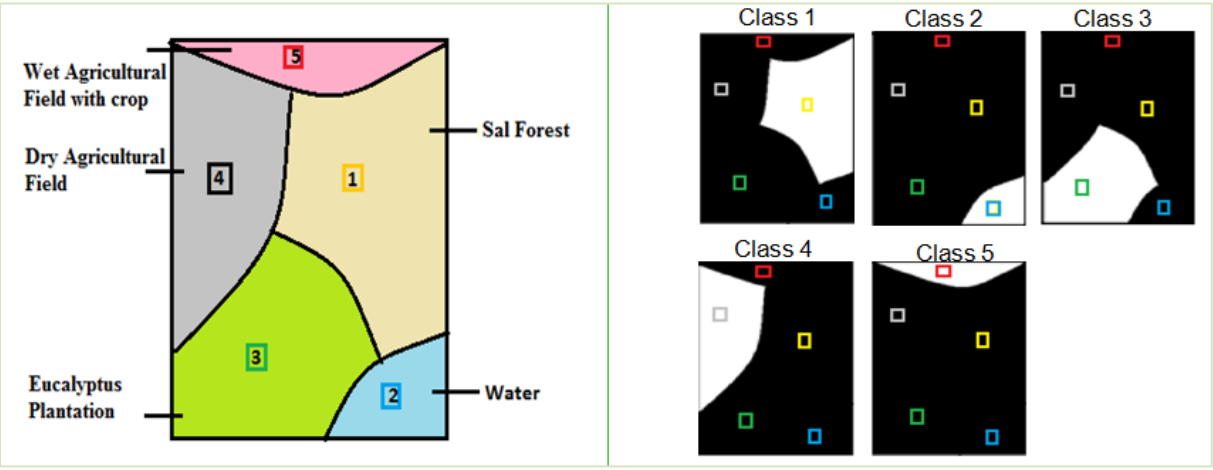

Figure 7-2: Sample locations selected for each class.

The objective of both methods was to estimate the optimal parameters 'm' and 'δ'. For δ beyond 10000, both of the entropy and membership value difference values seemed to saturate and so δ was kept constant at 10000 (See 3D Figure A.5 - A.10 provided in appendix A). On analysing the uncertainty graph drawn against constant δ, it was found that an optimal 'm' cannot be obtained using the method individually. Similarly a graph of membership value change against fuzzification factor was plotted with a constant δ. But it showed a continuous decreasing trend and hence couldn't provide any reliable estimate of 'm'. This was the case with all the six datasets from AWIFS, LISS-III, and LISS-IV from both Resourcesat-1 and Resourcesat-2. The Uncertainty and Membership Value Change graphs generated for AWIFS datasets from Resourcesat-1 and Resourcesat-2 are shows in Figure 7.3 and 7.4 respectively. The Uncertainty and Membership Value Change graphs generated for LISS-III and LISS-IV datasets are shown in Appendix A.

Since it was not possible to estimate the 'm' using the Uncertainty and Membership Value Change methods independently, a combination of both the methods was used to estimate the 'm' values. The graphs generated from both the methods were normalized (for each class) and plotted within common axis. The intersection point of the two plots (shown in Figure 7.3 and 7.4) was considered to corresponded to the optimal value of 'm'. Finally the 'm' of all the classes were averaged to obtain the optimal 'm' value for a particular dataset.

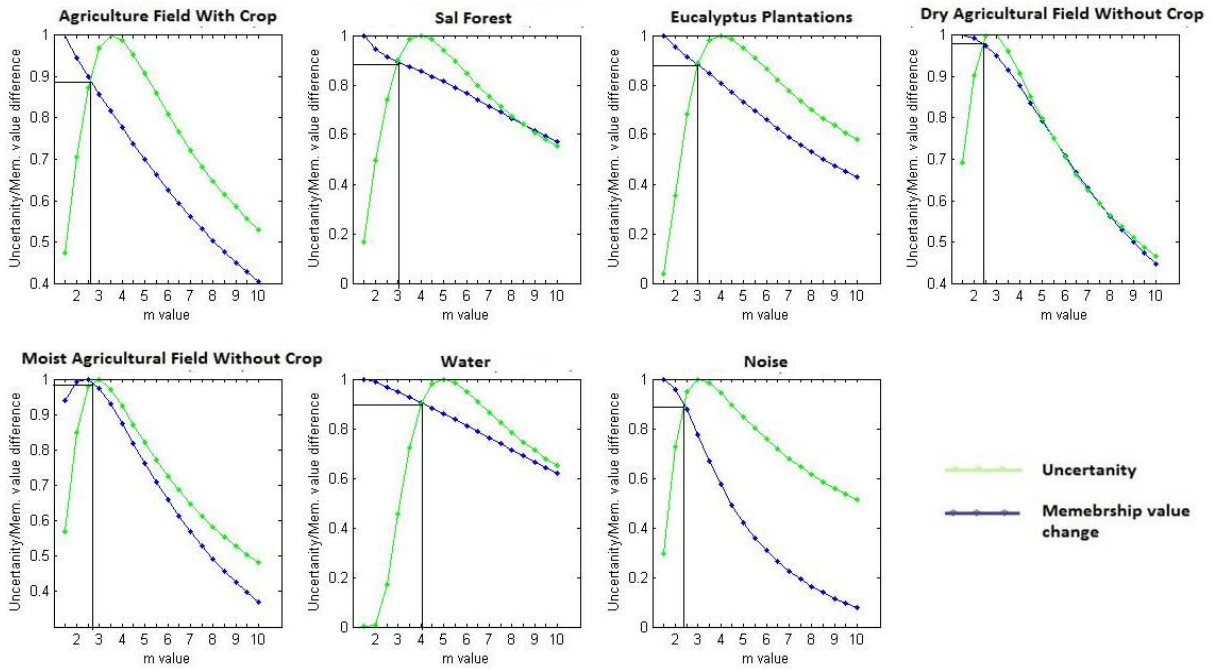

Figure 7-3: Estimated fuzzification factor (m) for AWIFS (from Resourcesat-1)

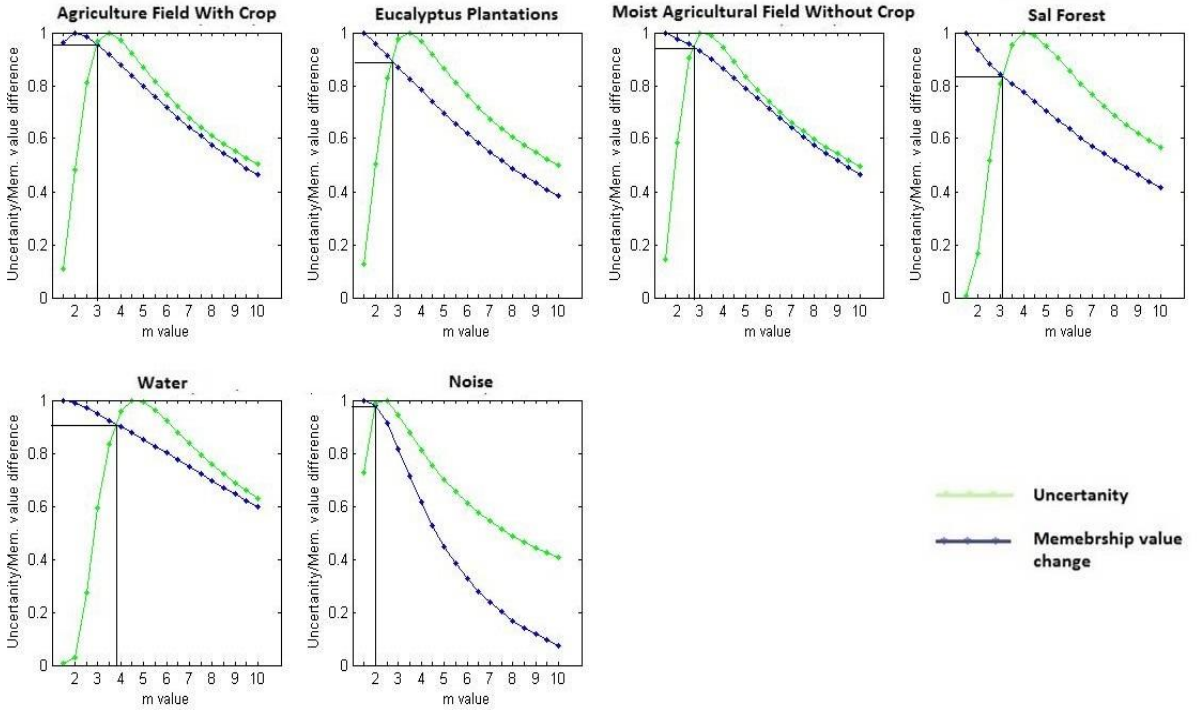

Figure 7-4: Estimated fuzzification factor (m) for AWIFS (from Resourcesat-2)

Table 7-1: Estimated 'm' values for Resourcesat-1 and Resourcesat-2

Dataset (Imagery)	fuzzification factor (m)	
	Resourcesat-1	Resourcesat-2
AWIFS	2.714	2.796
LISS-III	2.928	3.010
LISS-IV	3.064	3.225

Table 7.1 shows the estimated 'm' values for AWIFS, LISS-III and LISS-IV datasets from both Resourcesat-1 and Resourcesat-2. On inspecting the estimated fuzzification factors for AWIFS (coarser resolution), LISS-III (medium resolution) and LISS-IV (fine resolution) datasets, one can see that, an increase in spatial resolution of the image cause an increase trend in fuzzification factor. This trend was found applicable for both Resourcesat-1 and Resourcesat-2 datasets. A slight increase in the estimate fuzzification factor is also found in Resourcesat-2 datasets as when compared to Resourcesat-1 datasets.

7.2. Hybrid Classifier Parameter Estimation

Hybrid classifier parameter includes the weight factor which controls the spatial and spectral component (λ), neighbourhood weight in the case of in case of S-MRF models (β) and constant involved in the case DA model (γ) for AWIFS, LISS-III and LISS-IV datasets, the Initial temperature (T_0) and Temperature Update Rate (k). In this research the mean and variance method was used to estimate the values of λ, β/γ. The description of mean variance method can be found in section 5.4.5. The optimal parameters will be the one corresponding to the fractional image, which has the maximum mean difference across the boundary and minimum variance on either side of the boundary. Coming to Simulated Annealing parameters, the optimal value of $T_0$was kept at 3 for all experiments as this value gave the minimum entropy in the classification result, the value of k was chosen to be 0.90 as it gave the minimum variance in the estimated parameters on repeating the parameter estimation.

As discussed earlier, the classifier generates fractional images for each class considered for classification i.e. a set of images will be generated. A good classification result will have minimal uncertainty/contradiction i.e. suppose a pixel is given high membership value in a fractional image in the set, then it is expected to show low values in all the remaining fractional images in the set. This can be validated by taking the vertical entropy of the images in the set. To estimate the parameters λ and β/γ, image sets were generated for all combinations of the hybrid classifier parameters. λ was varied from 0 to 1 in intervals of 0.1, β was varied from 1 to 7 in intervals of 1 and γ was also varied from 0 to 1 in intervals of 0.1. The intervals have been selected by considering the extent of variability in the entropy for a small change in parameter value. Figure 7.5 shows the entropy values for all combination of λ and β/γ for LISS-III dataset of Resourcesat-1. In this it can be seen that the entropy is minimum for λ in the range 0.8 to 0.9 and γ in the range from 1 to 0.3. To find the optimal value of λ and β/γ from within the mentioned

range, the mean variance method was used. The entropy graph of classification results for AWIFS, LISS-III and LISS-IV for both Resourcesat-1 and 2 can be found in Figure A.11 – A.13 in Appendix A.

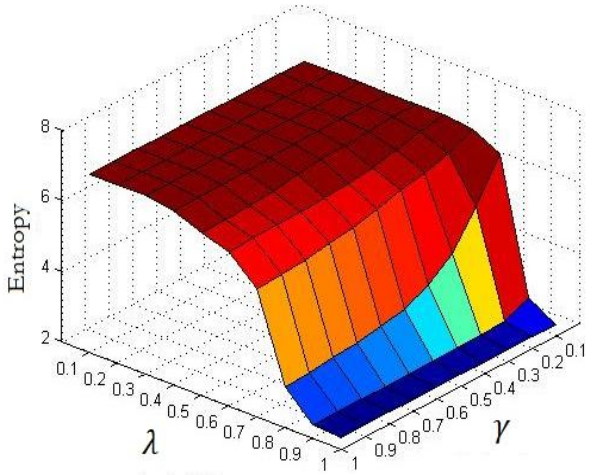

Figure 7-5: Entropy graph for LISS-III (from Resourcesat-1) classification results

A prior produces a smoothening effect on the image, depending on the prior's characteristics and for the same reason parameter estimation has to be separately conducted for each of the priors. Hence the optimal values of λ and β/γ have been estimated for AWIFS (Table 7.2), LISS-III (Table 7.3) and LISS-IV (Table 7.4) for both Resourcesat 1 and 2. The optimal values of λ and β/γ were found using the same method as that was conducted in the case of LISS-III (Resourcesat-1). The estimates are shown in Table 7.2 and it can be clearly seen that, the maximum mean difference across the boundary and the minimal variance on either side of the boundary is observed when MRF-DA4 is used as the prior to NC. Hence from among the different prior used, MRF-DA4 prior was identified to have the maximum edge preservation capability.

Table 7-2: Classifier Estimates for AWIFS Datasets

Model	λ	β/γ	Mean Difference		Variance on side of class A		Variance on side of class B	
			Water class	Eucalyptus class	Water class	Eucalyptus class	Water class	Eucalyptus class
			Resourcesat–1					
S-MRF	0.6	5	230.0	180.5	21.15	223.65	2.04	28.48
DA1-MRF	0.9	0.4	226.9	150.6	200.62	123.78	6.1	16.54
DA2-MRF	0.7	0.8	231.0	188.0	26.90	170.88	3.12	22.44
DA3-MRF	0.7	0.9	230.8	187.1	42.23	107.43	0.98	23.73
DA4-MRF	**0.8**	**0.8**	**233.2**	**189.3**	**13.28**	**84.71**	**2.00**	**60.54**
			Resourcesat–2					
S-MRF	0.6	5	226.3	119.5	88.76	93.77	22.4	47.38
DA1-MRF	0.9	0.4	221.1	132.2	108.10	146.94	35.37	20.01
DA2-MRF	0.7	0.8	216.8	126.0	196.17	86.23	38.26	79.12
DA3-MRF	0.7	0.9	229.9	120.6	30.90	237.87	2.93	114.72
DA4-MRF	**0.8**	**0.8**	**131.0**	**132.7**	**42.32**	**222.05**	**1.87**	**14.17**

Table 7-3: Classifier Estimates for LISS-III Datasets

Model	λ	β/γ	Mean Difference		Variance on side of class A		Variance on side of class B	
			Water class	Dry Agriculture class	Water class	Dry Agriculture class	Water class	Dry Agriculture class
			Resourcesat–1					
S-MRF	0.9	5	179.6	151.6	46.71	194.54	0.66	21.61
DA1-MRF	0.9	0.5	182.4	145.1	66.76	1245.78	133.61	10.40
DA2-MRF	0.8	0.4	190.0	144.7	68.88	108.66	0.23	32.67
DA3-MRF	0.8	0.5	191.2	140.7	102.22	298.32	0.40	58.17
DA4-MRF	**0.9**	**0.7**	**193.4**	**159.4**	**49.28**	**117.83**	**0.17**	**92.10**
			Resourcesat–2					
S-MRF	0.9	5	190.6	115.1	64.71	810.98	27.06	138.62
DA1-MRF	0.9	0.5	190.0	140.0	134.44	2550.54	69.06	560.22
DA2-MRF	0.8	0.4	194.0	113.4	49.56	442.01	8.90	134.40
DA3-MRF	0.8	0.5	196.2	130.0	122.76	461.87	1.65	36.32
DA4-MRF	**0.9**	**0.7**	**197.8**	**148.9**	**148.48**	**1043.06**	**0.62**	**0.45**

The LISS-IV classification result is used as a reference, and for the same reason the λ and β/γ needed to be estimated for generating the best possible reference images for each of the prior that was used. The estimated λ values have been found to be little low as when compared to LISS-III datasets.

Table 7-4: Classifier Estimates for LISS-IV Datasets

Model	λ	β/γ	Mean Difference		Variance on side of class A		Variance on side of class B	
			Water class	Dry Agriculture class	Water class	Dry Agriculture class	Water class	Dry Agriculture class
			Resourcesat–1					
S-MRF	0.6	6	163.0	182.9	128.98	316.10	2.62	1.33
DA1-MRF	0.9	0.4	180.8	174.6	201.60	461.56	5.56	1.43
DA2-MRF	0.7	0.5	177.0	204.5	267.55	245.06	0.44	0.23
DA3-MRF	0.7	0.7	184.2	179.0	456.54	456.44	0.98	0.29
DA4-MRF	**0.8**	**0.5**	**189.0**	**180.3**	**447.15**	**202.45**	**5.15**	**0.44**
			Resourcesat–2					
S-MRF	0.6	6	195.1	196.7	168.48	146.94	49.38	16.17
DA1-MRF	0.9	0.4	192.5	191.5	46.48	61.15	11.21	12.76
DA2-MRF	0.7	0.5	188.5	196.4	186.50	70.04	1.33	1.33
DA3-MRF	0.7	0.7	198.8	188.5	59.43	104.01	2.45	6.84
DA4-MRF	**0.8**	**0.5**	**213.4**	**200.2**	**173.34**	**118.84**	**9.78**	**1.15**

The images from 7.6 – 7.9 shows the fractional images generated for AWIFS and LISS-III for Resourcesat-1 and 2 using the respective parameter estimates i.e. for specific values of λ and β/γ.

The fractional image for LISS-IV generated against the optimal parameters is provided in Appendix A (Figure A.14 and Figure A.15).

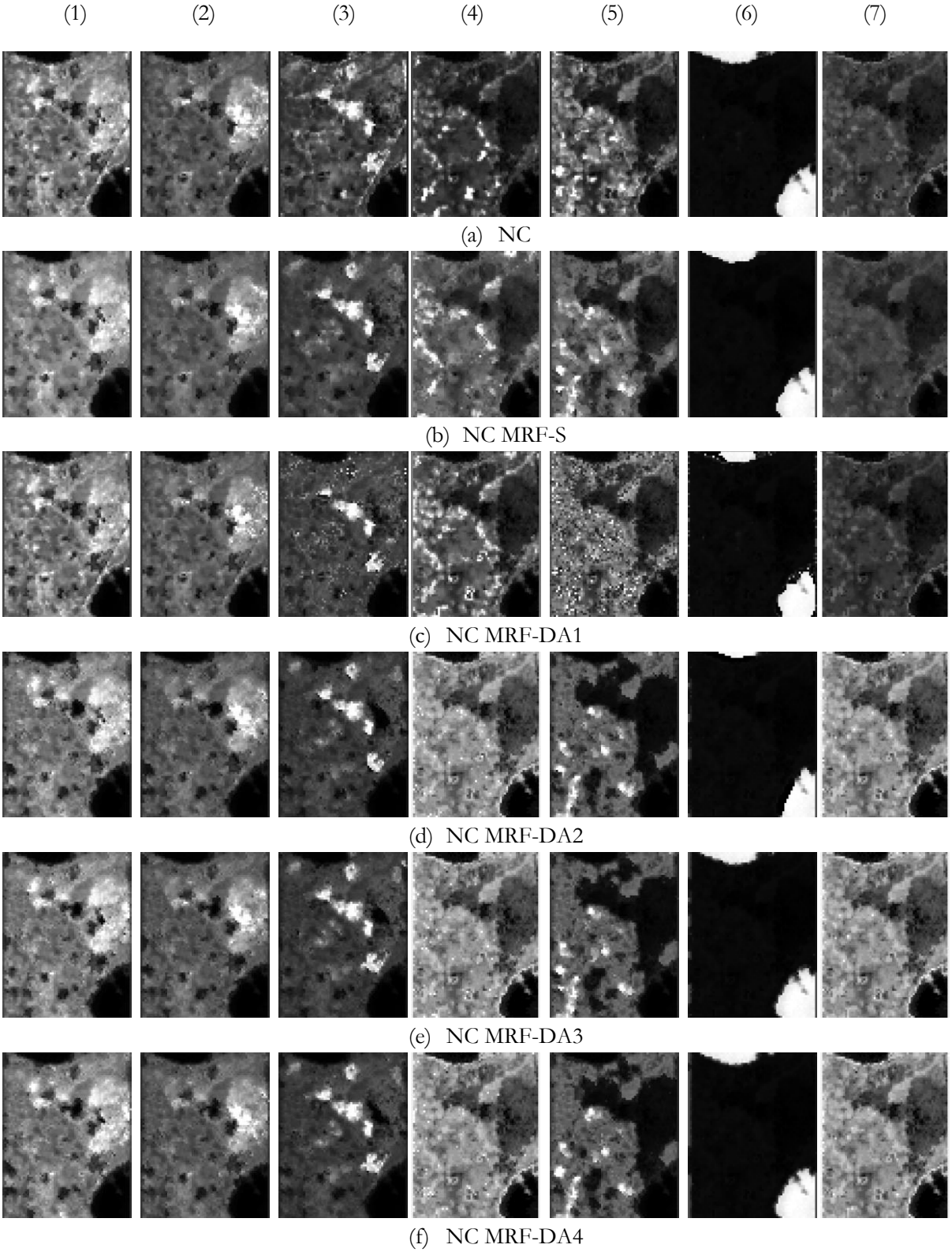

Figure 7-6: Fractional images obtained from NC, NC S-MRF and NC DA-MRF classifiers on AWIFS dataset from Resourcesat-1. The fractional images corresponds to Agriculture fields with crop (1), Sal Forest (2), Eucalyptus plantation (3), Dry agricultural field without crop (4), Moist agricultural field without crop (5), Water (6), Noise (7).

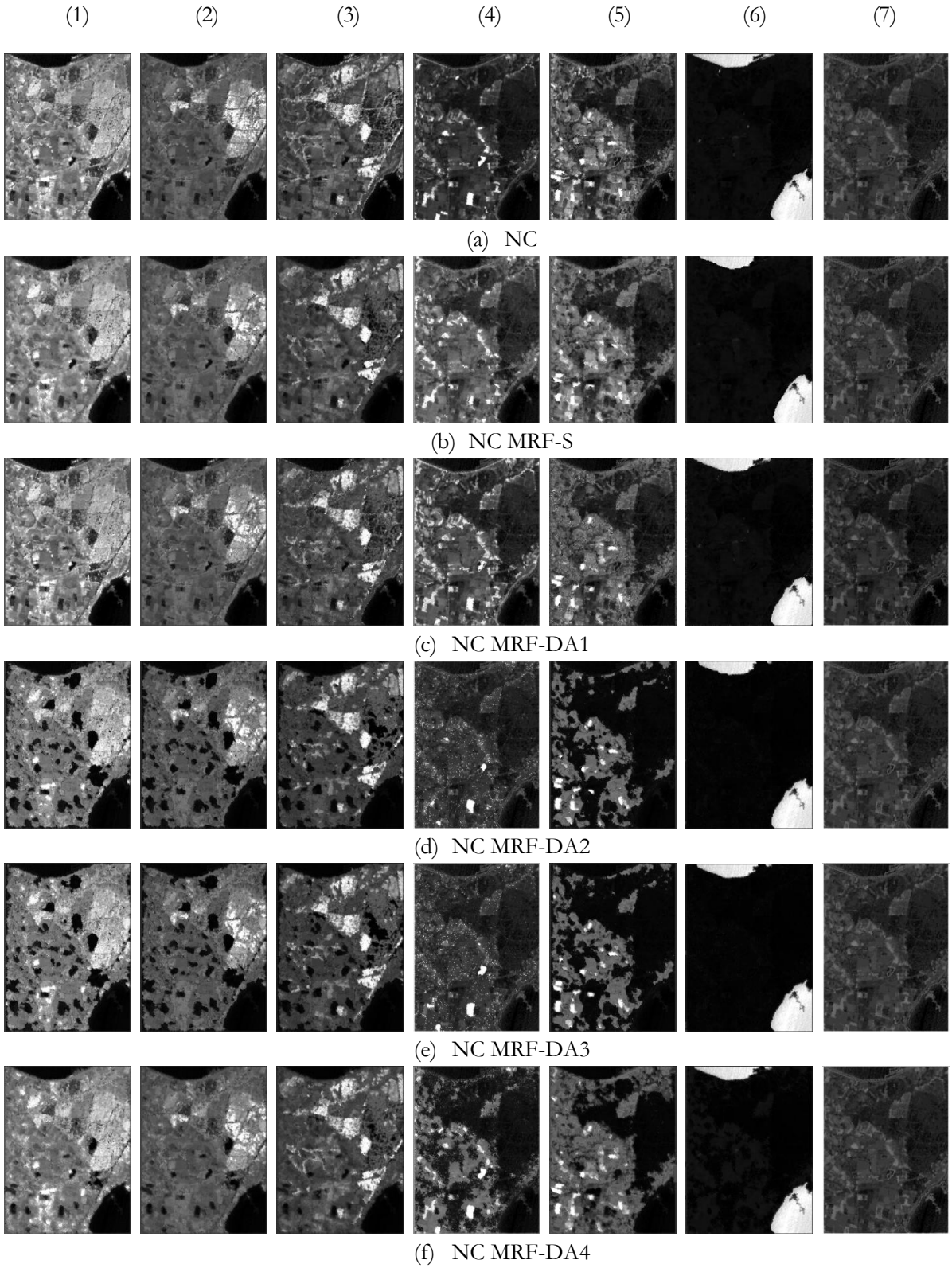

Figure 7-7: Fractional images obtained from NC, NC S-MRF and NC DA-MRF classifiers on LISS-III dataset from Resourcesat-1. The fractional images corresponds to Agriculture fields with crop (1), Sal Forest (2), Eucalyptus plantation (3), Dry agricultural field without crop (4), Moist agricultural field without crop (5), Water (6), Noise (7).

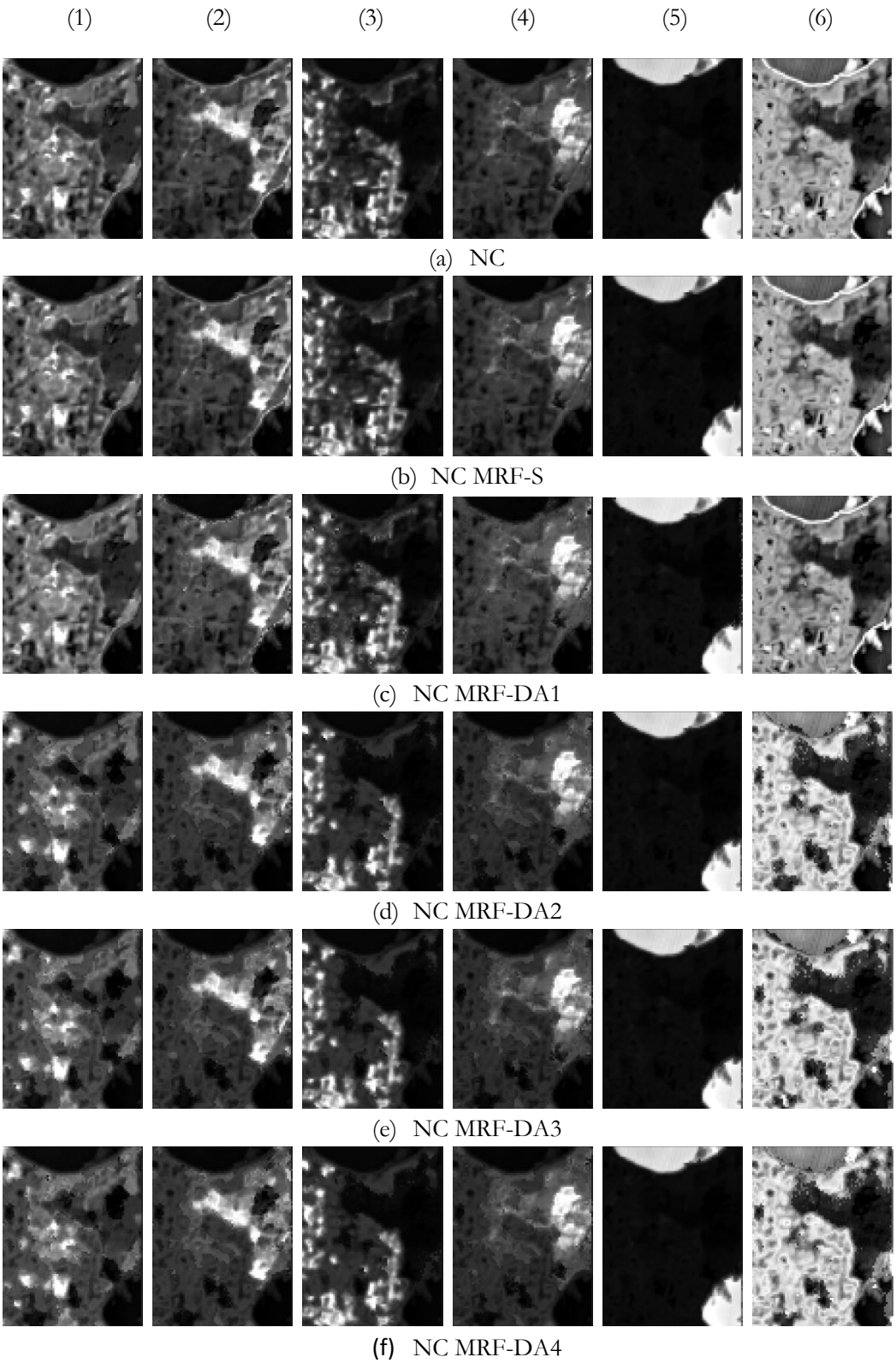

Figure 7-8: Fractional images obtained from NC, NC S-MRF and NC DA-MRF classifiers on AWIFS dataset from Resourcesat-2. The fractional images corresponds to Agriculture fields with crop (1), Sal Forest (2), Eucalyptus plantation (3), Dry agricultural field without crop (4), Moist agricultural field without crop (5), Water (6).

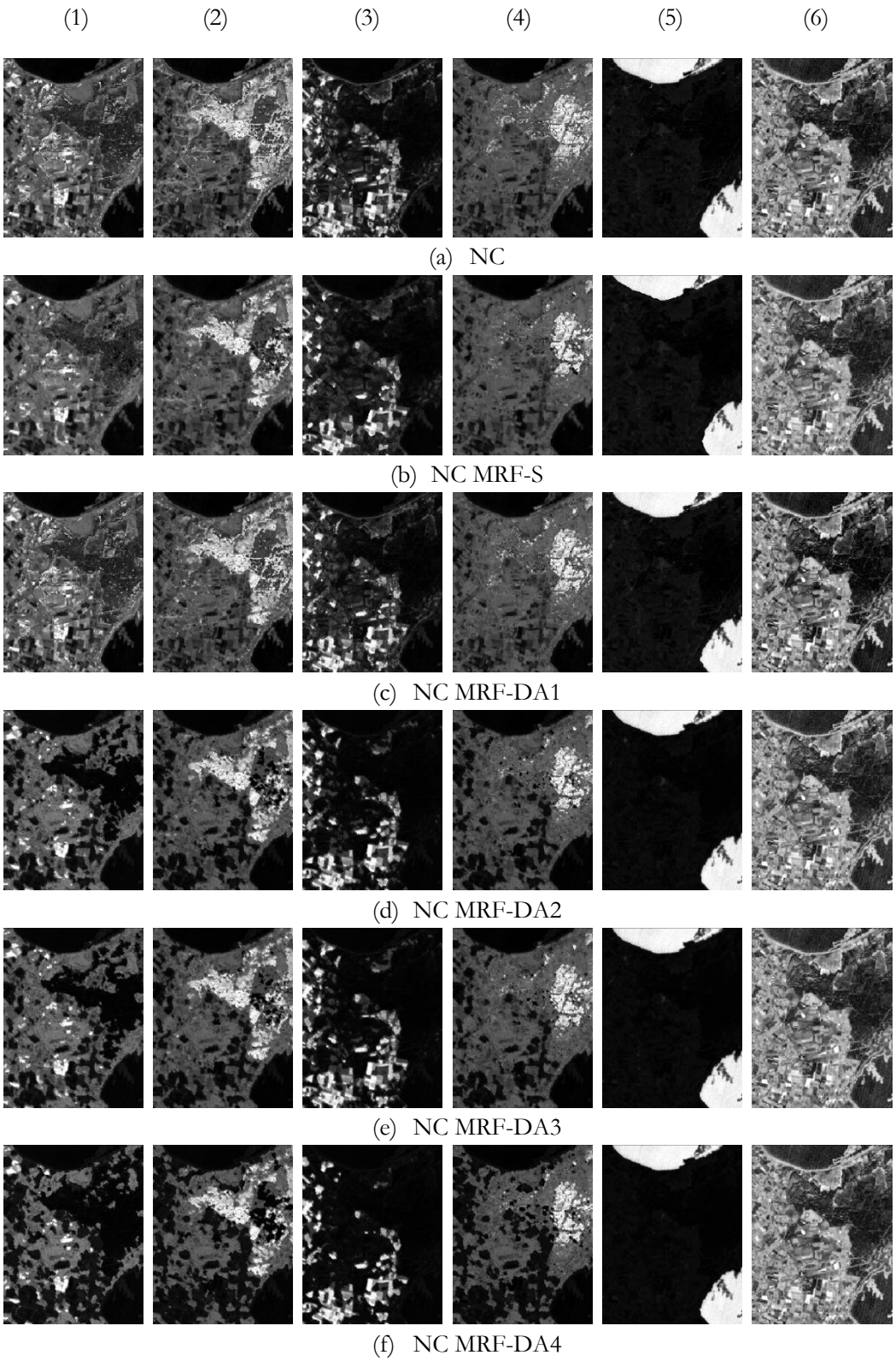

Figure 7-9: Fractional images obtained from NC, NC S-MRF and NC DA-MRF classifiers on LISS-III dataset from Resourcesat-2. The fractional images corresponds to Agriculture fields with crop (1), Sal Forest (2), Eucalyptus plantation (3), Dry agricultural field without crop (4), Moist agricultural field without crop (5), Water (6).

7.3. Accuracy Assessment Results

Having generated the fractional images against the estimated hybrid classifier parameters, the next step is to access the accuracy of the classification. In this research, point to point soft accuracy assessment was conducted. The fractional images generated from high resolution LISS-IV dataset against the optimal parameter values was considered as the reference dataset for AWIFS and LISS-III classification results. The accuracy of the AWIFS classification result has also been found against the reference dataset generated from relatively high resolution LISS-III images. Various fuzzy accuracy assessment techniques discussed in section 5.4. Among them FERM accuracy assessment was considered in this research due to it wide acceptance. Table 7.5 shows the FERM overall fuzzy accuracy of classification results from AWIFS against LISS-IV reference, LISS-III against LISS-IV reference and AWIFS against LISS-III reference, for NC, NC S-MRF, NC DA1-MRF, NC DA2-MRF, NC-DA3-MRF and NC DA4-MRF classifiers. In Table 7.5, R1 corresponds to Resourcesat-1 and R2 corresponds to Resourcesat-2.

Table 7-5: FERM Overall fuzzy accuracy for trained case

CLASSIFIER	AWIFS Vs LISS-IV		LISS-III Vs LISS-IV		AWIFS Vs LISS-III	
	R1 (%)	R2 (%)	R1 (%)	R2 (%)	R1 (%)	R2 (%)
NC	83.21	78.18	89.18	88.14	87.82	79.52
NC S-MRF	82.65	81.81	87.77	85.73	88.08	85.55
NC DA1-MRF	79.82	84.57	87.60	86.79	84.33	84.57
NC DA2-MRF	79.05	81.83	76.98	77.91	87.80	84.73
NC DA3-MRF	83.50	81.40	75.60	76.46	**90.60**	83.72
NC DA4-MRF	**87.26**	**85.27**	**89.40**	**89.37**	86.40	**87.25**

As one can see from Table 7.5, among the different classifiers used, NC DA4-MRF gave maximum overall fuzzy accuracy of 87.26% and 85.27% for AWIFS classification results from Resourcesat-1 and Resourcesat-2 against the NC DA4-MRF generated LISS-IV reference data. The NC DA4-MRF classifier gave a slightly higher overall fuzzy accuracy of 89.40% and 89.37% respectively for LISS-III datasets classification results when compared to LISS-IV classification results of the same classifier. This increase might be due to increase in the similarity in spatial resolution between the LISS-III and LISS-IV data. The accuracy of AWIFS dataset classification results were assessed against the relatively finer resolution LISS-III dataset classification results. In this case of AWIFS dataset from Resourcesat-1, NC DA3-MRF classifier had the highest fuzzy overall accuracy of 90.60% and the NC DA4-MRF models showed to be less accurate at around 86.40%. For AWIFS dataset from Resourcesat-2, the fuzzy overall accuracy of 87.35% was again the highest for NC DA4-MRF classifier as when compared to other classifiers. The detailed FERM and SCM (for comparison) accuracy assessment reports of all hybrid classifiers results for AWIFS and LISS-III data from Resourcesat-1 and 2 are provided in Appendix B.

7.4. Untrained Classes

Noise classifier assumes, any other class other than the trained classes to be noise. And to quantify the robustness of the Noise classifier to noise, a class was deliberately avoided while

training the classifier and the performance of the classifier is then evaluated. In this case the classifier was deprived of the signature information about one known class.

Table 7-6: Fuzzy User's Accuracy for trained and untrained case (i.e. not considering Agricultural field with Crop while training) on coarse resolution AWIFS (from Resourcesat-1) dataset

Accuracy assessment methods	NC		S-MRF		DA4-MRF	
	Untrained	Trained	Untrained	Trained	Untrained	Trained
Fuzzy user's accuracy (%)						
Sal Forest	72.37	89.37	69.96	88.29	52.89	65.67
Eucalyptus plantation	81.98	89.87	80.00	91.69	66.80	81.06
Dry agricultural without crop	74.85	84.83	82.61	91.57	55.58	66.76
Moist agricultural without crop	56.76	68.85	57.52	70.41	31.03	39.43
Water	88.01	87.89	87.78	89.31	68.69	76.46
Average user's accuracy (%)	**74.79**	**83.96**	**75.57**	**85.69**	**55.00**	**64.93**

Table 7-7: Fuzzy User's Accuracy for trained and untrained case (i.e. not considering Agricultural field with Crop while training) on coarse resolution AWIFS (from Resourcesat-2) dataset

Accuracy assessment methods	NC		S-MRF		DA4-MRF	
	Untrained	Trained	Untrained	Trained	Untrained	Trained
Fuzzy user's accuracy (%)						
Eucalyptus plantation	86.18	90.02	79.44	87.40	70.63	76.84
Dry agricultural without crop	72.84	88.86	71.20	79.24	59.68	70.18
Sal Forest	77.58	89.81	73.61	85.73	60.63	73.01
Water	97.13	98.29	97.34	98.30	86.88	92.71
Average user's accuracy (%)	**83.43**	**91.38**	**80.40**	**87.26**	**69.46**	**76.71**

Table 7-8: Fuzzy User's Accuracy for trained and untrained case (i.e. not considering Agricultural field with Crop while training) for medium resolution LISS-III (from Resourcesat-1) dataset

Accuracy assessment methods	NC		S-MRF		DA4-MRF	
	Untrained	Trained	Untrained	Trained	Untrained	Trained
Fuzzy user's accuracy (%)						
Sal Forest	74.14	91.32	72.06	93.21	59.85	65.65
Eucalyptus plantation	79.57	91.42	76.50	81.82	67.76	77.07
Dry agricultural without crop	75.50	87.35	78.53	84.75	85.38	89.71
Moist agricultural without crop	68.50	82.07	67.10	90.11	46.07	54.27
Water	88.22	92.95	87.20	83.30	87.81	90.37
Average user's accuracy (%)	**77.19**	**88.21**	**76.28**	**88.46**	**69.37**	**75.41**

Table 7-9: Fuzzy User's Accuracy for trained and untrained case (i.e. not considering Agricultural field with Crop while training) on medium resolution LISS-III (from Resourcesat-2) dataset

Accuracy assessment methods	NC		S-MRF		DA4-MRF	
	Untrained	Trained	Untrained	Trained	Untrained	Trained
Fuzzy user's accuracy (%)						
Eucalyptus plantation	77.37	89.29	72.71	86.48	63.03	78.29
Dry agricultural without crop	76.47	85.55	78.26	90.68	71.17	75.23
Sal Forest	70.61	87.56	68.36	85.77	55.93	81.12
Water	88.44	93.62	87.54	92.97	90.62	84.65
Average user's accuracy (%)	**78.22**	**88.75**	**76.72**	**88.47**	**70.19**	**79.82**

For untrained case, 'Agricultural field with Crop' class was kept untrained for both Resourcesat-1 and 2 datasets. Table 7.6 – 7.9 compares the user's accuracy of NC S-MRF classification results for AWIFS and LISS-III datasets from Resourcesat-1 and 2, for trained and untrained case. Here it is observed that the user's accuracy of classes for untrained case is less, as when compared to the user's accuracy of the classes for the trained case. The detailed accuracy assessment results are provided in the Appendix B.

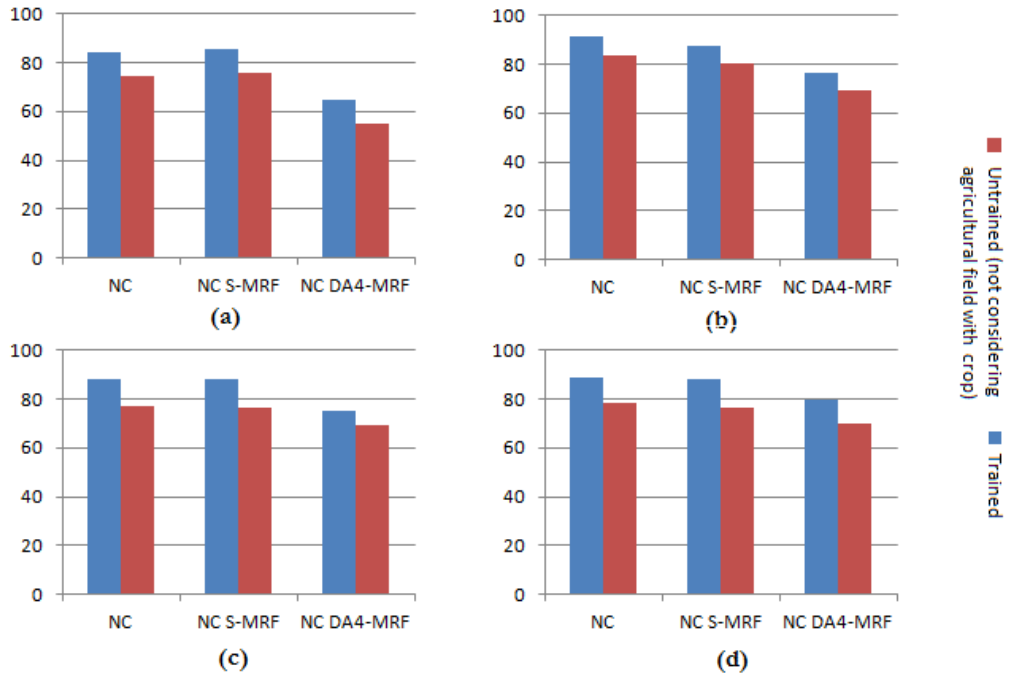

Figure 7-10: Graphical representation of user's accuracy for (a) AWIFS (Resourcesat-1), (b) AWIFS (Resourcesat-2), (c) LISS-III (Resourcesat-1) and (d) LISS-III (Resourcesat-2) for both trained and untrained case.

For untrained case, an overall decrease in user's accuracy was observed as when compared to that of the trained case for all the classifiers. For AWIFS dataset from Resourcesat-1, the decrease in user's accuracy for untrained classes were 9.17%, 10.12% and 9.93% for NC, NC S-MRF and NC DA4-MRF correspondingly. In case of AWIFS dataset from Resourcesat-2, the decrease in user's accuracy for untrained classes was 7.95%, 6.86% and 7.25% for NC, NC S-MRF and NC DA4-MRF correspondingly. For LISS-III dataset from Resourcesat-1, the decrease in user's accuracy for untrained classes were 11.02%, 12.18% and 6.04% for NC, NC S-MRF and NC DA4-MRF correspondingly. In case of LISS-III dataset from Resourcesat-2, the decrease in user's accuracy for untrained classes were 10.53%, 11.75% and 9.63% for NC, NC S-MRF and NC DA4-MRF correspondingly. The Figure 7.10 shows the graphical representation of the user's accuracy for AWIFS and LISS-III datasets from Resourcesat-1 and 2.

7.5. Entropy Measure of Classification Results

The entropy is a direct measure of uncertainty. Using entropy the uncertainty involved in the classification result i.e. fractional images, of a fuzzy classifier can be measured. In this research, an effort were made to study the effect of adding spatial contextual information using different

MRF priors such as Smoothness prior and four different discontinuity adaptive priors on the objective function of Noise classifier. A performance evaluation of all the classifiers using these five priors were conducted and the results are available in Table 7.5. The entropies of the most accurate classification results for different classifiers can be found in Table 7.10. It can be seen from Table 7.10 that the classification result of NC classifier (independently) gives the minimum entropy i.e. the uncertainty in the classification is minimal. Addition of spatial information to the NC classifier was found to have resulted in an increase in entropy. This is evident from the entropy values of classifier with different priors added to its objective function. The entropy of DA1-MRF classification results was found to have almost the same (little high) entropy values as that of the NC classification results and thus is the one with minimum uncertainty among the classifier created from different discontinuity adaptive prior. Even though the FERM fuzzy total accuracy is found to be the maximum for NC DA4-MRF classification results (refer Table 7.5), the uncertainty in the classification results is found to be the relatively high.

Table 7-10: Entropy values of classification results

CLASSIFIER	AWIFS		LISS-III	
	R1	R2	R1	R2
NC	2.049	1.786	1.989	1.694
NC S-MRF	3.184	2.346	3.129	2.000
NC DA1-MRF	2.092	1.807	2.066	1.781
NC DA2-MRF	2.918	2.435	2.357	2.040
NC DA3-MRF	2.813	2.431	2.327	2.002
NC DA4-MRF	3.358	2.814	3.326	2.005

7.6. Discussion of Results

In this research, spatial contextual information was modelled using Markov Random Fields and was incorporated into the objective function of the Noise classifier. The S-MRF prior model and four different DA-MRF prior models were mentioned in literature and all of them were used in this study for modelling spatial contextual information. Each prior has a unique Adaptive Interaction Function and incorporation of each prior into the Noise classifier objective function created one novel hybrid classifier. The so formed five hybrid classifiers are referred to in this thesis as the NC S-MRF, NC DA1-MRF, NC DA2-MRF, NC DA3-MRF and NC DA4-MRF classifiers. The primary objective of this research was to study the effect of DA-MRF models on the performance of Noise classifier. For studying this, classification was conducted using all six classifiers (see Table 7.10) on a coarse resolution AWIFS dataset and a medium resolution LISS-III dataset of the same area and date. Classification results of LISS-IV dataset was used as the reference data while using FERM accuracy assessment technique.

The estimation of Noise classifier parameter, fuzzification factor (m) and noise distance (δ), had been the initial priority of this research. Since there was no standard method for Noise classifier parameter estimation, the same was estimated by using entropy and 'membership value change' inputs as mentioned in section 7.1. For small value of Noise distance ($0<\delta<1000$), the entropy

was large and the difference in membership values between a class and non-class location (for each fractional image) was minimal. For large value of Noise distance (δ>1000), the entropy proved to be small and the membership value difference between class and non-class location became maximum within same fraction image. For δ beyond 10000, both the entropy and membership value difference values seemed to saturate and for that reason δ was made a constant ($\delta = 10000$) for further analysis. To estimate fuzzification factor (m), the entropy and membership value change between class and non-class location on the same fractional image was calculated by varying m values from 0 to 10. The m value at the crossing point of the two graphs was considered as the optimal. The optimal m values are mentioned in Table 7.1. The estimation of λ and β/γ for NC S-MRF and all four NC DA-MRF classifiers were conducted using the mean-variance method. The mean-variance method quantifies the clarity of edges in an image and ultimately the edge preserving capability of the classifier. Among the various DA-MRF models used, the DA4-MRF prior was found to give NC classifier, the maximum edge preservation.

AWIFS and LISS-III datasets from both Resourcesat-1 and 2 were classified using NC, S-MRF, NC DA1-MRF, NC DA2-MRF, NC DA3-MRF and NC DA4-MRF classifiers. Image to image fuzzy accuracy assessment technique was used in this thesis for reasons mentioned in section 6.4. The accuracy assessment of AWIFS and LISS-III classified data was conducted using LISS-IV reference data generated from same classifier as that of the classified data. For the purpose of accuracy assessment, the cell resolutions of AWIFS, LISS-III and LISS-IV datasets were made in the ratio 1:4:12 and hence 16 pixels (4 x 4) of LISS-III and 144 pixels (12 x 12) of AWIFS have to be combined to reach the pixel dimension of LISS-IV (Chawla, 2010). The resampling of the datasets and aggregation of pixels values to obtain a mean pixel value were sources of error, but were ignored in this research.

The NC DA4-MRF classification of AWIFS (from Resourcesat-1) and LISS-III (from Resourcesat-1) gave an overall fuzzy accuracy of 87.26% and 89.40% respectively. The overall fuzzy accuracy increase compared to NC classifier was 4.05% and 0.22% for AWIFS (from Resourcesat-1) and LISS-III datasets (from Resourcesat-1). The classification of AWIFS and LISS-III datasets both from Resourcesat-2 were also conducted, to study the effect of radiometric resolution of the input dataset on the classifier accuracy. The radiometric accuracy of AWIFS and LISS-III was 10 and 7 for Resourcesat-1 and 12 and 10 for Resourcesat-2. The NC DA4-MRF classification of AWIFS (from Resourcesat-2) and LISS-III (from Resourcesat-2) gave an overall fuzzy accuracy of 85.27% and 89.37% respectively and, was found to be slightly less than corresponding Resourcesat-1 dataset. The overall fuzzy accuracy increase compared to NC classifier was 7.09% and 1.23% for AWIFS (from Resourcesat-2) and LISS-III datasets (from Resourcesat-2).

In the past, studies were also conducted for evaluating the impact of incorporating spatial contextual information (modelled using MRF) on Fuzzy c-Means (FCM) and Possibilistic c-means. In case of FCM, the DA3-MRF prior gave the best result and the overall fuzzy accuracy for AWIFS and LISS-III datasets were 85.54% and 89.45% respectively (Singha, 2013). For PCM, DA2-MRF prior proved to be the best and its overall fuzzy accuracy for AWIFS and

LISS-III datasets were 81.97% and 87.31% respectively (Chawla, 2010). On comparing the overall fuzzy accuracy of NC DA4-MRF with FCM DA3-MRF, one can see that there is an improvement in accuracy of 1.72% for AWIFS dataset for NC DA4-MRF but almost the same for LISS-III dataset. When comparing the overall fuzzy accuracy of NC DA4-MRF with PCM DA2-MRF, one can see that there is an improvement in accuracy of 5.29% and 2.09% for NC DA4-MRF against AWIFS and LISS-III datasets respectively.

For all the five hybrid classifier used in this research, the presence of untrained class had found to cause a decrease in classification accuracy. In this study 'Agricultural Field with Crop' class was left untrained. The average user accuracy obtained while classifying LISS-III (from Resourcesat-1) using of NC DA4-MRF for untrained case was 69.37%, while it was 75.41% for the trained case. Thus the decrease in user's accuracy for the untrained case with respect to the fully trained case, for LISS-III classification of NC DA4-MRF was 6.04%. In the case of FCM DA3-MRF classification on LISS-III dataset, the user's accuracy for the untrained case was found to be 55.30%, while for the trained case it was 59.76% (Singha, 2013). The decrease in user's accuracy for the untrained case with respect to the fully trained case, for LISS-III classification of FCM DA3-MRF was 4.46%. Thus we can conclude that the user's accuracy of the NC DA4-MRF classified LISS-III data, for the untrained case, improves by 14.07% compared to the user's accuracy obtained for FCM DA3-MRF classified LISS-III data.

Considering the fuzzy accuracy obtained, it is true to say that the NC DA4-MRF does have the best performance among all classifier that is discussed in this section. This relatively better performance of NC DA4-MRF comes from the ability of Noise classifier to isolate noisy data from the input image. Further the fuzzy nature of Noise classifier enabled it to address the mixed pixel problem and the use of spatial contextual information helped in addressing the isolated pixel problem associated with any classifier. But the efficiency of the NC DA-MRF classifiers were evaluated by taking into account its performance on coarse resolution AWIFS (56 m spatial resolution) and a medium resolution LISS-III (23.5 m spatial resolution) datasets. But to confirm the usability of this classifier, its classification accuracy has to be evaluated for other resolution datasets with and without noise.

8. CONCLUSION AND RECOMMENDATION

8.1. Conclusion

This research work aimed at realizing a hybrid fuzzy noise robust classifier which used information from both spectral and spatial domains. Noise classifier was identified to be very robust against noise present in the datasets and hence was used as the base classifier in this research. The Noise classifier (fuzzy mode) does classification purely using the information from the spectral domain i.e. the digital number (DN) values of a pixel. Noise classifier (fuzzy mode) does handle the mixed pixel problem but using only the spectral information it isn't possible to address the isolated pixel problem. Use of spatial contextual information along with spectral information was identified as a possibility to address the isolated pixel problem that happens in a classification process and so, it was decided to incorporate the same with Noise classifier.

In this research, an effort was made to add contextual information modelled using different MRF models into the objective function of Noise classifier which purely works on spectral information. Here five MRF models including the S-MRF (smoothness prior) and four different DA-MRF (discontinuity adaptive prior) models have been used to model the contextual information and were then integrated into the objective function of Noise classifier. Technically saying, each MRF model when integrated with Noise classifier created a new classifier itself. In this research AWIFS, LISS-III and LISS-IV dataset from both Resourcesat-1 and 2 were used. Datasets from Resourcesat-2 has slightly higher radiometric accuracy and was included in this research to studying the effect of radiometric resolution on the hybrid classifier performance.

Initially the optimal parameters of the base classifier (Noise classifier) were estimated for each dataset to ensure optimal performance. The research then succeeded in studying the effect of different MRF models on the classifier accuracy and uncertainty, when integrated with the Noise classifier. FERM based fuzzy accuracy assessment was used to find the accuracy of the classification results. The reference data was generated from the high resolution LISS-IV imagery of the study area. Among the different discontinuity adaptive MRF models used NC DA4-MRF model was found to have the maximum accuracy of classification results for AWIFS and LISS-III dataset from both Resourcesat-1 and 2, but at the cost of slight increase in the entropy in the classification result. For Resourcesat-2 datasets, the entropy was found to be slightly low. The fuzzy error matrix (FERM) accuracy for AWIFS data was found to be equal to 87.26% for Resourcesat-1 and 89.40% for Resourcesat-2. FERM accuracy for LISS-III data was found to be 85.27% for Resourcesat-1 and 89.37% for Resourcesat-2.

Classification was also conducted by leaving one class untrained to study the effect on the NC DA-MRF classifier accuracy during the presence of untrained classes in the dataset. In this case a relative decrease in user's accuracy was observed when compared with the fully trained case. A decrease in user's accuracy of 9.93% and 7.25% was observed for AWIFS data from Resourcesat-1 and Resourcesat-2 respectively. A decrease in user's accuracy of 6.04% and 9.63% was observed for LISS-III data from Resourcesat-1 and Resourcesat-2 respectively.

8.2. Answers to Research Questions

A.1 How can the Noise classifier (NC) parameters be estimated?

Answer: The base classifier used in this research is Noise classifier. Estimation of optimal Noise classifier parameters which includes fuzzification factor (m) and noise distance (δ) is essential to ensure the optimal performance. These parameters are dataset dependent and so were estimated for all AWIFS, LISS-III and LISS-IV datasets separately. Uncertainty (entropy) involved in the classification results and 'membership value change' between pixels where a class is present and absent in the same fractional image, was identified as two prospective features by which optimal parameters can be estimated. But either of the features failed to provide an estimate of the parameters independently. Noise distance (δ) was found to have least impact on the both entropy and membership value change between class and non-class location on the same fractional image for δ beyond 10000. So the δ was made a constant at 10000 for this study. The optimal fuzzification factor (m) was then found from the crossing point of the normalized uncertainty and 'membership value difference' graphs. The so estimated optimal fuzzification factor (m) is listed in Table 7.1.

B.1 How can the Noise classifier objective function be modified to incorporate spatial contextual information modeled using S-MRF and DA-MRF models?

Answer:

To include spatial contextual information along with the spectral information for classification, an MRF model needs to be just added to the term in objective function of Noise classifier. In order to control the contribution from spectral and spatial domain, a term λ was introduced. Also each MRF model has a parameter which can be used to control the interaction of a pixel with its neighbours. Simulated Annealing was used to estimate the NC S-MRF and NC DA-MRF. In this study, the signature data of classes were available and so estimation of cluster centers was not conducted. A detail description about this integration is given in section 5.1.

C.1 Which DA-MRF prior model would be best suited for the Noise classifier?

Answer: The DA4-MRF prior model, when integrated with Noise classifier was found to give the maximum FERM total fuzzy accuracy and hence considered as the best prior model among the all models used in this research.

D.1 To what degree does the classification accuracy improve upon using the NC DA-MRF classifiers when compared to NC Classifier with and without training?

Answer: For trained case there was an increase in FERM overall accuracy for NC DA4-MRF classifier results over normal NC classifier results. When DA4-MRF prior model was used, the accuracy was found to have increased by 4.05 and 7.09 respectively for AWIFS

Resourcesat-1 and Resourcesat-2 datasets. And for LISS-III datasets from Resourcesat-1 and Resourcesat-2, the accuracy increase for NC DA4-MRF classifier over NC classifier results was 0.26 and 1.23 respectively. For untrained case, an overall decrease in user's accuracy was observed as when compared to that of the trained case for all the classifiers. More details about their accuracies and comparison with other classifiers are given in section 7.4 and 7.6.

8.3. Recommendation

A hundred percent accuracy in classification is still a myth. But the possibility for creating better classifier has been always looked upon by the research community and this research is one such effort to create a better and realistic classifier. The hybrid classifier developed and studied here necessarily does not handle every problem in classification and hence more effort has to be conducted to effectively address those problems. The following are few points that could be used for improving on the current classification technique.

a) A Noise clustering algorithm which could have a variable value for noise distance (Davé and Sen, 1997) claims to be more effective in dealing with noise and hence can be tried instead of Noise classifier. Kernel based clustering algorithms proposed by Chotiwattana, 2009 can also be tried instead of Noise classifier.
b) The effective estimation of the Noise classifier parameters is still a prospective research area. The estimation of Noise classifier parameters can be tried using methods other than that which is used in this research. A comparative study can also be done between various methods.
c) In this research, the cluster centers were obtained from the signature data of the classes. Hence optimal cluster centers were not considered as parameters to be estimated i.e. the approach here was supervised. It is recommended to try the unsupervised case as well where the cluster centers also need be estimated.
d) The optimization algorithm that was used in this research work is Simulated Annealing. Effect of using algorithms such as Iterated Conditional Modes (ICM) and Maximizer of Posterior Marginals can also be studied.

REFERENCES

BABU, G. P. & MURTY, M. N. 1994. Clustering with evolution strategies. *Pattern recognition,* 27**,** 321-329.

BARNI, M., CAPPELLINI, V. & MECOCCI, A. 1996. Comments on "A possibilistic approach to clustering". *Fuzzy Systems, IEEE Transactions on,* 4**,** 393-396.

BERNARDO, J. M. 2003. *Bayesian Statistics 7: Proceedings of the Seventh Valencia International Meeting*, Oxford University Press.

BERTSIMAS, D. & TSITSIKLIS, J. 1993. Simulated annealing. *Statistical Science***,** 10-15.

BESAG, J. 1974. Spatial interaction and the statistical analysis of lattice systems. *Journal of the Royal Statistical Society. Series B (Methodological)***,** 192-236.

BEZDEK, J. C. 1981. *Pattern recognition with fuzzy objective function algorithms*, Kluwer Academic Publishers.

BEZDEK, J. C., EHRLICH, R. & FULL, W. 1984. FCM: The fuzzy< i> c</i>-means clustering algorithm. *Computers & Geosciences,* 10**,** 191-203.

BINAGHI, E., BRIVIO, P. A., GHEZZI, P. & RAMPINI, A. 1999. A fuzzy set-based accuracy assessment of soft classification. *Pattern recognition letters,* 20**,** 935-948.

BINAGHI, E., MADELLA, P., GRAZIA MONTESANO, M. & RAMPINI, A. 1997. Fuzzy contextual classification of multisource remote sensing images. *Geoscience and Remote Sensing, IEEE Transactions on,* 35**,** 326-340.

CHAWLA, S. 2010. Possibilistic c-Means-Spatial Contexutal Information based sub-pixel classification approach for multi-spectral data. *University of Twente Faculty of Geo-Information and Earth Observation (ITC), Enschede.*

CHOTIWATTANA, W. Noise Clustering Algorithm based on Kernel Method. Advance Computing Conference, 2009. IACC 2009. IEEE International, 2009. IEEE, 56-60.

CONGALTON, R. G. 1991. A review of assessing the accuracy of classifications of remotely sensed data. *Remote sensing of Environment,* 37**,** 35-46.

DAVÉ, R. & SEN, S. Noise clustering algorithm revisited. Fuzzy Information Processing Society, 1997. NAFIPS'97., 1997 Annual Meeting of the North American, 1997. IEEE, 199-204.

DAVE, R. N. 1991. Characterization and detection of noise in clustering. *Pattern Recognition Letters,* 12**,** 657-664.

DAVE, R. N. Robust fuzzy clustering algorithms. Fuzzy Systems, 1993., Second IEEE International Conference on, 1993. IEEE, 1281-1286.

DAVE, R. N. & FU, T. 1994. Robust shape detection using fuzzy clustering: practical applications. *Fuzzy Sets and Systems,* 65**,** 161-185.

DAVÉ, R. N. & KRISHNAPURAM, R. 1997. Robust clustering methods: a unified view. *Fuzzy Systems, IEEE Transactions on,* 5**,** 270-293.

DEHGHAN, H. & GHASSEMIAN, H. 2006. Measurement of uncertainty by the entropy: application to the classification of MSS data. *International journal of remote sensing,* 27**,** 4005-4014.

DERIN, H. & ELLIOTT, H. 1987. Modeling and segmentation of noisy and textured images using Gibbs random fields. *Pattern Analysis and Machine Intelligence, IEEE Transactions on***,** 39-55.

DUTTA, A. 2009. *Fuzzy C-Means classification of multispectral data incorporating spatial contextual information by using Markov Random Field.* M. Sc Thesis, GFM, IIRS-ITC JEP.

FISHER, P. F. & PATHIRANA, S. 1990. The evaluation of fuzzy membership of land cover classes in the suburban zone. *Remote Sensing of Environment,* 34**,** 121-132.

FOODY, G. 1996. Approaches for the production and evaluation of fuzzy land cover classifications from remotely-sensed data. *International Journal of Remote Sensing,* 17**,** 1317-1340.

FOODY, G. M. 1995. Cross-entropy for the evaluation of the accuracy of a fuzzy land cover classification with fuzzy ground data. *ISPRS Journal of Photogrammetry and Remote Sensing,* 50**,** 2-12.

FOODY, G. M. 1997. Fully fuzzy supervised classification of land cover from remotely sensed imagery with an artificial neural network. *Neural Computing & Applications,* 5**,** 238-247.

FOODY, G. M. 2000. Estimation of sub-pixel land cover composition in the presence of untrained classes. *Computers & Geosciences,* 26**,** 469-478.

FOODY, G. M. 2002. Status of land cover classification accuracy assessment. *Remote sensing of environment,* 80**,** 185-201.

GEIGER, D. & GIROSI, F. 1991. Parallel and deterministic algorithms from MRFs: Surface reconstruction. *Pattern Analysis and Machine Intelligence, IEEE Transactions on,* 13**,** 401-412.

GEMAN, S. & GEMAN, D. 1984. Stochastic relaxation, Gibbs distributions, and the Bayesian restoration of images. *Pattern Analysis and Machine Intelligence, IEEE Transactions on***,** 721-741.

GEMAN, S. & GRAFFIGNE, C. Markov random field image models and their applications to computer vision. Proceedings of the International Congress of Mathematicians, 1986. AMS, Providence, RI, 2.

GREEN, K. & CONGALTON, R. G. 2004. *An error matrix approach to fuzzy accuracy assessment: The NIMA Geocover Project*, Boca Raton, FL: CRC Press.

JACKSON, Q. & LANDGREBE, D. A. 2002. Adaptive Bayesian contextual classification based on Markov random fields. *Geoscience and Remote Sensing, IEEE Transactions on,* 40**,** 2454-2463.

JOLION, J.-M. & ROSENFELD, A. 1989. Cluster detection in background noise. *Pattern Recognition,* 22**,** 603-607.

KANG, D.-J. & ROH, K.-S. 2001. A discontinuity adaptive Markov model for color image smoothing. *Image and Vision Computing,* 19**,** 369-379.

KASETKASEM, T., ARORA, M. K. & VARSHNEY, P. K. 2005. Super-resolution land cover mapping using a Markov random field based approach. *Remote Sensing of Environment,* 96**,** 302-314.

KRISHNAPURAM, R. & FREG, C.-P. 1992. Fitting an unknown number of lines and planes to image data through compatible cluster merging. *Pattern Recognition,* 25**,** 385-400.

KRISHNAPURAM, R. & KELLER, J. M. 1993. A possibilistic approach to clustering. *Fuzzy Systems, IEEE Transactions on,* 1**,** 98-110.

KRISHNAPURAM, R. & KELLER, J. M. 1996. The possibilistic c-means algorithm: insights and recommendations. *Fuzzy Systems, IEEE Transactions on,* 4**,** 385-393.

KUMAR, A. & DADHWAL, V. 2010. Entropy-based fuzzy classification parameter optimization using uncertainty variation across spatial resolution. *Journal of the Indian Society of Remote Sensing,* 38**,** 179-192.

KUMAR, A., GHOSH, S. & DADHWAL, V. 2006. Sub-pixel land cover mapping: SMIC system. *ISPRS Int. Sym."Geospatial Databases for Sustainable Development", Goa, India*.

LI, S. Z. 1995. On discontinuity-adaptive smoothness priors in computer vision. *Pattern Analysis and Machine Intelligence, IEEE Transactions on,* 17**,** 576-586.

LI, S. Z. 2009. *Markov random field modeling in image analysis*, Springer.

MA, L., SMITH, D. & MILNER, B. Environmental noise classification for context-aware applications. Database and Expert Systems Applications, 2003. Springer, 360-370.

MATHER, P. & TSO, B. 2010. *Classification methods for remotely sensed data*, CRC press.

MELGANI, F. & SERPICO, S. B. 2003. A Markov random field approach to spatio-temporal contextual image classification. *Geoscience and Remote Sensing, IEEE Transactions on,* 41**,** 2478-2487.

MOSER, G. & SERPICO, S. B. Contextual remote-sensing image classification by support vector machines and Markov random fields. Geoscience and Remote Sensing Symposium (IGARSS), 2010 IEEE International, 2010. IEEE, 3728-3731.

OKEKE, F. & KARNIELI, A. 2006. Methods for fuzzy classification and accuracy assessment of historical aerial photographs for vegetation change analyses. Part I: Algorithm development. *International journal of remote sensing,* 27**,** 153-176.

PHAM, D. L. 2001. Spatial models for fuzzy clustering. *Computer vision and image understanding,* 84**,** 285-297.

PIZURICA, A. 2002. *Image denoising using wavelets and spatial context modeling*. Ghent University.

PONTIUS JR, R. G. & CHEUK, M. L. 2006. A generalized cross-tabulation matrix to compare soft-classified maps at multiple resolutions. *International Journal of Geographical Information Science,* 20**,** 1-30.

RANGARAJAN, A., CHELLAPPA, R. & MANJUNATH, B. 1991. *Markov random fields and neural networks with applications to early vision problems*, Citeseer.

RICHARDS, J. A. 2013. *Remote sensing digital image analysis: an introduction*, Springer.

RICOTTA, C. & AVENA, G. 2002. Evaluating the degree of fuzziness of thematic maps with a generalized entropy function: a methodological outlook. *International Journal of Remote Sensing,* 23**,** 4519-4523.

SEN, S. & DAVE, R. Application of noise clustering in group technology. Fuzzy Information Processing Society, 1999. NAFIPS. 18th International Conference of the North American, 1999. IEEE, 366-370.

SILVÁN-CÁRDENAS, J. & WANG, L. 2008. Sub-pixel confusion–uncertainty matrix for assessing soft classifications. *Remote Sensing of Environment,* 112**,** 1081-1095.

SINGHA, M. 2013. Study the effect of discontinuity adaptive MRF models in fuzzy based classifier.

SMITS, P. C. & DELLEPIANE, S. G. 1997. Synthetic aperture radar image segmentation by a detail preserving Markov random field approach. *Geoscience and Remote Sensing, IEEE Transactions on,* 35**,** 844-857.

SOLBERG, A. H., TAXT, T. & JAIN, A. K. 1996. A Markov random field model for classification of multisource satellite imagery. *Geoscience and Remote Sensing, IEEE Transactions on,* 34**,** 100-113.

SOMAN, K., DIWAKAR, S. & AJAY, V. 2006. *DATA MINING: THEORY AND PRACTICE [WITH CD]*, PHI Learning Pvt. Ltd.

TOLPEKIN, V. A. & STEIN, A. 2009. Quantification of the effects of land-cover-class spectral separability on the accuracy of Markov-random-field-based superresolution mapping. *Geoscience and Remote Sensing, IEEE Transactions on,* 47**,** 3283-3297.

YANG, M.-S. & WU, K.-L. 2006. Unsupervised possibilistic clustering. *Pattern Recognition,* 39**,** 5-21.

ZADEH, L. A. 1965. Fuzzy sets. *Information and control,* 8**,** 338-353.

ZHANG, J. & FOODY, G. 1998. A fuzzy classification of sub-urban land cover from remotely sensed imagery. *International Journal of Remote Sensing,* 19**,** 2721-2738.

ZHANG, J. & FOODY, G. 2001. Fully-fuzzy supervised classification of sub-urban land cover from remotely sensed imagery: statistical and artificial neural network approaches. *International Journal of Remote Sensing,* 22**,** 615-628.

ZHANG, J. & KIRBY, R. P. 1997. An evaluation of fuzzy approaches to mapping land cover from aerial photographs. *ISPRS journal of photogrammetry and remote sensing,* 52**,** 193-201.

APPENDIX A

A.1: Variation of 'Uncertainty' Vs 'Membership Value Change' against fuzzification factor (m) (Noise distance(δ=10000)

The graphs show the variation of entropy and 'membership value change' happening across different classes within same fractional image for different fuzzification factor(m). Here the x-axis shows the fuzzification factor (m) and the y-axis shows the 'Uncertainty' and 'Membership Value Change' values.

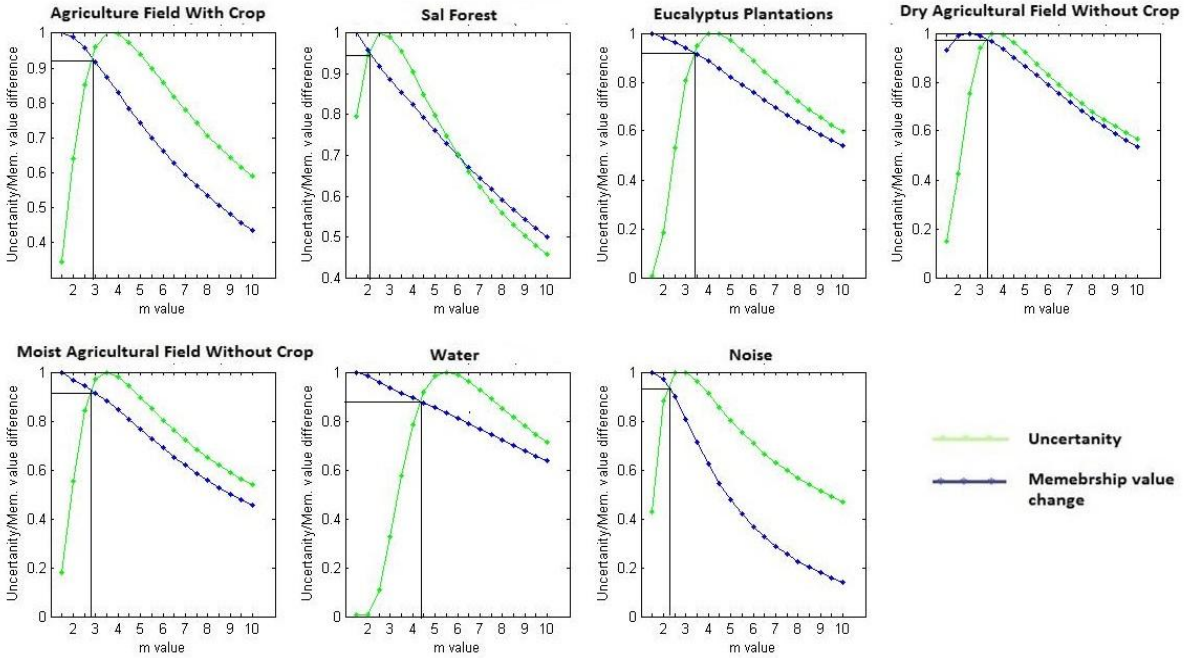

Figure A-1: Estimated fuzzification factor (m) for LISS-III (from Resourcesat-1) fractional images

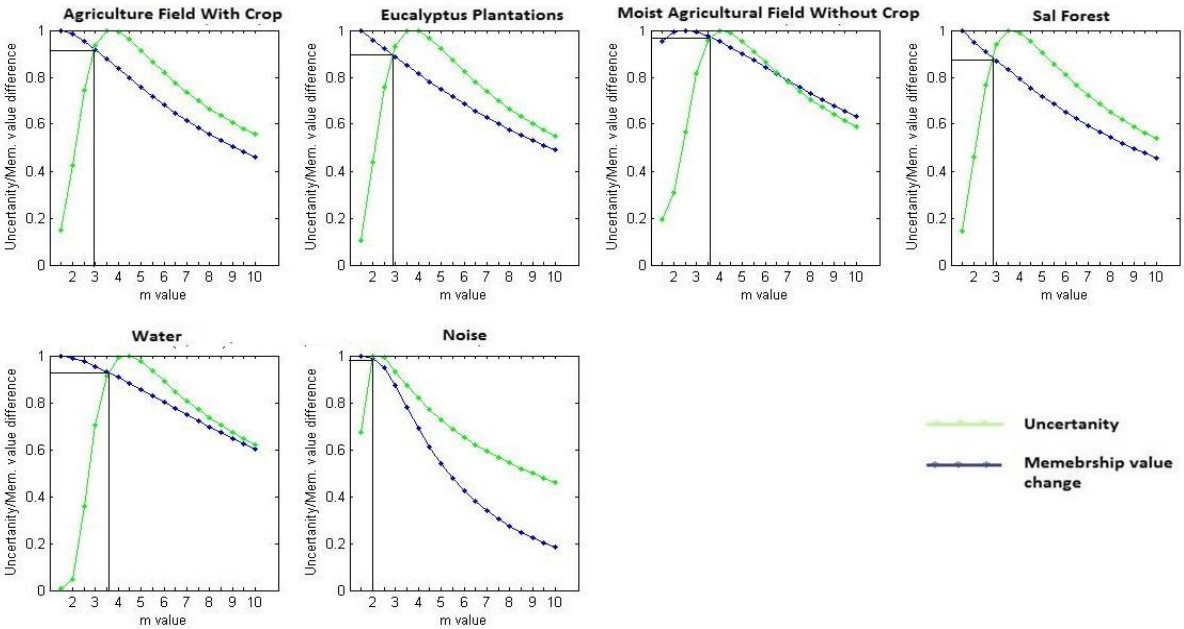

Figure A-2: Estimated fuzzification factor (m) for LISS-III (from Resourcesat-2) fractional images

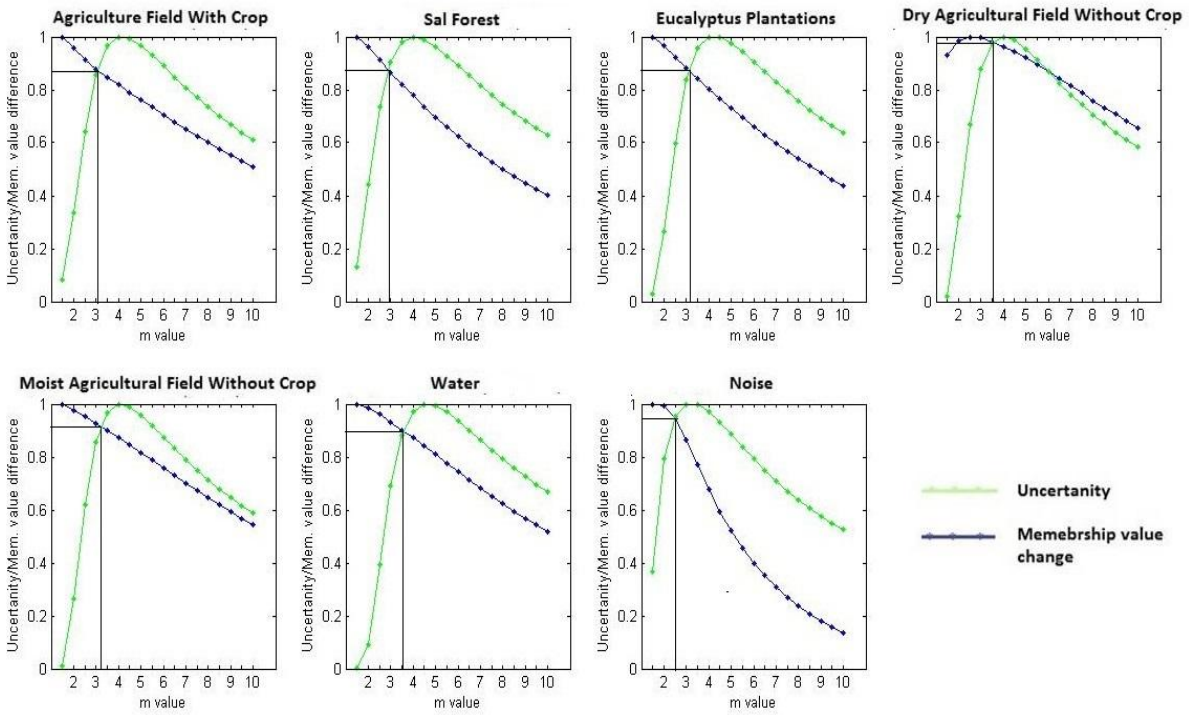

Figure A-3: Estimated fuzzification factor (m) for LISS-IV (from Resourcesat-1) fractional images

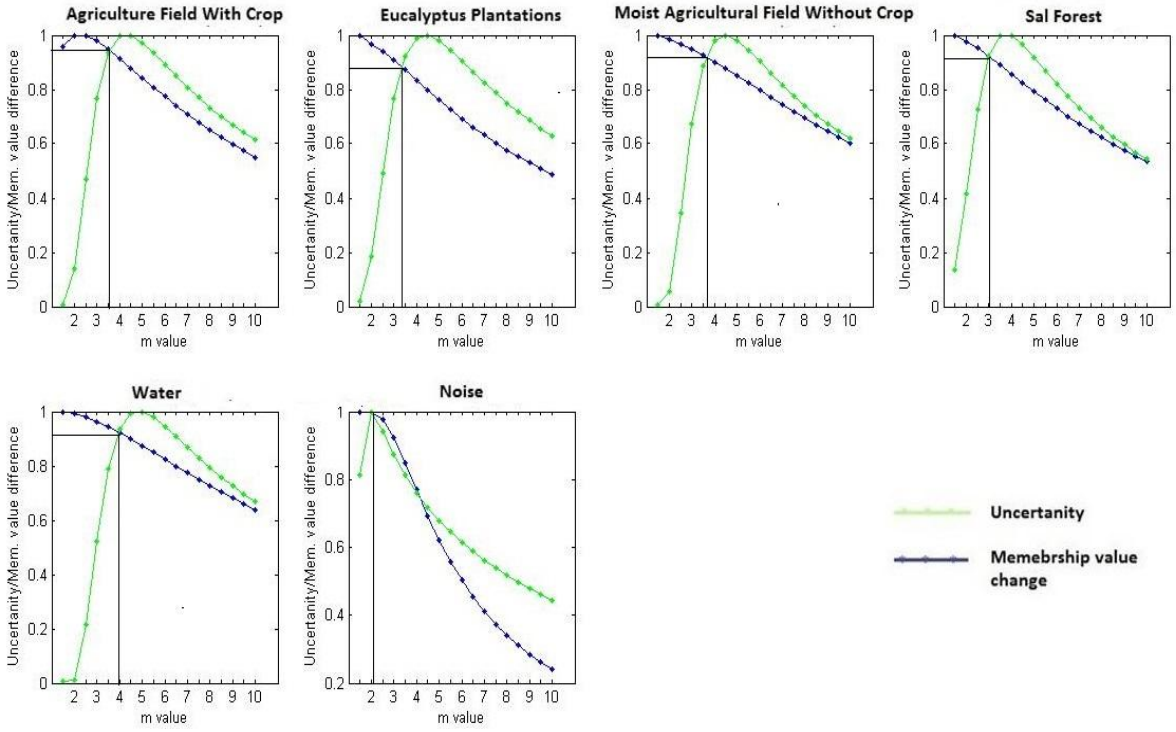

Figure A-4: Estimated fuzzification factor (m) for LISS-IV (from Resourcesat-2) fractional images

A.2: Variation of 'Uncertainty' and 'Membership Value Change' values against fuzzification factor (m) and Noise distance (δ)

The 3D graphs are obtained by plotting the value of entropy and 'membership value change' happening across different classes within same fractional image. Here the x-axis shows the fuzzification factor (m), the y-axis shows the Noise distance $(\boldsymbol{\delta})$ and z-axis shows the 'Uncertainty' and 'Membership Value Change' values.

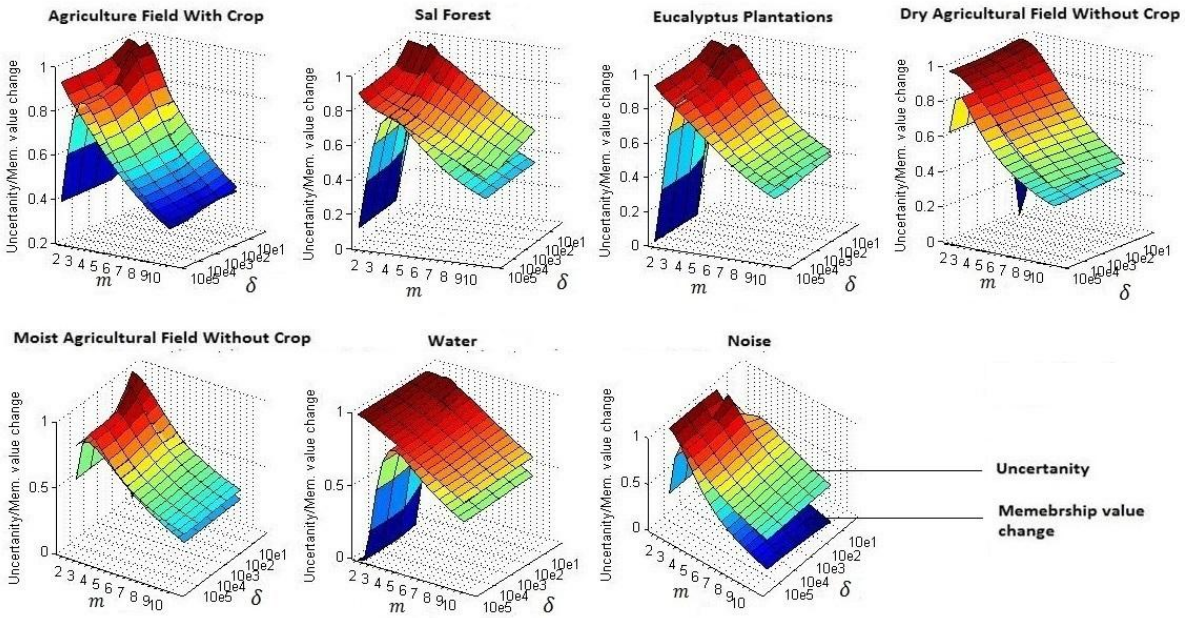

Figure A-5: Uncertainty' and 'Membership Value Change' graph for AWIFS (from Resourcesat-1)

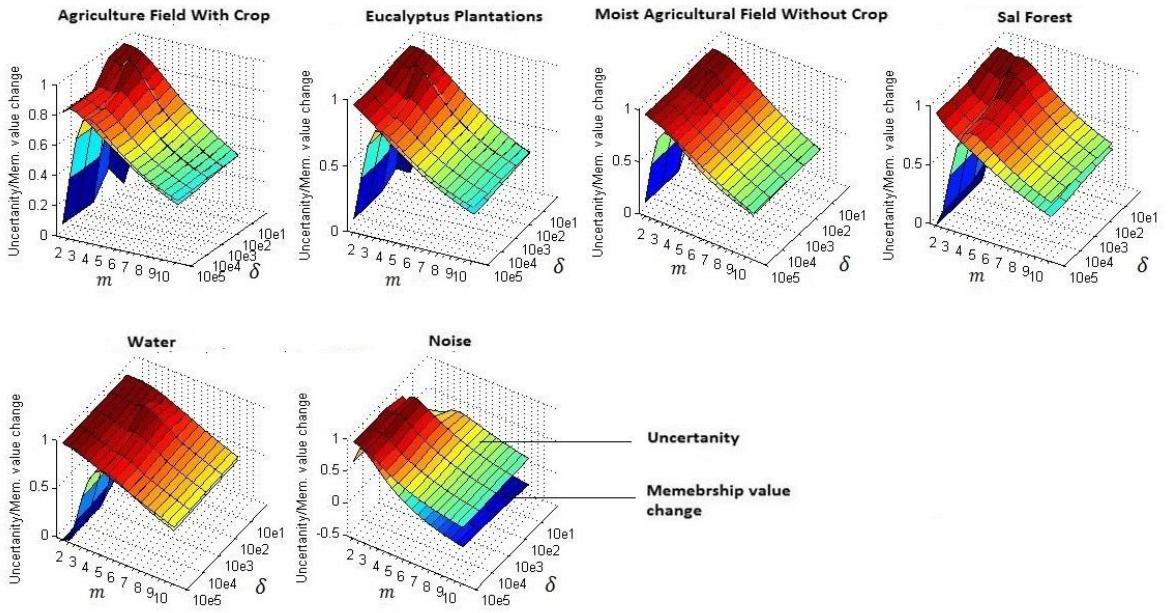

Figure A-6: Uncertainty' and 'Membership Value Change' graph for AWIFS (from Resourcesat-2)

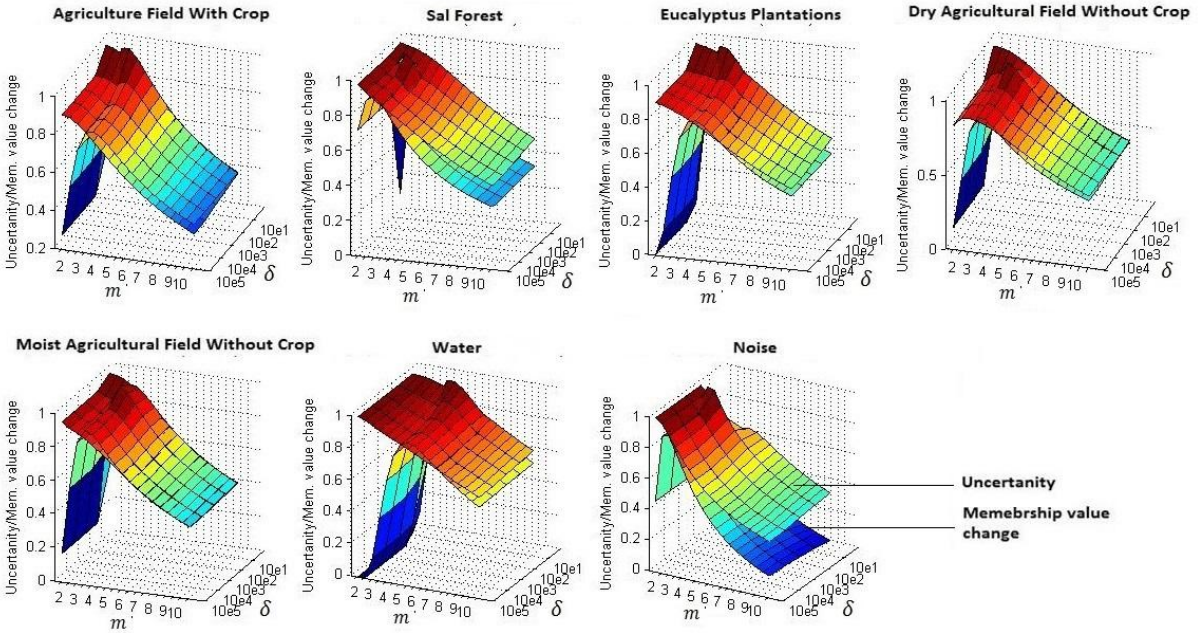

Figure A-7: Uncertainty' and 'Membership Value Change' graph for LISS-III (from Resourcesat-1)

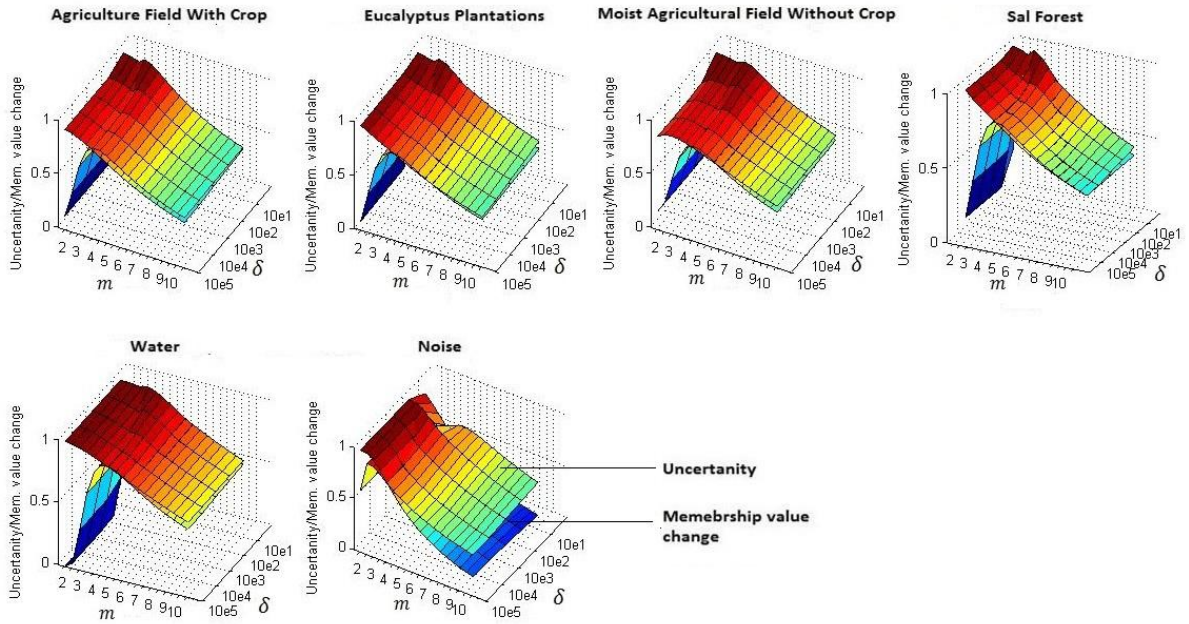

Figure A-8: Uncertainty' and 'Membership Value Change' graph for LISS-III (from Resourcesat-2)

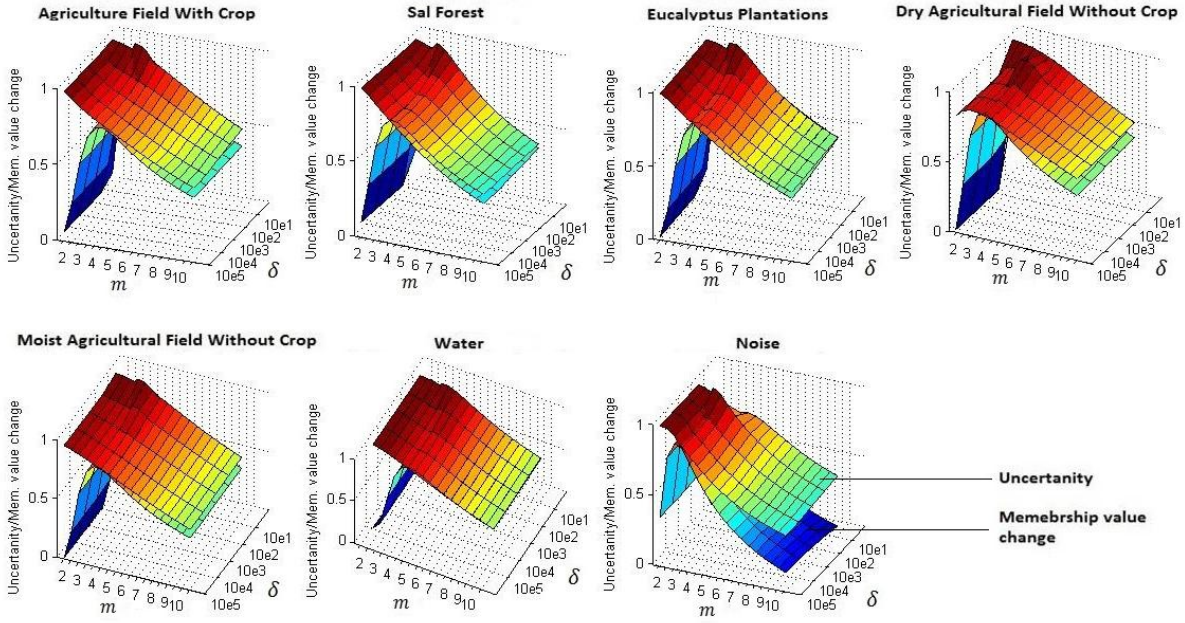

Figure A-9: Uncertainty' and 'Membership Value Change' graph for LISS-IV (from Resourcesat-1)

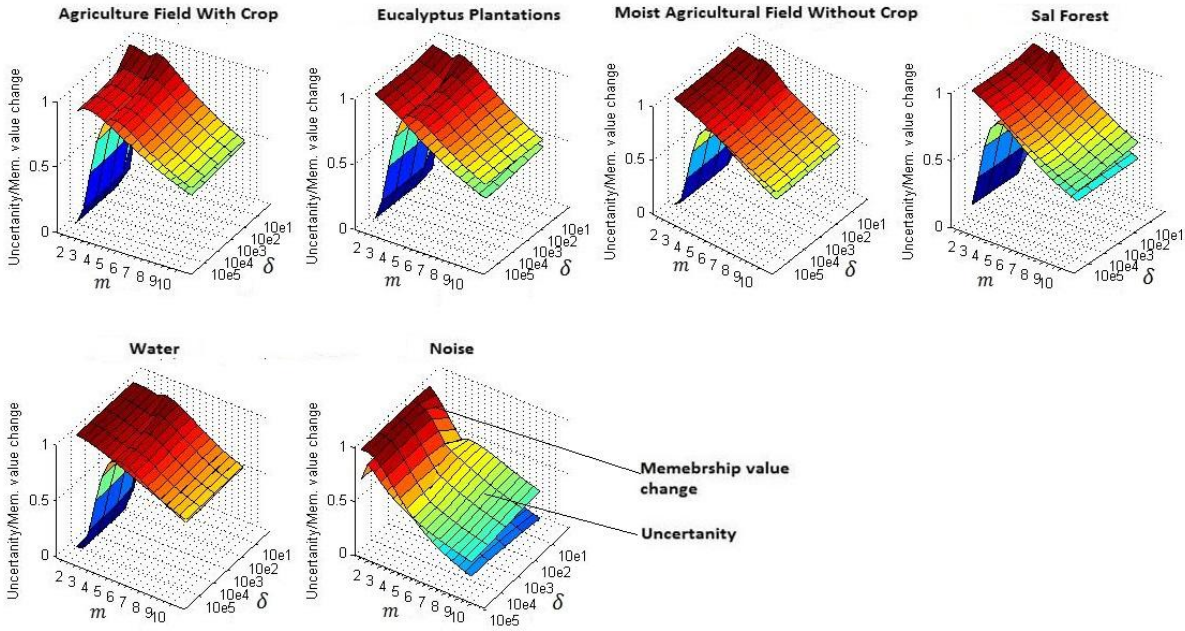

Figure A-10: Uncertainty' and 'Membership Value Change' graph for LISS-IV (from Resourcesat-2)

A.3: Entropy graphs

The 3D graph shows the variation of entropy for all combination of λ and γ. λ and γ are parameters that need to be estimated in the objective function of NC DA4-MRF classifier.

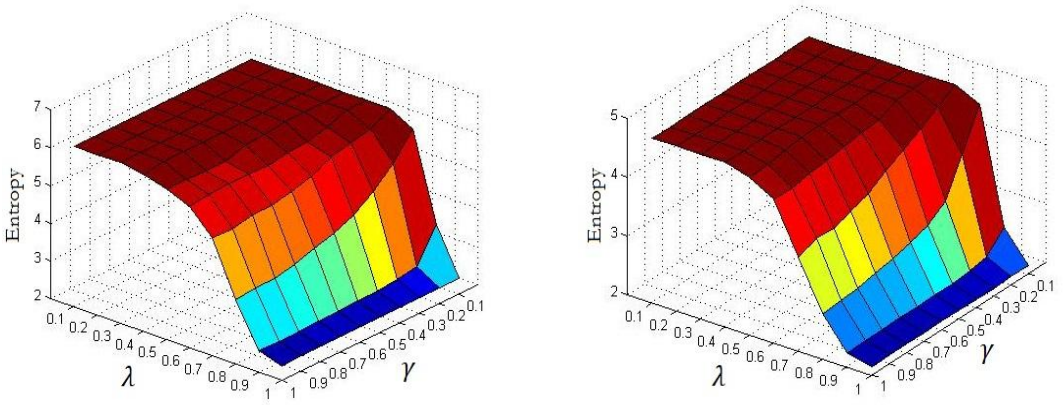

(a) (b)

Figure A-11: (a) Entropy graph for NC DA4-MRF classified AWIFS data (from Resourcesat-1) (b) Entropy graph for NC DA4-MRF classified AWIFS data (from Resourcesat-2).

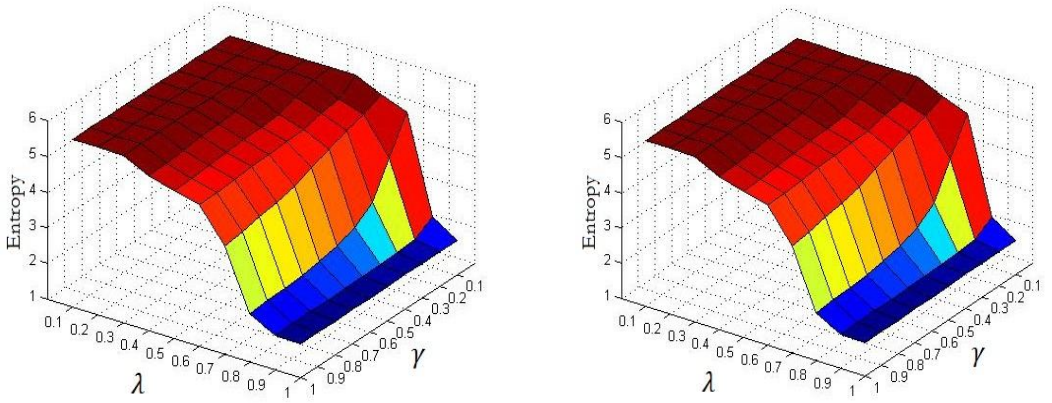

(a) (b)

Figure A-12: (a) Entropy graph for NC DA4-MRF classified LISS-III data (from Resourcesat-1) (b) Entropy graph for NC DA4-MRF classified LISS-III data (from Resourcesat-2)

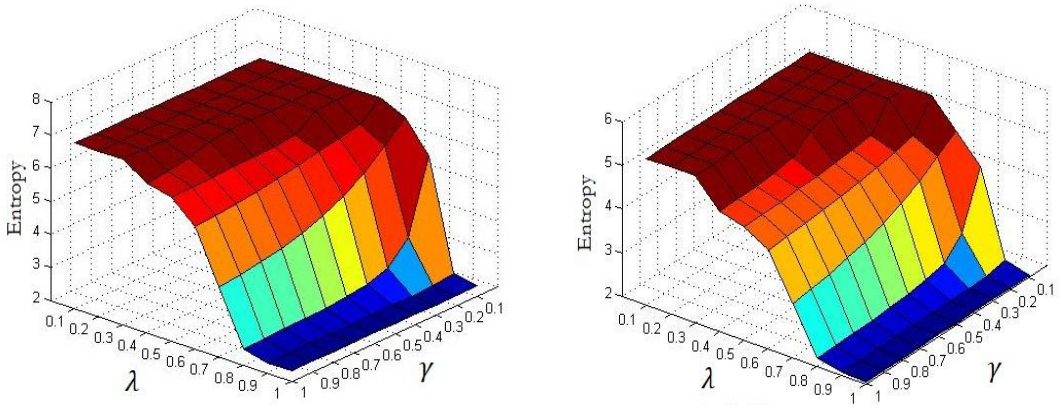

(a) (b)

Figure A-13: (a) Entropy graph for NC DA4-MRF classified LISS-IV data (from Resourcesat-1) (b) Entropy graph for NC DA4-MRF classified LISS-IV data (from Resourcesat-2).

A.4: LISS-IV Fractional Images

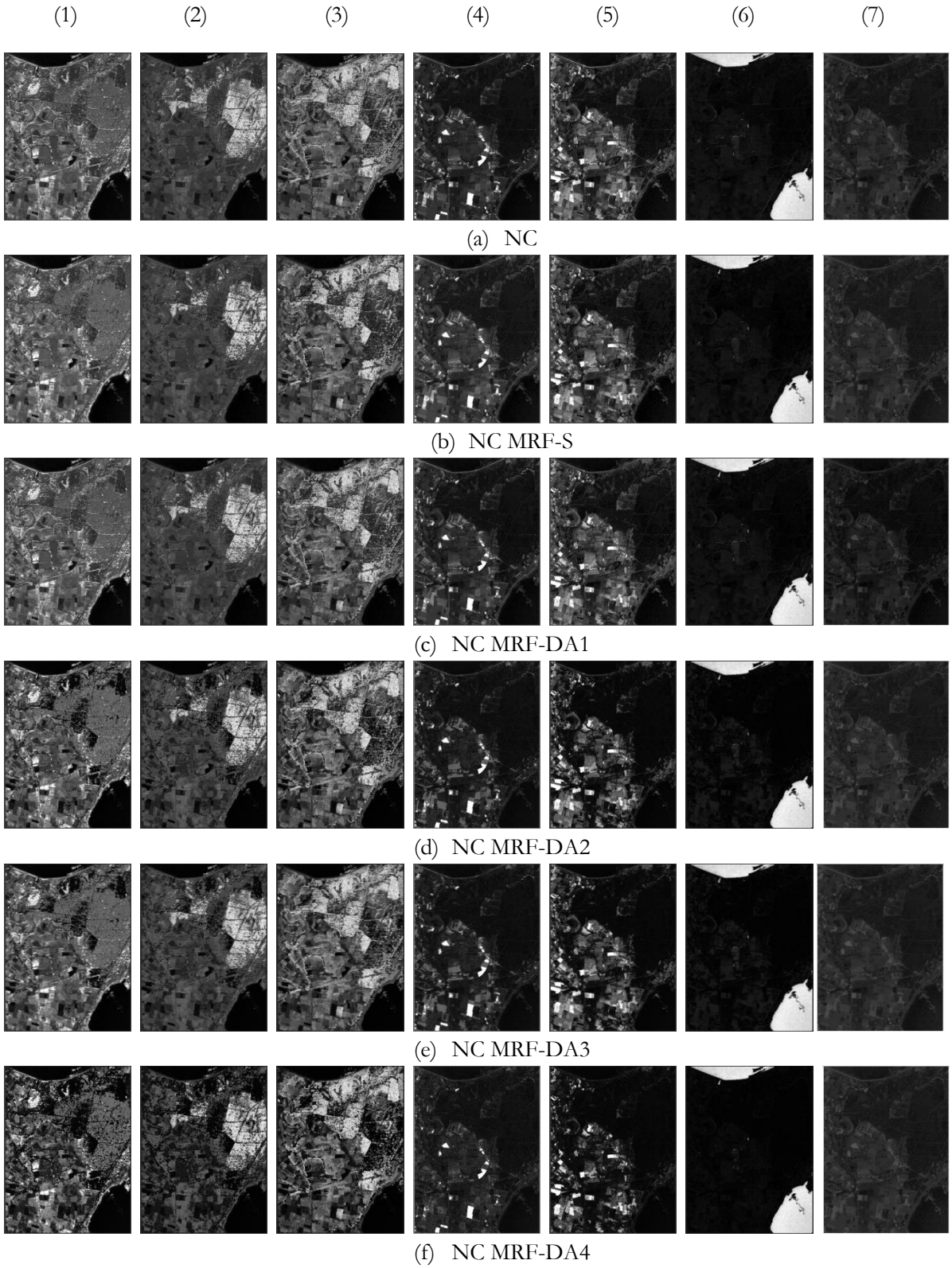

Figure A-14: Fractional images obtained from NC, NC S-MRF and NC DA-MRF classifiers on LISS-IV dataset from Resourcesat-1. The fractional images corresponds to Agriculture fields with crop (1), Sal Forest (2), Eucalyptus plantation (3), Dry agricultural field without crop (4), Moist agricultural field without crop (5), Water (6), Noise (7).

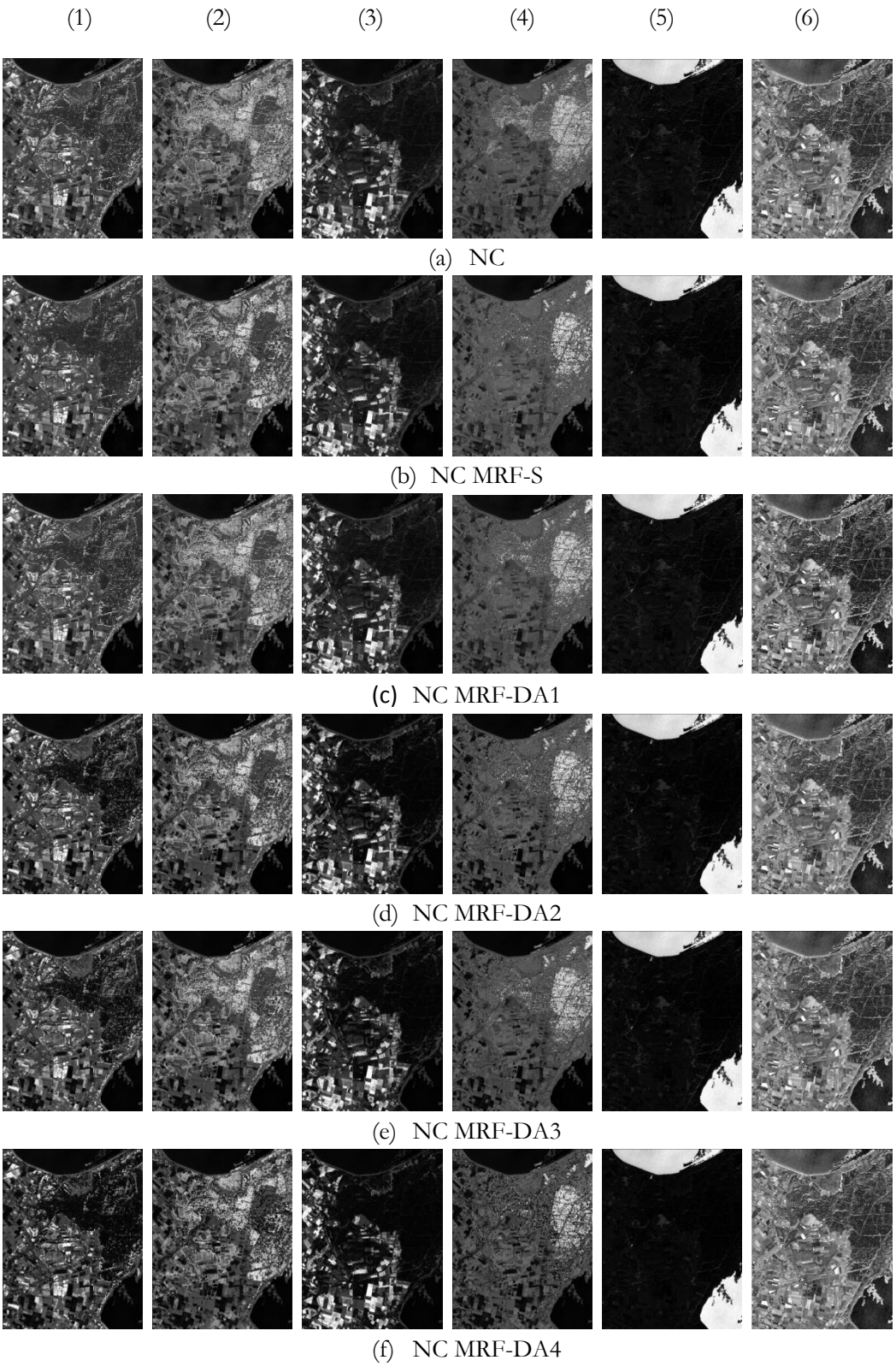

Figure A-15: Fractional images obtained from NC, NC S-MRF and NC DA-MRF classifiers on LISS-IV dataset from Resourcesat-2. The fractional images corresponds to Agriculture fields with crop (1), Sal Forest (2), Eucalyptus plantation (3), Dry agricultural field without crop (4), Moist agricultural field without crop (5), Water (6).

A.5 Noise Clustering Algorithm

For unsupervised case, the following steps should be followed to end up in an optimal solution.

1. Fix the number of clusters and initialize them; also assume a suitable value of delta (δ).
2. Membership values for each class are calculated using equation 3.2 -3.3.
3. Cluster centers are calculated using equation 3.3
4. Objective Function value is calculated using equation 3.1.
5. Steps 2 through 4 are repeated until the objective function value converges.

In this research work, information about the optimal cluster centers are available (i.e. signature class is available). Supervised classification is one in which the training data is available and in this light it is more suitable to replace the name 'noise clustering' by 'noise classifier'. Also, since the cluster centers are fixed, the first iteration of noise clustering algorithm will provide the optimal membership values.

APPENDIX B

B.1 Accuracy assessment of coarser resolution data (AWIFS from Resourcesat-1) against fine resolution (LISS-IV from Resourcesat-1) reference data, with all the classes trained.

Table B-1: Accuracy assessment results for NC classified AWIFS data (Resourcesat-1) against NC classified LISS-IV (Resourcesat-1) reference data

Accuracy assessment methods	FERM (%)	SCM (%)
Fuzzy user's accuracy (%)		
Agriculture fields with crop	82.92	86.05 ± 8.40
Sal Forest	89.37	90.72 ± 7.49
Eucalyptus plantation	89.87	91.98 ± 3.62
Dry agricultural field without crop	84.83	85.99 ± 13.85
Moist agricultural field without crop	68.85	76.06 ± 14.21
Water	87.89	91.59 ± 3.46
Fuzzy producer's accuracy (%)		
Agriculture fields with crop	90.75	93.31 ± 4.63
Sal Forest	89.92	91.97 ± 3.95
Eucalyptus plantation	75.89	82.36 ± 9.67
Dry agricultural field without crop	78.81	84.42 ± 12.74
Moist agricultural field without crop	91.32	93.50 ± 4.49
Water	72.01	78.08 ± 14.98
Fuzzy overall accuracy (%)	83.21	87.28 ± 8.04
Fuzzy Kappa	-	0.84 ± 0.09

Table B-2: Accuracy assessment results for NC S-MRF classified AWIFS data (Resourcesat-1) against NC S-MRF classified LISS-IV (Resourcesat-1) reference data

Accuracy assessment methods	FERM (%)	SCM (%)
Fuzzy user's accuracy (%)		
Agriculture fields with crop	82.85	89.11 ± 9.52
Sal Forest	88.29	90.47 ± 8.94
Eucalyptus plantation	91.69	94.65 ± 3.30
Dry agricultural field without crop	91.57	91.62 ± 8.37
Moist agricultural field without crop	70.41	80.18 ± 15.97
Water	89.31	93.96 ± 3.01
Fuzzy producer's accuracy (%)		
Agriculture fields with crop	91.08	95.16 ± 3.54
Sal Forest	91.65	94.76 ± 3.39
Eucalyptus plantation	77.27	86.90 ± 10.69
Dry agricultural field without crop	69.50	82.09 ± 15.96
Moist agricultural field without crop	86.84	94.67 ± 4.04
Water	71.13	81.76 ± 16.13
Fuzzy overall accuracy (%)	82.65	89.85 ± 8.31
Fuzzy Kappa	-	0.87 ± 0.10

Table B-3: Accuracy assessment results for NC DA1-MRF classified AWIFS data (Resourcesat-1) against NC DA1-MRF classified LISS-IV (Resourcesat-1) reference data

Accuracy assessment methods	FERM (%)	SCM (%)
Fuzzy user's accuracy (%)		
Agriculture fields with crop	81.10	72.45 ± 3.61
Sal Forest	94.73	90.11 ± 1.86
Eucalyptus plantation	93.13	88.25 ± 4.01
Dry agricultural field without crop	73.26	61.38 ± 4.95
Moist agricultural field without crop	64.56	52.04 ± 7.03
Water	91.18	84.38 ± 4.45
Fuzzy producer's accuracy (%)		
Agriculture fields with crop	92.70	88.93 ± 3.48
Sal Forest	84.79	80.22 ± 3.00
Eucalyptus plantation	70.78	67.10 ± 3.31
Dry agricultural field without crop	87.67	75.25 ± 13.58
Moist agricultural field without crop	86.22	87.92 ± 3.52
Water	62.93	57.34 ± 1.61
Fuzzy overall accuracy (%)	79.82	75.47 ± 3.72
Fuzzy Kappa	-	0.69 ± 0.04

Table B-4: Accuracy assessment results for NC DA2-MRF classified AWIFS data (Resourcesat-1) against NC DA2-MRF classified LISS-IV (Resourcesat-1) reference data

Accuracy assessment methods	FERM (%)	SCM (%)
Fuzzy user's accuracy (%)		
Agriculture fields with crop	74.95	88.87 ± 11.10
Sal Forest	81.18	90.59 ± 9.37
Eucalyptus plantation	88.16	95.41 ± 4.26
Dry agricultural field without crop	76.42	84.48 ± 15.51
Moist agricultural field without crop	52.50	77.21 ± 21.43
Water	80.92	92.83 ± 7.01
Fuzzy producer's accuracy (%)		
Agriculture fields with crop	89.70	93.87 ± 5.99
Sal Forest	90.98	94.78 ± 4.74
Eucalyptus plantation	73.00	83.66 ± 15.94
Dry agricultural field without crop	70.18	82.38 ± 17.55
Moist agricultural field without crop	85.13	93.12 ± 6.83
Water	59.91	88.29 ± 11.70
Fuzzy overall accuracy (%)	79.05	89.40 ± 10.33
Fuzzy Kappa	-	0.86 ± 0.13

Table B-5: Accuracy assessment results for NC DA3-MRF classified AWIFS data (Resourcesat-1) against NC DA3-MRF classified LISS-IV (Resourcesat-1) reference data.

Accuracy assessment methods	FERM (%)	SCM (%)
Fuzzy user's accuracy (%)		
Agriculture fields with crop	75.69	89.33 ± 10.55
Sal Forest	81.68	90.97 ± 8.70
Eucalyptus plantation	88.26	95.94 ± 3.75
Dry agricultural field without crop	75.48	83.67 ± 16.32
Moist agricultural field without crop	53.11	77.35 ± 22.47
Water	81.82	92.91 ± 6.96
Fuzzy producer's accuracy (%)		
Agriculture fields with crop	90.14	93.99 ± 5.69
Sal Forest	90.40	93.88 ± 5.75
Eucalyptus plantation	74.46	84.21 ± 15.56
Dry agricultural field without crop	72.11	84.28 ± 15.63
Moist agricultural field without crop	88.23	94.67 ± 5.29
Water	85.00	90.59 ± 9.40
Fuzzy overall accuracy (%)	83.50	89.87 ± 9.91
Fuzzy Kappa	-	0.87 ± 0.12

Table B-6: Accuracy assessment results for NC DA4-MRF classified AWIFS data (Resourcesat-1) against NC DA4-MRF classified LISS-IV (Resourcesat-1) reference data.

Accuracy assessment methods	FERM (%)	SCM (%)
Fuzzy user's accuracy (%)		
Agriculture fields with crop	60.19	87.39 ± 12.57
Sal Forest	65.67	89.50 ± 10.47
Eucalyptus plantation	81.06	96.50 ± 3.48
Dry agricultural field without crop	66.76	83.63 ± 16.36
Moist agricultural field without crop	39.43	78.09 ± 21.90
Water	76.46	92.84 ± 7.14
Fuzzy producer's accuracy (%)		
Agriculture fields with crop	92.26	93.33 ± 6.63
Sal Forest	92.99	94.89 ± 5.10
Eucalyptus plantation	78.35	82.92 ± 17.05
Dry agricultural field without crop	86.70	93.62 ± 6.36
Moist agricultural field without crop	89.98	90.33 ± 9.65
Water	92.01	94.90 ± 5.09
Fuzzy overall accuracy (%)	87.26	89.81 ± 10.17
Fuzzy Kappa	-	0.87 ± 0.12

B.1 Accuracy assessment of medium resolution data (LISS-III data from Resourcesat-1) against fine resolution (LISS-IV data from Resourcesat-1) reference data, with all the classes trained.

Table B-7: Accuracy assessment results for NC classified LISS-III data (Resourcesat-1) against NC classified LISS-IV (Resourcesat-1) reference data.

Accuracy assessment methods	FERM (%)	SCM (%)
Fuzzy user's accuracy (%)		
Agriculture fields with crop	84.13	87.45 ± 7.34
Sal Forest	91.32	92.76 ± 5.86
Eucalyptus plantation	91.42	93.49 ± 3.81
Dry agricultural field without crop	87.35	90.36 ± 8.75
Moist agricultural field without crop	82.07	86.99 ± 9.40
Water	92.95	96.06 ± 2.73
Fuzzy producer's accuracy (%)		
Agriculture fields with crop	94.57	95.89 ± 2.81
Sal Forest	91.09	92.75 ± 3.31
Eucalyptus plantation	84.65	88.32 ± 6.51
Dry agricultural field without crop	85.50	88.05 ± 11.53
Moist agricultural field without crop	92.76	94.07 ± 5.22
Water	86.51	87.84 ± 10.91
Fuzzy overall accuracy (%)	89.18	91.23 ± 5.99
Fuzzy Kappa	-	0.89 ± 0.07

Table B-8: Accuracy assessment results for NC S-MRF classified LISS-III data (Resourcesat-1) against NC S-MRF classified LISS-IV (Resourcesat-1) reference data.

Accuracy assessment methods	FERM (%)	SCM (%)
Fuzzy user's accuracy (%)		
Agriculture fields with crop	83.78	91.20 ± 7.77
Sal Forest	89.45	93.03 ± 6.47
Eucalyptus plantation	91.58	95.95 ± 3.20
Dry agricultural field without crop	91.64	93.39 ± 6.60
Moist agricultural field without crop	82.23	88.43 ± 9.98
Water	92.09	95.79 ± 2.60
Fuzzy producer's accuracy (%)		
Agriculture fields with crop	93.59	96.57 ± 2.79
Sal Forest	93.21	95.89 ± 2.98
Eucalyptus plantation	81.82	90.79 ± 7.60
Dry agricultural field without crop	84.75	88.38 ± 10.84
Moist agricultural field without crop	90.11	94.85 ± 4.53
Water	83.30	89.88 ± 9.78
Fuzzy overall accuracy (%)	87.77	93.10 ± 5.94
Fuzzy Kappa	-	0.91 ± 0.07

Table B-9: Accuracy assessment results for NC DA1-MRF classified LISS-III data (Resourcesat-1) against NC DA1-MRF classified LISS-IV (Resourcesat-1) reference data.

Accuracy assessment methods	FERM (%)	SCM (%)
Fuzzy user's accuracy (%)		
Agriculture fields with crop	74.65	61.01 ± 12.77
Sal Forest	94.19	84.89 ± 7.01
Eucalyptus plantation	94.10	86.49 ± 7.19
Dry agricultural field without crop	83.00	62.69 ± 14.50
Moist agricultural field without crop	78.55	63.10 ± 11.03
Water	96.21	82.66 ± 11.43
Fuzzy producer's accuracy (%)		
Agriculture fields with crop	97.93	90.15 ± 6.94
Sal Forest	90.37	77.67 ± 10.00
Eucalyptus plantation	77.40	64.39 ± 10.79
Dry agricultural field without crop	90.01	67.22 ± 18.74
Moist agricultural field without crop	93.31	79.46 ± 12.90
Water	83.37	65.46 ± 9.39
Fuzzy overall accuracy (%)	87.60	73.65 ± 10.89
Fuzzy Kappa	-	0.67 ± 0.13

Table B-10: Accuracy assessment results for NC DA2-MRF classified LISS-III data (Resourcesat-1) against NC DA2-MRF classified LISS-IV (Resourcesat-1) reference data.

Accuracy assessment methods	FERM (%)	SCM (%)
Fuzzy user's accuracy (%)		
Agriculture fields with crop	79.39	87.63 ± 12.34
Sal Forest	84.72	89.98 ± 9.99
Eucalyptus plantation	89.58	94.39 ± 5.55
Dry agricultural field without crop	93.95	94.58 ± 5.41
Moist agricultural field without crop	72.91	81.45 ± 18.54
Water	91.14	96.92 ± 3.07
Fuzzy producer's accuracy (%)		
Agriculture fields with crop	83.73	95.34 ± 4.64
Sal Forest	82.26	93.67 ± 6.26
Eucalyptus plantation	73.88	89.54 ± 10.43
Dry agricultural field without crop	54.74	75.66 ± 24.33
Moist agricultural field without crop	69.85	88.88 ± 11.11
Water	78.37	87.84 ± 12.15
Fuzzy overall accuracy (%)	76.98	90.55 ± 9.42
Fuzzy Kappa	-	0.87 ±0.12

Table B-11: Accuracy assessment results for NC DA3-MRF classified LISS-III data (Resourcesat-1) against NC DA3-MRF classified LISS-IV (Resourcesat-1) reference data.

Accuracy assessment methods	FERM (%)	SCM (%)
Fuzzy user's accuracy (%)		
Agriculture fields with crop	80.34	88.31 ± 11.68
Sal Forest	86.10	90.19 ± 9.77
Eucalyptus plantation	88.44	93.57 ± 6.40
Dry agricultural field without crop	92.03	93.72 ± 6.27
Moist agricultural field without crop	77.09	84.00 ± 15.99
Water	91.0	97.73 ± 2.26
Fuzzy producer's accuracy (%)		
Agriculture fields with crop	79.20	95.14 ± 4.85
Sal Forest	80.93	93.91 ± 6.05
Eucalyptus plantation	72.81	90.73 ± 9.24
Dry agricultural field without crop	60.35	78.03 ± 21.96
Moist agricultural field without crop	67.48	88.51 ± 11.48
Water	79.72	89.12 ± 10.87
Fuzzy overall accuracy (%)	75.60	91.06 ± 8.92
Fuzzy Kappa	-	0.88 ± 0.11

Table B-12: Accuracy assessment results for NC DA4-MRF classified LISS-III data (Resourcesat-1) against NC DA4-MRF classified LISS-IV (Resourcesat-1) reference data.

Accuracy assessment methods	FERM (%)	SCM (%)
Fuzzy user's accuracy (%)		
Agriculture fields with crop	58.49	87.23 ± 12.68
Sal Forest	65.65	89.93 ± 10.06
Eucalyptus plantation	77.07	95.17 ± 4.82
Dry agricultural field without crop	89.71	89.11 ± 9.66
Moist agricultural field without crop	54.27	80.78 ± 19.21
Water	90.37	95.69 ± 4.30
Fuzzy producer's accuracy (%)		
Agriculture fields with crop	93.17	94.79 ± 5.08
Sal Forest	92.42	94.65 ± 5.23
Eucalyptus plantation	84.68	86.70 ± 13.22
Dry agricultural field without crop	79.95	81.15 ± 18.76
Moist agricultural field without crop	90.71	90.80 ± 9.19
Water	93.06	93.41 ± 6.56
Fuzzy overall accuracy (%)	89.40	90.67 ± 9.24
Fuzzy Kappa	-	0.88 ± 0.11

B.2 Accuracy assessment of coarser resolution data (AWIFS data from Resourcesat-1) against medium resolution (LISS-III data from Resourcesat-1) reference data, with all the classes trained.

Table B-13: Accuracy assessment results for NC classified AWIFS data (Resourcesat-1) against NC classified LISS-III (Resourcesat-1) reference data.

Accuracy assessment methods	FERM (%)	SCM (%)
Fuzzy user's accuracy (%)		
Agriculture fields with crop	91.57	92.62 ± 5.11
Sal Forest	90.47	91.44 ± 6.12
Eucalyptus plantation	90.42	92.37 ± 4.05
Dry agricultural field without crop	90.00	89.91 ± 9.87
Moist agricultural field without crop	79.64	84.67 ± 11.66
Water	93.24	95.89 ± 3.02
Fuzzy producer's accuracy (%)		
Agriculture fields with crop	89.78	92.79 ± 4.71
Sal Forest	92.58	94.69 ± 3.39
Eucalyptus plantation	84.12	89.0 ± 6.85
Dry agricultural field without crop	79.16	85.53 ± 11.62
Moist agricultural field without crop	91.33	93.67 ± 5.38
Water	85.24	88.91 ± 8.82
Fuzzy overall accuracy (%)	87.82	91.32 ± 6.13
Fuzzy Kappa	-	0.89 ± 0.07

Table B-14: Accuracy assessment results for NC S-MRF classified AWIFS data (Resourcesat-1) against NC S-MRF classified LISS-III (Resourcesat-1) reference data.

Accuracy assessment methods	FERM (%)	SCM (%)
Fuzzy user's accuracy (%)		
Agriculture fields with crop	92.63	95.29 ± 4.13
Sal Forest	89.95	93.57 ± 5.03
Eucalyptus plantation	90.55	94.70 ± 3.42
Dry agricultural field without crop	91.56	90.79 ± 9.20
Moist agricultural field without crop	78.53	86.87 ± 12.15
Water	92.36	96.79 ± 2.42
Fuzzy producer's accuracy (%)		
Agriculture fields with crop	90.02	94.52 ± 4.25
Sal Forest	92.46	95.76 ± 3.38
Eucalyptus plantation	83.46	92.30 ± 5.93
Dry agricultural field without crop	82.44	88.07 ± 10.78
Moist agricultural field without crop	91.62	95.58 ± 3.72
Water	85.98	90.06 ± 9.28
Fuzzy overall accuracy (%)	88.08	93.34 ± 5.54
Fuzzy Kappa	-	0.91 ± 0.06

Table B-15: Accuracy assessment results for NC DA1-MRF classified AWIFS data (Resourcesat-1) against NC DA1-MRF classified LISS-III (Resourcesat-1) reference data.

Accuracy assessment methods	FERM (%)	SCM (%)
Fuzzy user's accuracy (%)		
Agriculture fields with crop	94.86	84.32 ± 8.91
Sal Forest	93.07	79.60 ± 10.20
Eucalyptus plantation	93.39	81.48 ± 9.96
Dry agricultural field without crop	82.04	55.19 ± 10.53
Moist agricultural field without crop	74.34	54.97 ± 15.45
Water	94.78	78.28 ± 15.59
Fuzzy producer's accuracy (%)		
Agriculture fields with crop	84.77	74.46 ± 10.38
Sal Forest	89.89	79.04 ± 10.32
Eucalyptus plantation	81.14	71.55 ± 12.16
Dry agricultural field without crop	91.61	68.20 ± 21.00
Moist agricultural field without crop	85.27	80.84 ± 11.33
Water	75.91	65.78 ± 12.96
Fuzzy overall accuracy (%)	84.33	73.76 ± 12.21
Fuzzy Kappa	-	0.67 ± 0.15

Table B-16: Accuracy assessment results for NC DA2-MRF classified AWIFS data (Resourcesat-1) against NC DA2-MRF classified LISS-III (Resourcesat-1) reference data.

Accuracy assessment methods	FERM (%)	SCM (%)
Fuzzy user's accuracy (%)		
Agriculture fields with crop	82.40	96.35 ± 3.64
Sal Forest	81.03	95.97 ± 3.69
Eucalyptus plantation	82.85	97.05 ± 2.54
Dry agricultural field without crop	53.33	79.81 ± 20.18
Moist agricultural field without crop	52.66	87.48 ± 12.51
Water	78.53	92.95 ± 7.04
Fuzzy producer's accuracy (%)		
Agriculture fields with crop	91.79	94.63 ± 4.90
Sal Forest	93.98	95.50 ± 4.25
Eucalyptus plantation	84.46	90.84 ± 9.09
Dry agricultural field without crop	96.87	97.58 ± 2.41
Moist agricultural field without crop	88.82	94.39 ± 5.60
Water	76.89	97.22 ± 2.77
Fuzzy overall accuracy (%)	87.80	94.18 ± 5.62
Fuzzy Kappa	-	0.92 ± 0.07

Table B-17: Accuracy assessment results for NC DA3-MRF classified AWIFS data (Resourcesat-1) against NC DA3-MRF classified LISS-III (Resourcesat-1) reference data.

Accuracy assessment methods	FERM (%)	SCM (%)
Fuzzy user's accuracy (%)		
Agriculture fields with crop	82.87	96.40±3.49
Sal Forest	80.76	96.26±3.61
Eucalyptus plantation	82.76	96.52±2.97
Dry agricultural field without crop	53.57	79.05±20.94
Moist agricultural field without crop	55.04	87.48±12.51
Water	80.06	93.53±6.46
Fuzzy producer's accuracy (%)		
Agriculture fields with crop	90.93	94.16±5.58
Sal Forest	92.00	94.24±5.34
Eucalyptus plantation	87.21	92.27±7.60
Dry agricultural field without crop	95.32	96.59±3.40
Moist agricultural field without crop	90.64	94.12±5.87
Water	93.16	96.58±3.41
Fuzzy overall accuracy (%)	90.60	94.10±5.71
Fuzzy Kappa	-	0.92±0.07

Table B-18: Accuracy assessment results for NC DA4-MRF classified AWIFS data (Resourcesat-1) against NC DA4-MRF classified LISS-III (Resourcesat-1) reference data.

Accuracy assessment methods	FERM (%)	SCM (%)
Fuzzy user's accuracy (%)		
Agriculture fields with crop	92.03	96.08 ± 3.88
Sal Forest	90.72	95.47 ± 4.30
Eucalyptus plantation	92.53	96.35 ± 3.31
Dry agricultural field without crop	78.23	84.50 ± 15.49
Moist agricultural field without crop	78.38	88.22 ± 11.53
Water	84.53	92.41 ± 7.58
Fuzzy producer's accuracy (%)		
Agriculture fields with crop	89.57	94.80 ± 4.84
Sal Forest	90.36	95.35 ± 4.43
Eucalyptus plantation	82.97	92.59 ± 7.23
Dry agricultural field without crop	70.41	87.60 ± 12.34
Moist agricultural field without crop	84.40	94.43 ± 5.56
Water	89.40	93.87 ± 6.10
Fuzzy overall accuracy (%)	86.40	93.87 ± 5.94
Fuzzy Kappa	-	0.92 ± 0.07

B.3 Accuracy assessment of coarser resolution data (AWIFS data from Resourcesat-2) against fine resolution (LISS-IV data from Resourcesat-2) reference data, with all the classes trained.

Table B-19: Accuracy assessment results for NC classified AWIFS data (Resourcesat-2) against NC classified LISS-IV (Resourcesat-2) reference data.

Accuracy assessment methods	FERM (%)	SCM (%)
Fuzzy user's accuracy (%)		
Agriculture fields with crop	89.95	90.25 ± 8.27
Eucalyptus plantation	90.02	91.56 ± 5.20
Dry agricultural field without crop	88.86	88.53 ± 11.30
Sal Forest	89.81	91.44 ± 4.86
Water	98.29	98.25 ± 1.73
Fuzzy producer's accuracy (%)		
Agriculture fields with crop	80.49	91.48 ± 6.16
Eucalyptus plantation	73.10	90.89 ± 7.22
Dry agricultural field without crop	79.23	93.26 ± 5.87
Sal Forest	83.90	93.15 ± 5.65
Water	74.59	89.20 ± 7.13
Fuzzy overall accuracy (%)	78.18	91.64 ± 6.41
Fuzzy Kappa	-	0.89 ± 0.08

Table B-20: Accuracy assessment results for NC S-MRF classified AWIFS data (Resourcesat-2) against NC S-MRF classified LISS-IV (Resourcesat-2) reference data.

Accuracy assessment methods	FERM (%)	SCM (%)
Fuzzy user's accuracy (%)		
Agriculture fields with crop	85.62	89.45 ± 8.07
Eucalyptus plantation	87.40	94.53 ± 3.79
Dry agricultural field without crop	79.24	84.00 ± 12.23
Sal Forest	85.73	93.20 ± 4.42
Water	98.30	98.45 ± 1.44
Fuzzy producer's accuracy (%)		
Agriculture fields with crop	84.76	92.77 ± 4.92
Eucalyptus plantation	77.10	89.72 ± 7.71
Dry agricultural field without crop	83.19	93.26 ± 5.67
Sal Forest	87.72	93.56 ± 4.70
Water	76.60	88.62 ± 8.51
Fuzzy overall accuracy (%)	81.81	91.58 ± 6.31
Fuzzy Kappa	-	0.89 ± 0.07

Table B-21: Accuracy assessment results for NC DA1-MRF classified AWIFS data (Resourcesat-2) against NC DA1-MRF classified LISS-IV (Resourcesat-2) reference data.

Accuracy assessment methods	FERM (%)	SCM (%)
Fuzzy user's accuracy (%)		
Agriculture fields with crop	85.07	75.37 ± 5.60
Eucalyptus plantation	88.55	82.58 ± 4.85
Dry agricultural field without crop	77.83	65.97 ± 8.27
Sal Forest	85.72	77.57 ± 5.37
Water	95.97	87.24 ± 6.55
Fuzzy producer's accuracy (%)		
Agriculture fields with crop	85.35	78.96 ± 5.43
Eucalyptus plantation	80.40	72.37 ± 7.68
Dry agricultural field without crop	84.46	77.30 ± 6.32
Sal Forest	91.31	85.98 ± 4.50
Water	81.80	73.83 ± 5.84
Fuzzy overall accuracy (%)	84.57	77.48 ± 6.14
Fuzzy Kappa	-	0.71 ± 0.07

Table B-22: Accuracy assessment results for NC DA2-MRF classified AWIFS data (Resourcesat-2) against NC DA2-MRF classified LISS-IV (Resourcesat-2) reference data.

Accuracy assessment methods	FERM (%)	SCM (%)
Fuzzy user's accuracy (%)		
Agriculture fields with crop	79.76	90.43 ± 9.56
Eucalyptus plantation	85.94	96.49 ± 3.45
Dry agricultural field without crop	76.13	84.80 ± 15.19
Sal Forest	80.26	94.10 ± 5.07
Water	93.68	95.34 ± 4.44
Fuzzy producer's accuracy (%)		
Agriculture fields with crop	80.16	91.67 ± 7.76
Eucalyptus plantation	75.48	89.30 ± 10.25
Dry agricultural field without crop	77.96	92.46 ± 7.52
Sal Forest	87.19	93.62 ± 6.19
Water	89.60	95.76 ± 4.22
Fuzzy overall accuracy (%)	81.83	92.38 ± 7.36
Fuzzy Kappa	-	0.90 ± 0.09

Table B-23: Accuracy assessment results for NC DA3-MRF classified AWIFS data (Resourcesat-2) against NC DA3-MRF classified LISS-IV (Resourcesat-2) reference data.

Accuracy assessment methods	FERM (%)	SCM (%)
Fuzzy user's accuracy (%)		
Agriculture fields with crop	82.02	90.75 ± 8.92
Eucalyptus plantation	86.61	96.04 ± 3.73
Dry agricultural field without crop	75.94	85.05 ± 14.73
Sal Forest	82.23	93.31 ± 5.79
Water	94.64	95.49 ± 4.50
Fuzzy producer's accuracy (%)		
Agriculture fields with crop	78.74	90.85 ± 8.57
Eucalyptus plantation	75.40	89.34 ± 10.07
Dry agricultural field without crop	81.21	93.01 ± 6.92
Sal Forest	86.11	93.30 ± 6.40
Water	87.47	94.89 ± 4.91
Fuzzy overall accuracy (%)	81.40	92.08 ± 7.56
Fuzzy Kappa	-	0.90 ± 0.09

Table B-24: Accuracy assessment results for NC DA4-MRF classified AWIFS data (Resourcesat-2) against NC DA4-MRF classified LISS-IV (Resourcesat-2) reference data.

Accuracy assessment methods	FERM (%)	SCM (%)
Fuzzy user's accuracy (%)		
Agriculture fields with crop	70.83	89.65 ± 10.29
Eucalyptus plantation	76.84	95.62 ± 4.27
Dry agricultural field without crop	70.18	85.88 ± 14.07
Sal Forest	73.01	93.13 ± 6.44
Water	92.71	95.52 ± 4.47
Fuzzy producer's accuracy (%)		
Agriculture fields with crop	84.03	91.41 ± 8.43
Eucalyptus plantation	79.61	88.29 ± 11.53
Dry agricultural field without crop	86.61	92.36 ± 7.61
Sal Forest	90.95	94.39 ± 5.60
Water	86.11	94.43 ± 5.24
Fuzzy overall accuracy (%)	85.27	92.00 ± 7.85
Fuzzy Kappa	-	0.89 ± 0.09

B.4 Accuracy assessment of medium resolution data (LISS-III data from Resourcesat-2) against fine resolution (LISS-IV data from Resourcesat-2) reference data, with all the classes trained.

Table B-25: Accuracy assessment results for NC classified LISS-III data (Resourcesat-2) against NC classified LISS-IV (Resourcesat-2) reference data.

Accuracy assessment methods	FERM (%)	SCM (%)
Fuzzy user's accuracy (%)		
Agriculture fields with crop	87.73	90.71 ± 6.48
Eucalyptus plantation	89.29	91.77 ± 3.85
Dry agricultural field without crop	85.55	90.53 ± 7.10
Sal Forest	87.56	89.98 ± 5.57
Water	93.62	96.32 ± 3.33
Fuzzy producer's accuracy (%)		
Agriculture fields with crop	87.53	91.45 ± 4.64
Eucalyptus plantation	86.62	90.86 ± 5.31
Dry agricultural field without crop	81.50	87.56 ± 9.09
Sal Forest	92.60	94.66 ± 2.75
Water	91.43	93.73 ± 4.76
Fuzzy overall accuracy (%)	88.14	91.78 ± 5.17
Fuzzy Kappa	-	0.89 ± 0.06

Table B-26: Accuracy assessment results for NC S-MRF classified LISS-III data (Resourcesat-2) against NC S-MRF classified LISS-IV (Resourcesat-2) reference data.

Accuracy assessment methods	FERM (%)	SCM (%)
Fuzzy user's accuracy (%)		
Agriculture fields with crop	86.46	91.26 ± 7.64
Eucalyptus plantation	86.48	94.24 ± 4.15
Dry agricultural field without crop	90.68	94.40 ± 4.00
Sal Forest	85.77	92.20 ± 6.69
Water	92.97	95.94 ± 3.18
Fuzzy producer's accuracy (%)		
Agriculture fields with crop	86.55	95.04 ± 3.41
Eucalyptus plantation	85.42	93.36 ± 5.19
Dry agricultural field without crop	73.75	86.82 ± 11.16
Sal Forest	92.99	97.01 ± 2.11
Water	87.63	93.95 ± 5.46
Fuzzy overall accuracy (%)	85.73	93.49 ± 5.25
Fuzzy Kappa	-	0.91 ± 0.06

Table B-27: Accuracy assessment results for NC DA1-MRF classified LISS-III data (Resourcesat-2) against NC DA1-MRF classified LISS-IV (Resourcesat-2) reference data.

Accuracy assessment methods	FERM (%)	SCM (%)
Fuzzy user's accuracy (%)		
Agriculture fields with crop	86.69	72.95 ± 9.76
Eucalyptus plantation	89.86	80.99 ± 8.47
Dry agricultural field without crop	87.65	73.91 ± 12.24
Sal Forest	85.93	73.77 ± 9.52
Water	94.92	82.75 ± 10.78
Fuzzy producer's accuracy (%)		
Agriculture fields with crop	89.51	79.84 ± 10.02
Eucalyptus plantation	82.50	73.75 ± 10.38
Dry agricultural field without crop	80.46	68.09 ± 10.60
Sal Forest	92.20	84.21 ± 8.42
Water	89.38	77.79 ± 10.18
Fuzzy overall accuracy (%)	86.79	76.79 ± 10.01
Fuzzy Kappa	-	0.70 ± 0.12

Table B-28: Accuracy assessment results for NC DA2-MRF classified LISS-III data (Resourcesat-2) against NC DA2-MRF classified LISS-IV (Resourcesat-2) reference data.

Accuracy assessment methods	FERM (%)	SCM (%)
Fuzzy user's accuracy (%)		
Agriculture fields with crop	81.78	89.16 ± 10.83
Eucalyptus plantation	87.47	94.79 ± 5.20
Dry agricultural field without crop	83.50	89.58 ± 10.38
Sal Forest	82.86	90.47 ± 9.31
Water	93.31	96.71 ± 3.28
Fuzzy producer's accuracy (%)		
Agriculture fields with crop	69.75	90.19 ± 9.69
Eucalyptus plantation	76.39	91.41 ± 8.43
Dry agricultural field without crop	70.67	89.52 ± 10.47
Sal Forest	85.82	95.82 ± 4.17
Water	86.29	93.22 ± 6.77
Fuzzy overall accuracy (%)	77.91	92.18 ± 7.76
Fuzzy Kappa	-	0.90 ± 0.09

Table B-29: Accuracy assessment results for NC DA3-MRF classified LISS-III data (Resourcesat-2) against NC DA3-MRF classified LISS-IV (Resourcesat-2) reference data.

Accuracy assessment methods	FERM (%)	SCM (%)
Fuzzy user's accuracy (%)		
Agriculture fields with crop	79.49	87.74 ± 12.15
Eucalyptus plantation	84.85	93.08 ± 6.91
Dry agricultural field without crop	81.98	87.55 ± 12.44
Sal Forest	82.18	88.47 ± 10.91
Water	94.26	97.67 ± 2.32
Fuzzy producer's accuracy (%)		
Agriculture fields with crop	66.47	87.82 ± 12.08
Eucalyptus plantation	71.60	89.45 ± 9.94
Dry agricultural field without crop	70.85	88.19 ± 11.80
Sal Forest	85.24	95.26 ± 4.72
Water	87.24	92.97 ± 7.02
Fuzzy overall accuracy (%)	76.46	90.97 ± 8.86
Fuzzy Kappa	-	0.88 ± 0.11

Table B-30: Accuracy assessment results for NC DA4-MRF classified LISS-III data (Resourcesat-2) against NC DA4-MRF classified LISS-IV (Resourcesat-2) reference data.

Accuracy assessment methods	FERM (%)	SCM (%)
Fuzzy user's accuracy (%)		
Agriculture fields with crop	79.44	88.41 ± 11.58
Eucalyptus plantation	78.29	93.19 ± 6.74
Dry agricultural field without crop	75.23	10.24 ± 11.78
Sal Forest	81.12	89.31 ± 10.68
Water	84.65	97.82 ± 2.17
Fuzzy producer's accuracy (%)		
Agriculture fields with crop	83.31	88.24 ± 11.73
Eucalyptus plantation	85.55	89.74 ± 10.24
Dry agricultural field without crop	82.12	89.59 ± 10.40
Sal Forest	92.38	93.82 ± 6.07
Water	91.42	96.14 ± 3.85
Fuzzy overall accuracy (%)	89.37	91.92 ± 8.04
Fuzzy Kappa	-	0.89 ± 0.10

B.5 Accuracy assessment of coarse resolution data (AWIFS data from Resourcesat-2) against medium resolution (LISS-III data from Resourcesat-2) reference data, with all the classes trained.

Table B-31: Accuracy assessment results for NC classified AWIFS data (Resourcesat-2) against NC classified LISS-III (Resourcesat-2) reference data.

Accuracy assessment methods	FERM (%)	SCM (%)
Fuzzy user's accuracy (%)		
Agriculture fields with crop	92.23	93.04 ± 6.17
Eucalyptus plantation	93.91	94.83 ± 3.55
Dry agricultural field without crop	81.00	83.01 ± 16.77
Sal Forest	93.02	94.20 ± 3.17
Water	97.56	97.87 ± 2.02
Fuzzy producer's accuracy (%)		
Agriculture fields with crop	81.59	92.22 ± 6.17
Eucalyptus plantation	75.89	91.0 ± 7.20
Dry agricultural field without crop	80.68	95.02 ± 4.46
Sal Forest	81.46	92.27 ± 6.70
Water	78.57	93.12 ± 5.96
Fuzzy overall accuracy (%)	79.52	92.48 ± 6.28
Fuzzy Kappa	-	0.90 ± 0.07

Table B-32: Accuracy assessment results for NC S-MRF classified AWIFS data (Resourcesat-2) against NC S-MRF classified LISS-III (Resourcesat-2) reference data.

Accuracy assessment methods	FERM (%)	SCM (%)
Fuzzy user's accuracy (%)		
Agriculture fields with crop	87.31	93.15 ± 6.00
Eucalyptus plantation	89.83	95.36 ± 3.18
Dry agricultural field without crop	74.71	83.99 ± 15.06
Sal Forest	89.22	95.61 ± 2.80
Water	97.10	98.39 ± 1.60
Fuzzy producer's accuracy (%)		
Agriculture fields with crop	87.53	94.12 ± 4.81
Eucalyptus plantation	83.15	92.25 ± 6.52
Dry agricultural field without crop	88.98	96.37 ± 2.83
Sal Forest	86.50	92.57 ± 6.21
Water	83.06	93.34 ± 6.04
Fuzzy overall accuracy (%)	85.55	93.45 ± 5.53
Fuzzy Kappa	-	0.91 ± 0.06

Table B-33: Accuracy assessment results for NC DA1-MRF classified AWIFS data (Resourcesat-2) against NC DA1-MRF classified LISS-III (Resourcesat-2) reference data.

Accuracy assessment methods	FERM (%)	SCM (%)
Fuzzy user's accuracy (%)		
Agriculture fields with crop	85.07	81.47 ± 5.82
Eucalyptus plantation	88.55	85.54 ± 5.86
Dry agricultural field without crop	77.83	61.88 ± 9.16
Sal Forest	85.72	82.07 ± 6.64
Water	95.97	86.66 ± 7.77
Fuzzy producer's accuracy (%)		
Agriculture fields with crop	85.35	78.73 ± 7.32
Eucalyptus plantation	80.40	77.00 ± 7.53
Dry agricultural field without crop	84.46	81.77 ± 6.88
Sal Forest	91.31	83.53 ± 5.33
Water	81.80	74.97 ± 9.28
Fuzzy overall accuracy (%)	84.57	79.28 ± 7.19
Fuzzy Kappa		0.73 ± 0.09

Table B-34: Accuracy assessment results for NC DA2-MRF classified AWIFS data (Resourcesat-2) against NC DA2-MRF classified LISS-III (Resourcesat-2) reference data.

Accuracy assessment methods	FERM (%)	SCM (%)
Fuzzy user's accuracy (%)		
Agriculture fields with crop	69.19	89.92 ± 9.97
Eucalyptus plantation	83.47	95.52 ± 4.00
Dry agricultural field without crop	62.27	82.27 ± 17.60
Sal Forest	82.05	95.45 ± 4.19
Water	85.82	90.25 ± 9.74
Fuzzy producer's accuracy (%)		
Agriculture fields with crop	83.28	90.73 ± 9.08
Eucalyptus plantation	83.25	89.58 ± 10.06
Dry agricultural field without crop	81.59	90.62 ± 9.37
Sal Forest	86.86	91.08 ± 8.43
Water	88.48	95.94 ± 4.05
Fuzzy overall accuracy (%)	84.73	91.23 ± 8.51
Fuzzy Kappa	-	0.88 ± 0.10

Table B-35: Accuracy assessment results for NC DA3-MRF classified AWIFS data (Resourcesat-2) against NC DA3-MRF classified LISS-III (Resourcesat-2) reference data.

Accuracy assessment methods	FERM (%)	SCM (%)
Fuzzy user's accuracy (%)		
Agriculture fields with crop	74.80	90.19 ± 9.80
Eucalyptus plantation	83.17	94.72 ± 5.09
Dry agricultural field without crop	60.63	81.85 ± 18.14
Sal Forest	83.62	94.31 ± 5.35
Water	86.85	91.61 ± 8.38
Fuzzy producer's accuracy (%)		
Agriculture fields with crop	84.09	90.50 ± 9.27
Eucalyptus plantation	82.09	88.58 ± 11.25
Dry agricultural field without crop	81.23	90.45 ± 9.54
Sal Forest	83.57	89.47 ± 10.34
Water	87.68	95.43 ± 4.56
Fuzzy overall accuracy (%)	83.72	90.66 ± 9.22
Fuzzy Kappa	-	0.88 ± 0.11

Table B-36: Accuracy assessment results for NC DA4-MRF classified AWIFS data (Resourcesat-2) against NC DA4-MRF classified LISS-III (Resourcesat-2) reference data.

Accuracy assessment methods	FERM (%)	SCM (%)
Fuzzy user's accuracy (%)		
Agriculture fields with crop	58.57	89.08 ± 10.91
Eucalyptus plantation	70.66	94.42 ± 5.25
Dry agricultural field without crop	54.15	83.78 ± 16.17
Sal Forest	73.00	95.29 ± 4.52
Water	89.15	94.70 ± 5.29
Fuzzy producer's accuracy (%)		
Agriculture fields with crop	88.78	92.93 ± 7.06
Eucalyptus plantation	84.36	89.45 ± 10.34
Dry agricultural field without crop	85.31	89.92 ± 10.07
Sal Forest	86.88	90.37 ± 9.32
Water	90.64	96.35 ± 3.63
Fuzzy overall accuracy (%)	87.25	91.80 ± 8.07
Fuzzy Kappa	-	0.89 ± 0.10

B.6 Accuracy assessment of coarse resolution data (AWIFS data from Resourcesat-1) against fine resolution (LISS-IV data from Resourcesat-1) reference data, with one untrained classes.

Table B-37: Accuracy assessment results for NC classified AWIFS data (Resourcesat-1) against NC classified LISS-IV (Resourcesat-1) reference data.

Accuracy assessment methods	FERM (%)	SCM (%)
Fuzzy user's accuracy (%)		
Sal Forest	72.37	91.68 ± 7.57
Eucalyptus plantation	81.98	94.42 ± 3.58
Dry agricultural field without crop	74.85	87.36 ± 12.25
Moist agricultural field without crop	56.76	84.91 ± 13.36
Water	88.01	93.25 ± 2.22
Fuzzy producer's accuracy (%)		
Sal Forest	95.27	96.16 ± 1.59
Eucalyptus plantation	88.74	90.40 ± 7.99
Dry agricultural field without crop	90.20	91.29 ± 7.56
Moist agricultural field without crop	94.44	95.69 ± 2.04
Water	82.63	84.11 ± 13.45
Fuzzy overall accuracy (%)	90.05	91.15 ± 6.86
Fuzzy Kappa	-	0.88 ± 0.09

Table B-38: Accuracy assessment results for NC S-MRF classified AWIFS data (Resourcesat-1) against NC S-MRF classified LISS-IV (Resourcesat-1) reference data.

Accuracy assessment methods	FERM (%)	SCM (%)
Fuzzy user's accuracy (%)		
Sal Forest	69.96	91.07 ± 7.85
Eucalyptus plantation	80.00	94.62 ± 3.26
Dry agricultural field without crop	82.61	91.86 ± 8.13
Moist agricultural field without crop	57.52	86.76 ± 12.38
Water	87.78	94.45 ± 2.41
Fuzzy producer's accuracy (%)		
Sal Forest	95.45	96.97 ± 1.46
Eucalyptus plantation	89.07	92.15 ± 6.50
Dry agricultural field without crop	80.26	88.22 ± 9.64
Moist agricultural field without crop	92.70	96.12 ± 2.06
Water	80.31	84.32 ± 13.54
Fuzzy overall accuracy (%)	88.84	91.96 ± 6.37
Fuzzy Kappa	-	0.89 ± 0.08

Table B-39: Accuracy assessment results for NC DA4-MRF classified AWIFS data (Resourcesat-1) against NC DA4-MRF classified LISS-IV (Resourcesat-1) reference data.

Accuracy assessment methods	FERM (%)	SCM (%)
Fuzzy user's accuracy (%)		
Sal Forest	52.89	93.17 ± 6.78
Eucalyptus plantation	66.80	97.71 ± 2.28
Dry agricultural field without crop	55.58	88.72 ± 11.27
Moist agricultural field without crop	31.03	85.80 ± 14.19
Water	68.69	94.24 ± 5.72
Fuzzy producer's accuracy (%)		
Sal Forest	97.36	97.95 ± 2.03
Eucalyptus plantation	90.29	91.13 ± 8.82
Dry agricultural field without crop	77.57	85.90 ± 14.07
Moist agricultural field without crop	91.82	94.26 ± 5.72
Water	92.84	96.59 ± 3.40
Fuzzy overall accuracy (%)	92.03	93.77 ± 6.20
Fuzzy Kappa	-	0.91 ± 0.08

B.7 Accuracy assessment of medium resolution data (LISS-III data from Resourcesat-1) against fine resolution (LISS-IV data from Resourcesat-1) reference data, with one untrained classes.

Table B-40: Accuracy assessment results for NC classified LISS-III data (Resourcesat-1) against NC classified LISS-IV (Resourcesat-1) reference data.

Accuracy assessment methods	FERM (%)	SCM (%)
Fuzzy user's accuracy (%)		
Sal Forest	74.14	95.97 ± 3.30
Eucalyptus plantation	79.57	96.77 ± 2.01
Dry agricultural field without crop	75.50	93.93 ± 6.06
Moist agricultural field without crop	68.50	94.02 ± 5.81
Water	88.22	96.03 ± 2.24
Fuzzy producer's accuracy (%)		
Sal Forest	96.17	96.54 ± 2.01
Eucalyptus plantation	94.69	94.66 ± 4.36
Dry agricultural field without crop	94.77	95.78 ± 3.88
Moist agricultural field without crop	96.65	97.32 ± 1.96
Water	95.61	95.39 ± 4.11
Fuzzy overall accuracy (%)	95.54	95.75 ± 3.32
Fuzzy Kappa	-	0.94 ± 0.04

Table B-41: Accuracy assessment results for NC S-MRF classified LISS-III data (Resourcesat-1) against NC S-MRF classified LISS-IV (Resourcesat-1) reference data.

Accuracy assessment methods	FERM (%)	SCM (%)
Fuzzy user's accuracy (%)		
Sal Forest	72.06	95.13 ± 4.57
Eucalyptus plantation	76.50	96.87 ± 2.27
Dry agricultural field without crop	78.53	94.02 ± 5.97
Moist agricultural field without crop	67.10	93.47 ± 6.16
Water	87.20	95.60 ± 2.95
Fuzzy producer's accuracy (%)		
Sal Forest	94.02	96.11 ± 2.63
Eucalyptus plantation	91.93	94.05 ± 5.48
Dry agricultural field without crop	88.73	93.83 ± 5.10
Moist agricultural field without crop	93.57	95.90 ± 3.09
Water	93.12	96.90 ± 2.90
Fuzzy overall accuracy (%)	92.69	95.41 ± 3.87
Fuzzy Kappa	-	0.94 ± 0.05

Table B-42: Accuracy assessment results for NC DA4-MRF classified LISS-III data (Resourcesat-1) against NC DA4-MRF classified LISS-IV (Resourcesat-1) reference data.

Accuracy assessment methods	FERM (%)	SCM (%)
Fuzzy user's accuracy (%)		
Sal Forest	59.85	93.20 ± 6.75
Eucalyptus plantation	67.76	96.51 ± 3.48
Dry agricultural field without crop	85.38	95.61 ± 4.38
Moist agricultural field without crop	46.07	84.74 ± 15.25
Water	87.81	98.22 ± 1.77
Fuzzy producer's accuracy (%)		
Sal Forest	89.17	96.01 ± 3.98
Eucalyptus plantation	86.43	93.46 ± 6.50
Dry agricultural field without crop	75.46	89.80 ± 10.19
Moist agricultural field without crop	81.91	93.90 ± 6.09
Water	94.19	96.49 ± 3.50
Fuzzy overall accuracy (%)	87.65	94.58 ± 5.40
Fuzzy Kappa	-	0.92 ±0.07

B.8 Accuracy assessment of coarse resolution data (AWIFS data from Resourcesat-1) against medium resolution (LISS-III data from Resourcesat-1) reference data, with one untrained classes.

Table B-43: Accuracy assessment results for NC classified AWIFS data (Resourcesat-1) against NC classified LISS-III (Resourcesat-1) reference data.

Accuracy assessment methods	FERM (%)	SCM (%)
Fuzzy user's accuracy (%)		
Sal Forest	89.30	91.40 ± 4.65
Eucalyptus plantation	92.31	93.79 ± 3.34
Dry agricultural field without crop	89.93	91.33 ± 7.65
Moist agricultural field without crop	82.16	86.48 ± 9.86
Water	94.59	96.34 ± 1.95
Fuzzy producer's accuracy (%)		
Sal Forest	90.84	93.65 ± 3.50
Eucalyptus plantation	86.65	90.96 ± 4.54
Dry agricultural field without crop	81.74	88.90 ± 9.79
Moist agricultural field without crop	92.36	95.08 ± 3.70
Water	81.23	87.57 ± 9.24
Fuzzy overall accuracy (%)	87.65	91.75 ± 5.20
Fuzzy Kappa	-	0.89 ± 0.06

Table B-44: Accuracy assessment results for NC S-MRF classified AWIFS data (Resourcesat-1) against NC S-MRF classified LISS-III (Resourcesat-1) reference data.

Accuracy assessment methods	FERM (%)	SCM (%)
Fuzzy user's accuracy (%)		
Sal Forest	89.66	94.38 ± 4.67
Eucalyptus plantation	91.01	94.77 ± 2.63
Dry agricultural field without crop	93.54	94.05 ± 5.90
Moist agricultural field without crop	81.01	87.96 ± 10.10
Water	94.16	97.60 ± 1.98
Fuzzy producer's accuracy (%)		
Sal Forest	89.91	95.17 ± 2.94
Eucalyptus plantation	86.05	93.92 ± 4.53
Dry agricultural field without crop	93.54	88.45 ± 9.68
Moist agricultural field without crop	91.31	96.30 ± 2.64
Water	85.12	90.25 ± 8.60
Fuzzy overall accuracy (%)	87.34	93.65 ± 4.83
Fuzzy Kappa	-	0.91 ± 0.06

Table B-45: Accuracy assessment results for NC DA4-MRF classified AWIFS data (Resourcesat-1) against NC DA4-MRF classified LISS-III (Resourcesat-1) reference data.

Accuracy assessment methods	FERM (%)	SCM (%)
Fuzzy user's accuracy (%)		
Sal Forest	73.38	94.85 ± 4.47
Eucalyptus plantation	82.15	98.17 ± 1.56
Dry agricultural field without crop	53.00	82.31 ± 17.68
Moist agricultural field without crop	51.63	89.48 ± 10.31
Water	75.77	93.60 ± 6.39
Fuzzy producer's accuracy (%)		
Sal Forest	93.95	95.53 ± 4.18
Eucalyptus plantation	87.25	90.99 ± 8.45
Dry agricultural field without crop	91.94	94.38 ± 5.61
Moist agricultural field without crop	92.65	96.12 ± 3.87
Water	96.25	97.98 ± 1.77
Fuzzy overall accuracy (%)	91.54	94.20 ± 5.47
Fuzzy Kappa	-	0.92 ± 0.07

B.9 Accuracy assessment of coarse resolution data (AWIFS - Resourcesat-2) against fine resolution (LISS-IV -Resourcesat-2) reference data, with one untrained classes.

Table B-46: Accuracy assessment results for NC classified AWIFS data (Resourcesat-2) against NC classified LISS-IV (Resourcesat-2) reference data.

Accuracy assessment methods	FERM (%)	SCM (%)
Fuzzy user's accuracy (%)		
Eucalyptus plantation	86.18	95.05 ± 3.49
Dry agricultural field without crop	72.84	90.12 ± 9.62
Sal Forest	77.58	92.37 ± 5.71
Water	97.13	98.33 ± 1.62
Fuzzy producer's accuracy (%)		
Eucalyptus plantation	87.48	92.24 ± 6.31
Dry agricultural field without crop	89.85	94.01 ± 5.68
Sal Forest	94.05	96.49 ± 2.47
Water	85.99	91.82 ± 6.78
Fuzzy overall accuracy (%)	89.50	93.69 ± 5.22
Fuzzy Kappa	-	0.91 ± 0.07

Table B-47: Accuracy assessment results for NC S-MRF classified AWIFS data (Resourcesat-2) against NC S-MRF classified LISS-IV (Resourcesat-2) reference data.

Accuracy assessment methods	FERM (%)	SCM
Fuzzy user's accuracy (%)		
Eucalyptus plantation	79.44	96.02 ± 3.54
Dry agricultural field without crop	71.20	90.83 ± 8.23
Sal Forest	73.61	93.78 ± 5.25
Water	97.34	98.75 ± 1.24
Fuzzy producer's accuracy (%)		
Eucalyptus plantation	89.71	93.76 ± 5.29
Dry agricultural field without crop	90.11	94.72 ± 5.11
Sal Forest	95.75	97.57 ± 1.96
Water	88.01	93.19 ± 6.19
Fuzzy overall accuracy (%)	91.00	94.83 ± 4.58
Fuzzy Kappa	-	0.93 ± 0.06

Table B-48: Accuracy assessment results for NC DA4-MRF classified AWIFS data (Resourcesat-2) against NC DA4-MRF classified LISS-IV (Resourcesat-2) reference data.

Accuracy assessment methods	FERM (%)	SCM (%)
Fuzzy user's accuracy (%)		
Eucalyptus plantation	70.63	97.15 ± 2.77
Dry agricultural field without crop	59.68	93.54 ± 6.36
Sal Forest	60.63	95.23 ± 4.67
Water	86.88	96.95 ± 3.04
Fuzzy producer's accuracy (%)		
Eucalyptus plantation	91.59	93.37 ± 6.54
Dry agricultural field without crop	93.54	94.98 ± 5.01
Sal Forest	96.98	97.98 ± 1.95
Water	94.31	97.25 ± 2.64
Fuzzy overall accuracy (%)	94.03	95.77 ± 4.15
Fuzzy Kappa	-	0.94 ± 0.05

B.10 Accuracy assessment of medium resolution data (LISS-III data from Resourcesat-2) against fine resolution (LISS-IV data from Resourcesat-2) reference data, with one untrained classes.

Table B-49: Accuracy assessment results for NC classified LISS-III data (Resourcesat-2) against NC classified LISS-IV (Resourcesat-2) reference data.

Accuracy assessment methods	FERM (%)	SCM (%)
Fuzzy user's accuracy (%)		
Eucalyptus plantation	77.37	94.97 ± 3.06
Dry agricultural field without crop	76.47	96.73 ± 2.75
Sal Forest	70.61	94.34 ± 3.71
Water	88.44	97.06 ± 2.39
Fuzzy producer's accuracy (%)		
Eucalyptus plantation	94.92	95.95 ± 2.38
Dry agricultural field without crop	90.31	91.75 ± 6.88
Sal Forest	95.98	96.99 ± 1.13
Water	96.58	97.39 ± 2.30
Fuzzy overall accuracy (%)	94.63	95.64 ± 3.02
Fuzzy Kappa	-	0.94 ± 0.04

Table B-50: Accuracy assessment results for NC S-MRF classified LISS-III data (Resourcesat-2) against NC S-MRF classified LISS-IV (Resourcesat-2) reference data.

Accuracy assessment methods	FERM (%)	SCM (%)
Fuzzy user's accuracy (%)		
Eucalyptus plantation	72.71	95.34 ± 4.26
Dry agricultural field without crop	78.26	96.36 ± 2.95
Sal Forest	68.36	94.07 ± 5.32
Water	87.54	96.56 ± 2.95
Fuzzy producer's accuracy (%)		
Eucalyptus plantation	94.92	96.79 ± 2.56
Dry agricultural field without crop	80.65	89.60 ± 9.69
Sal Forest	95.89	97.96 ± 1.53
Water	92.25	96.32 ± 3.44
Fuzzy overall accuracy (%)	91.53	95.44 ± 4.03
Fuzzy Kappa	-	0.93 ± 0.05

Table B-51: Accuracy assessment results for NC DA4-MRF classified LISS-III data (Resourcesat-2) against NC DA4-MRF classified LISS-IV (Resourcesat-2) reference data.

Accuracy assessment methods	FERM (%)	SCM (%)
Fuzzy user's accuracy (%)		
Eucalyptus plantation	63.03	94.40 ± 5.59
Dry agricultural field without crop	71.17	91.61 ± 8.38
Sal Forest	55.93	91.47 ± 8.46
Water	90.62	98.00 ± 1.99
Fuzzy producer's accuracy (%)		
Eucalyptus plantation	88.52	94.75 ± 5.19
Dry agricultural field without crop	77.13	88.21 ± 11.78
Sal Forest	89.93	95.88 ± 4.11
Water	93.58	95.91 ± 4.08
Fuzzy overall accuracy (%)	88.00	94.06 ± 5.92
Fuzzy Kappa	-	0.91 ± 0.08

B.11 Accuracy assessment of coarse resolution data (AWIFS data from Resourcesat-2) against medium resolution (LISS-III data from Resourcesat-2) reference data, with one untrained classes.

Table B-52: Accuracy assessment results for NC classified AWIFS data (Resourcesat-2) against NC classified LISS-III (Resourcesat-2) reference data.

Accuracy assessment methods	FERM (%)	SCM (%)
Fuzzy user's accuracy (%)		
Eucalyptus plantation	95.38	96.16 ± 1.67
Dry agricultural field without crop	83.55	85.93 ± 12.51
Sal Forest	92.81	93.87 ± 2.42
Water	97.58	97.77 ± 2.05
Fuzzy producer's accuracy (%)		
Eucalyptus plantation	77.45	90.51 ± 5.51
Dry agricultural field without crop	85.95	96.28 ± 2.68
Sal Forest	83.72	93.91 ± 4.73
Water	79.25	92.40 ± 5.44
Fuzzy overall accuracy (%)	81.42	93.07 ± 4.70
Fuzzy Kappa	-	0.90 ± 0.06

Table B-53: Accuracy assessment results for NC S-MRF classified AWIFS data (Resourcesat-2) against NC S-MRF classified LISS-III (Resourcesat-2) reference data.

Accuracy assessment methods	FERM (%)	SCM (%)
Fuzzy user's accuracy (%)		
Eucalyptus plantation	90.40	95.93 ± 2.33
Dry agricultural field without crop	78.05	85.30 ± 13.37
Sal Forest	90.50	95.42 ± 2.19
Water	97.21	98.79 ± 1.20
Fuzzy producer's accuracy (%)		
Eucalyptus plantation	81.59	92.33 ± 5.51
Dry agricultural field without crop	88.16	96.39 ± 2.26
Sal Forest	83.65	92.93 ± 5.55
Water	80.43	92.95 ± 6.14
Fuzzy overall accuracy (%)	83.36	93.42 ± 4.98
Fuzzy Kappa	-	0.90 ± 0.06

Table B-54: Accuracy assessment results for NC DA4-MRF classified AWIFS data (Resourcesat-2) against NC DA4-MRF classified LISS-III (Resourcesat-2) reference data

Accuracy assessment methods	FERM (%)	SCM (%)
Fuzzy user's accuracy (%)		
Eucalyptus plantation	84.70	95.37 ± 3.53
Dry agricultural field without crop	60.83	83.22 ± 15.97
Sal Forest	84.67	95.40 ± 3.55
Water	86.80	91.92 ± 7.92
Fuzzy producer's accuracy (%)		
Eucalyptus plantation	80.79	89.59 ± 9.27
Dry agricultural field without crop	88.34	93.84 ± 5.62
Sal Forest	84.27	90.70 ± 8.08
Water	87.92	95.58 ± 4.33
Fuzzy overall accuracy (%)	84.61	91.83 ± 7.33
Fuzzy Kappa	-	0.88 ± 0.09

APPENDIX C

C.1: Implementation code of Noise classifier in R

```
rm(list=ls(all=TRUE))

require(rgdal)
require(mvtnorm)
require(rgl)
require(scatterplot3d)
require(R.utils)

# Read the input image and extract the dimensionality details
Path <- "C:\\Users\\ABC\\Desktop\\Data"
str_name<-"AWIFS.tif"
imageObj <- readGDAL(paste(Path , "\\", str_name, sep=""))
imageObjArray <- as.array(imageObj)
d <- dim(imageObjArray)
Bands <-d[3]
N <- d[2]
M <- d[1]
n <- M*N

#fuzzification Factor
m =2.7

#Delta value
Delta <- 10000

# number of classes
Ncl <- 6

# Maximum DN Value
maxDN <- 255

# Randomly initialize membership values
MembValArray = array(0,c(M,N,Ncl+1))

# Assign mean values for each class and initialization of cluster centers
MeanClassVal <- array(0,c(Bands,Ncl))
MeanClassVal[,] <- c(c(83,39.77,102.45,55.4),c(76.27,36,103.83,54.77),
c(77.78,39.15,84.15,47.31),
c(113.22,82.27,101.05,125.05),c(91.88,54.88,56,71.88),
c(70.76,34,27.03,16))

# Function to find initial optimal membership values for all classes and
pixels
getAllUValues <- function(){
  Md <- array(0,c(Ncl,n))
  Mdk <- array(0,c(Ncl,Ncl,n))
  Mdy <- array(0,c(Ncl,1,n))

  aa = array(imageObjArray, c(n,Bands))
  bb = t(MeanClassVal)

  for(k in 1:Ncl)
    Md[k,] <- sqrt(rowSums((t(t(aa)-bb[k,]))^2,1))
```

```
  for(l in 1:Ncl)
    for (k in 1:Ncl){
      Mdk[k,l,] <- (Md[l,]/Md[k,])^(2/(m-1)) + (Md[l,]/Delta)^(2/(m-1))
    }

  for(l in 1:1)
    for (k in 1:Ncl){
        Mdy[k,l,] <- (Delta/Md[k,])^(2/(m-1))
    }

  NoiseClsVector <- t(1.0/(colSums(Mdy,1)+1))
  ClassVectors <- t(1.0/colSums(Mdk,1))

  m1=array(0,c(M,N,Ncl+1))

  for(bnd in 1:(Ncl))
    m1[,,bnd] <- matrix(ClassVectors[,bnd], nrow=M, ncol=N)
  m1[,,(Ncl+1)] <- matrix(NoiseClsVector[,(Ncl+1)], nrow=M, ncol=N)

  return(m1)
}

# # Function to find initial optimal cluster centers for a specific class
Vvalues <- function (cls){

  MemValueVector <- array(rep(MembValArray[,,cls]^m,times=Bands) ,
dim=c(M,N,Bands))
  cc <- MemValueVector * imageObjArray

  aaa <- c(sum(cc[,,1]), sum(cc[,,2]), sum(cc[,,3]), sum(cc[,,4]))
  return(aaa/(sum(MemValueVector)/4))
}

# Function to find initial optimal cluster centers for all classes
getAllVvalues <- function (){
  for (cl in 1: Ncl)
    MeanClassVal[,cl] <- Vvalues(cl)
  return(MeanClassVal)
}

# Function to stretch the histogram for better results
hist_stretch<-function(data)
{
  cur.lim<-quantile(data,c(0.025,0.975),na.rm=TRUE)
  data<-pmax(cur.lim[1],pmin(cur.lim[2],data))
  data<-floor(255*(data-cur.lim[1])/(cur.lim[2]-cur.lim[1]))
  data[is.na(data)]<-0
  data
}

# Objective function of NC
NC <- function(){
  firstTerm <- 0
  secondTerm <- 0

  for (i in 1:M)
    for (j in 1:N){
      for(cl in 1:Ncl) {
```

```
        firstTerm <- firstTerm +
((MembValArray[i,j,cl])^m)*(sqrt(sum((imageObjArray[i,j,] -
MeanClassVal[,cl])^2)))
      }
      secondTerm <- secondTerm + ((MembValArray[i,j,Ncl+1])^m)*Delta
    }
  return(firstTerm+secondTerm)
}

temp <- MembValArray

objfunvalold <- 0
objfunvalnew <- 0
Objerr <- 0

# Code to create a SpatialGridDataFrame
gsd <- 56
xyoffset <- c(271761.75, 5822778.0)
xyoffset <- xyoffset - 0.5*c(gsd,gsd)
Refdata <-data.frame(as.vector(imageObjArray[,,1]))
names(Refdata) <- "class"
refgrid <-
GridTopology(cellcentre.offset=xyoffset,cellsize=c(gsd,gsd),cells.dim=c(M,N
))
Ref <- SpatialGridDataFrame(refgrid, Refdata, proj4string = "+proj=utm
+zone=44 +datum=WGS84 +units=m +no_defs +ellps=WGS84
                            +towgs84=0,0,0")
Ref$class <-  hist_stretch(Ref$class)
windows()

#The following code implements the main process of NC algorithm

iter<-0
for (iter in 1:1){ #Since Noise classifier is used stopped at iteration 1
  ptm <- proc.time()

  #get U values (i.e membership values)
  MembValArray <- getAllUValues()
  MembValArray[MembValArray==Inf] <-0

  objfunvalnew <- NC()

  # Divergence/Convergence value of objective function (i.e current
iteration value - previous iteration value)
  Objerr <- max(abs(objfunvalold-objfunvalnew))
  objfunvalold <- objfunvalnew
  print(Objerr)

  # Loop exit condition
  if(Objerr<50)
    break

  MLC <- Ref
  MLC$class <- array(0,n)

  # Code for display
  par(mfrow=c(2,4))
  for(i in 1:(Ncl+1)){
    F <- as.vector(MembValArray[,,i])
    MLC$class <- round((F/max(F)) * 255)
```

```
    image(MLC, col=gray((0:255)/255), axes=TRUE)
    title(paste({"Class "}, {i-1} ,{" - Iteration "},iter, sep=""))
  }

  #get V values (i.e. cluster centers/ mean vector for each class)
  MeanClassVal <- getAllVvalues()

  print(proc.time() - ptm)
}
```

C.2: Implementation code of NC S-MRF and NC DA-MRF Classifiers in R

```
rm(list=ls(all=TRUE))
require(rgdal)
require(mvtnorm)
require(rgl)
require(scatterplot3d)
require(R.utils)

# Read the input image & extract the dimensionality details
Path <- "C:\\Users\\ABC\\Desktop\\Data"
str_name<-"AWIFS.tif"
imageObj <- readGDAL(paste(Path , "\\", str_name, sep=""))
imageObjArray <- as.array(imageObj)
d <- dim(imageObjArray)
Bands <-d[3]
N <- d[2]
M <- d[1]
n <- M*N

# Actual window size is 2*WSize+1
WSize  <- 1

# Maximum number of neighbours
Nn  <- (WSize*2+1)^2-1

#fuzzification Factor
m =2.7

#Delta value
Delta <- 10000

# number of classes
Ncl <- 6

# The weightage to spatial and spectral components
lambda <- 0.5

# Gamma value
gamma <- 0.9

# Beeta value
beeta <- 2

#Selected Prior
prior = "DA1"  #  Options: "SA", "DA1", "DA2", "DA3", "DA4"

# Maximum DN Value
maxDN <- 255
```

```
Neigh_Coord  <- array(0, c(M, N, Bands))
Weight       <- array(0, c(2*WSize+1, 2*WSize+1))

# Randomly initialize membership values
MembValArray = array(runif(N*M*(Ncl+1)),c(M,N,(Ncl+1)))

# Assign mean values for each class (Since it is supervised method)
MeanClassVal <- array(0,c(Bands,Ncl))
MeanClassVal[,] <- c(c(83,39.77,102.45,55.4),c(76.27,36,103.83,54.77),
c(77.78,39.15,84.15,47.31),
c(113.22,82.27,101.05,125.05),c(91.88,54.88,56,71.88),
c(70.76,34,27.03,16))

# Function to find initial optimal memebrship values for all classes and
pixels
getInitMembValues <- function(){
  Md <- array(0,c(Ncl,n))
  Mdk <- array(0,c(Ncl,Ncl,n))
  Mdy <- array(0,c(Ncl,1,n))

  # Vectorized bands for easy computation
  vectorizedBands = array(imageObjArray, c(n,Bands))
  meanVector = t(MeanClassVal)

  # Computation steps
  for(k in 1:Ncl)
    Md[k,] <- sqrt(rowSums((t(t(vectorizedBands)-meanVector[k,]))^2,1))

  for(l in 1:Ncl)
    for (k in 1:Ncl){
      Mdk[k,l,] <- (Md[l,]/Md[k,])^(2/(m-1)) + (Md[l,]/Delta)^(2/(m-1))
    }

  for(l in 1:1)
    for (k in 1:Ncl){
      Mdy[k,l,] <- (Delta/Md[k,])^(2/(m-1))
    }

  # New membership values in Vector form
  NoiseClassVector <- t(1.0/(colSums(Mdy,1)+1))
  ClassVectors <- t(1.0/colSums(Mdk,1))

  #Convert back to Matrix of dimension  M*N*Bands (Rows/Column is set to
M/N to match with 'MembValArray')
  m1=array(0,c(M,N,Ncl+1))
  for (bnd in 1:Ncl){
    m1[,,bnd] <- matrix(ClassVectors[,bnd], nrow=M, ncol=N)
  }
  m1[,,(Ncl+1)] <- matrix(NoiseClassVector, nrow=M, ncol=N) # For new Noise
Membership (Equation is different)

  return(m1)
}

# Get Updated Membership values for each class.
UNew <- function(UMat){

  tempBands = array(UMat, c(n,Ncl+1))
  tempBands1 = array(UMat, c(n,Ncl+1))
```

```
  # Code for generating membership value from shuffling membership values
(not within bands but across bands) of input UMat
  for (J in 1:Ncl)
    for (val in 1:n){
      tempBands1[val,J]=
tempBands[val,(round(runif(1,min=1,max=977))%%Ncl)+1]
    }

  # OR use Code for generating random membership value generation
#     for (val in 1:n){
#       tempBands1[val,(1:Ncl)]= sample_frac()
#     }

  m1=array(0,c(M,N,Ncl+1))

  for(bnd in 1:(Ncl))
    m1[,,bnd] <- matrix(tempBands1[,bnd], nrow=M, ncol=N)
  m1[,,(Ncl+1)] <- matrix(tempBands1[,(Ncl+1)], nrow=M, ncol=N)

  return(m1)
}

# Find the L2 norm of a vector
L2distObjFunc <- function(rowNo, colNo, classNo){
  dist <-sqrt(sum((imageObjArray[rowNo,colNo,] -
MeanClassVal[,classNo])^2))
  return(dist)
}

# Noise Clustering Objective Function
NC <- function(i,j,cl){
  totVal <- 0
  totVal <- totVal + ((f[i,j,cl])^m)*L2distObjFunc(i,j,cl) +
((f[i,j,(Ncl+1)])^m)*Delta
  return(totVal)
}

# Function assigning weights in the neighbourhood
Fw <- function(a,b){
  val <- a^2 + b^2
  val <- 1 / val
  val <- val^(0.5)
  val[val==Inf]<-0
  return(val)
}

sample_frac<-function()
{
  val <- array(0,Ncl)

  k <- round(runif(1,min=0,max=Ncl)+0.5)

  val[k] <- runif(1,min=1/Ncl,max=1.0)

  k_rest <- (1:Ncl)[-k]

  f_lim <- 1-val[k]

  f_rest <- runif(Ncl-1,min=0,max=f_lim)
```

```
  s<-sum(f_rest)

  while(s==0)
  {
    f_rest <- runif(Ncl-1,min=0,max=1)
    s<-sum(f_rest)
  }

  val[k_rest] <- f_rest*f_lim/s

  return(val)
}

# Use in case of weight factors has to be give to the neighbourhood
# for(k in 1:(2*WSize+1))
#   for(l in 1:(2*WSize+1))
#   {
#     Weight[k, l] <- Fw(k-(WSize+1),l-(WSize+1))
#   }
#
# Weight <- Weight/ sum(Weight)

for(i in 1:M)
  for(j in 1:N)
  {
    imin <- i - WSize
    imax <- i + WSize
    jmin <- j - WSize
    jmax <- j + WSize

    if(imin<1)  imin <-1
    if(imax>M) imax <-M
    if(jmin<1)  jmin <-1
    if(jmax>N) jmax <-N

    Neigh_Coord[i, j, ] <- c(imin,imax,jmin,jmax)
  }

Uprior <- function(i,j,cl){
  val <- 0

  f1 <-
f[((Neigh_Coord[i,j,1]):(Neigh_Coord[i,j,2])),((Neigh_Coord[i,j,3]):(Neigh_
Coord[i,j,4])),cl]
  #W1 <- Weight[(Neigh_Coord[i,j,1]-i+1+WSize):(Neigh_Coord[i,j,2]-
i+1+WSize),(Neigh_Coord[i,j,3]-j+1+WSize):(Neigh_Coord[i,j,4]-j+1+WSize)]

  f0 <- (f1 - f[i,j,cl])^2

  for (ct in 1:(dim(f0)[1]*dim(f0)[2])){
  #  if(ct == (round((dim(f0)[1]*dim(f0)[2])/2)+1))
   #   next
    val <- val + (beeta * (f0[ct]))
  }

  return(val)
}

DA1prior <- function(i,j,cl){
  val <- 0
```

```
  f1 <-
f[((Neigh_Coord[i,j,1]):(Neigh_Coord[i,j,2])),((Neigh_Coord[i,j,3]):(Neigh_
Coord[i,j,4])),cl]
  #W1 <- Weight[(Neigh_Coord[i,j,1]-i+1+WSize):(Neigh_Coord[i,j,2]-
i+1+WSize),(Neigh_Coord[i,j,3]-j+1+WSize):(Neigh_Coord[i,j,4]-j+1+WSize)]

  f0 <- (f1 - f[i,j,cl])^2

  for (ct in 1:(dim(f0)[1]*dim(f0)[2])){
    val <- val + (-gamma * (exp((-(f0[ct])/gamma))))
  }
  return(val)
}

DA2prior <- function(i,j,cl){
  val <- 0

  f1 <-
f[((Neigh_Coord[i,j,1]):(Neigh_Coord[i,j,2])),((Neigh_Coord[i,j,3]):(Neigh_
Coord[i,j,4])),cl]
  #W1 <- Weight[(Neigh_Coord[i,j,1]-i+1+WSize):(Neigh_Coord[i,j,2]-
i+1+WSize),(Neigh Coord[i,j,3]-j+1+WSize):(Neigh Coord[i,j,4]-j+1+WSize)]

  f0 <- (f1 - f[i,j,cl])^2

 for (ct in 1:(dim(f0)[1]*dim(f0)[2])){
#    if(ct == (round((dim(f0)[1]*dim(f0)[2])/2)+1))
#      next
    val <- val + (-gamma/(1 + ((f0[ct])/gamma)))
  }
  return(val)
}

DA3prior <- function(i,j,cl){
  val <- 0

  f1 <-
f[((Neigh_Coord[i,j,1]):(Neigh_Coord[i,j,2])),((Neigh_Coord[i,j,3]):(Neigh_
Coord[i,j,4])),cl]
  #W1 <- Weight[(Neigh_Coord[i,j,1]-i+1+WSize):(Neigh_Coord[i,j,2]-
i+1+WSize),(Neigh_Coord[i,j,3]-j+1+WSize):(Neigh_Coord[i,j,4]-j+1+WSize)]

  f0 <- (f1 - f[i,j,cl])^2

  for (ct in 1:(dim(f0)[1]*dim(f0)[2])){
    val <- val + (gamma * log(1 + ((f0[ct])/gamma)))
  }

  return(val)
}

DA4prior <- function(i,j,cl){
  val <- 0

  f1 <-
f[((Neigh_Coord[i,j,1]):(Neigh_Coord[i,j,2])),((Neigh_Coord[i,j,3]):(Neigh_
Coord[i,j,4])),cl]
  #W1 <- Weight[(Neigh_Coord[i,j,1]-i+1+WSize):(Neigh_Coord[i,j,2]-
i+1+WSize),(Neigh_Coord[i,j,3]-j+1+WSize):(Neigh_Coord[i,j,4]-j+1+WSize)]
```

```
  f0<- (f1 - f[i,j,cl])

  for (ct in 1:(dim(f0)[1]*dim(f0)[2])){
    val <- val + (gamma*abs((f0[ct])) - (gamma^2)*log(1 +
(abs((f0[ct]))/gamma)))
  }

  return(val)
}

U <- function(i,j,clv){
  val <- 0
  if(prior == "SA")
    val <-  (1.0-lambda) * NC(i,j,clv) + lambda * Uprior(i,j,clv)
  else if(prior == "DA1")
    val <-  (1.0-lambda) * NC(i,j,clv) + lambda * DA1prior(i,j,clv)
  else if(prior == "DA2")
    val <-  (1.0-lambda) * NC(i,j,clv) + lambda * DA2prior(i,j,clv)
  else if(prior == "DA3")
    val <-  (1.0-lambda) * NC(i,j,clv) + lambda * DA3prior(i,j,clv)
  else
    val <-  (1.0-lambda) * NC(i,j,clv) + lambda * DA4prior(i,j,clv)

  return(val)
}

#=============================================================================
======================
# Block 5:  Energy optimisation with simulated annealing
#=============================================================================
======================

# Maximum allowed number of iterations
Niter <- 20

# SA cooling schedule parameters
T0 <- 2.0

# Convergence criterion for SA
min_acc_thr <- 0.1*10^(-2)*n*Ncl

T <- T0

par(mfrow=c(1,1))
stop_crit <- 0

# Initialize SpatialGridDataFrame
gsd <- 20
xyoffset <- c(271761.75, 5822778.0)
xyoffset <- xyoffset - 0.5*c(gsd,gsd)
#Refdata <- data.frame(as.vector(array(0,c(M,N))))
Refdata <-data.frame(as.vector(imageObjArray[,,1]))
names(Refdata) <- "MembVal"
refgrid <-
GridTopology(cellcentre.offset=xyoffset,cellsize=c(gsd,gsd),cells.dim=c(M,N
))
Ref <- SpatialGridDataFrame(refgrid, Refdata, proj4string = "+proj=utm
+zone=44 +datum=WGS84 +units=m +no_defs +ellps=WGS84
                            +towgs84=0,0,0")
```

```
windows()

# Initialize the NC Array
NCA <- Ref
NCA$MembVal <- array(0,n)

# Get the initial membership values
f <- getInitMembValues()
#f[f==Inf] <-0

MembValArray <- f
UpdatedUVal=UNew(MembValArray)

for(iter in 1:Niter)
{
  upd_count <- 0

  for(cl in 1:Ncl)
  {
    if(iter == 1)
      next

    for(i in 1:M)
    {
      for(j in 1:N)
      {
        f_update <-  UpdatedUVal[i,j,cl]
        ft <- f[i,j,cl]

        if(f_update!=ft)
        {
          u1 <- U(i,j,cl)
          f[i,j,cl] <- f_update

          u2 <- U(i,j,cl)

          u1 <- u2-u1

          if(T!=0)
          {
            if(u1>0)
            {
              f[i,j,cl] <- ft
            }
            else
            {
              u1 <- exp(-u1/T)
              xi <- runif(1, min=0, max=1)

              if(xi>u1)
              {
                f[i,j,cl] <- ft
              }
              else
                upd_count<-upd_count+1
            }
          }
        }
      }
```

```
    }
  }

  if(iter!= 1 && upd_count<=min_acc_thr) # Iter 1 is just output of Simple
NC i.e Initial Membership values
    break

  if(iter!= 1) # Iter 1 is just output of Simple NC i.e Initial Membership
values
    print(upd_count)

  # Update Temperature
  T <- (log(1+iter)/log(2+iter))*T0

  # Print the NC-MRF output for each class. (i.e Membership values for each
class)
  par(mfrow=c(2,4))

  for(i in 1:(Ncl+1)){
    F <- as.vector(f[,,i])
    NCA$MembVal <- round((F/max(F)) * 255)
    image(NCA, col=gray((0:255)/255), axes=TRUE)

    if(iter==1)
      title(paste({"Class "}, {i-1}, {" Init Membership Values"}))
    else
      title(paste({"Class "}, {i-1}, {" - Iteration "},(iter-1), sep=""))
# First iter is just skipped over
  }

}
```

APPENDIX D

D.1 Publications

Aravind H., A. Kumar, A. Stein- The effect of spatial contextual information on Noise classifier". (Draft prepared. To be submitted in a peer reviewed journal)